2001

Study of the electrical and optical properties of CuO and CdS thin films prepared by spray method and formation of CuO/CdS heterojunction

Muhibbullah, Md.

University of Rajshahi

Study of the electrical and optical properties of CuO and CdS thin films prepared by spray method and formation of CuO/CdS heterojunction

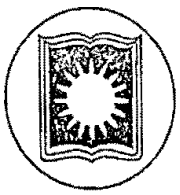

by

MD. MUHIBBULLAH

A Thesis Submitted for the
Degree of M. Phil. in the Department
of Physics, University of Rajshahi, Rajshahi-6205
Bangladesh

September 2001

DEDICATED
TO
MY PARENTS

ACKNOWLEDGEMENT

It is a great pleasure for me to express my profound sense of gratitude to my honourable teachers Professor M. G. M. Chaudhury and Professor M. O. Hakim for their kind and constant supervision throughout the whole of my work and preparation of the thesis.

I offer my thanks to the chairman of the department of Physics for giving me the opportunity to use the departmental facilities.

I am greatly indebted to my teacher Professor A. K. M. Azharul Islam for his learned advice and helpful suggestions in my work.

I also pay my gratitude to my teachers Dr. M. Mozibur Rahman and Mr. A. F. M. Abdul Wahed for their valuable learned advice and helpful suggestions in the process of my work. I am grateful to my respectable teachers Mr. Nurul Islam and Professor M. Nazrul Islam for their encouragement and valuable suggestions.

I am thankful to all other teachers of the department of physics specially , Professor M. Golam Mortuza for his encouragement and helpful suggestions.

My thanks to Mr. M. Moksed Ali, glass blower and Mr. M. Bodoroddoza of Physics department for their kind help in the course of the experimental work.

The award of a research fellowship (N. S. T.) by the Ministry of Science and Technology, Bangladesh and the most valuable service rendered by the BANSDOC in supplying me some of the photocopies of the references are gratefully acknowledged.

Finally, I would like to thank my wife Mafruha and daughter Meem for their encouragement and many sacrifices during the course of my research work.

ABSTRACT

Cupric oxide (CuO) and Cadmium sulphide (CdS) thin films have been deposited on glass substrates by chemical spray pyrolysis technique and their structural, electrical and optical properties were studied. Film growth aspects have been reported in addition to optimization procedures.

X-ray diffraction study indicated that cupric oxide (CuO) deposit is crystalline and has monoclinic crystal structure with a=4.704Å, b=3.414Å and c=5.004Å. For CdS films, X-ray diffraction pattern exhibit that the samples have hexagonal crystalline structure with a=4.136Å and c=6.713Å.

Hall effect and thermoelectric power measurements show that CuO is p-type with carrier concentration about 10^{15}-10^{16} cm^{-3} and CdS is n-type with low carrier concentration of order 10^{14} cm^{-3}. In both the materials Fermi levels position changes with the thickness of the film.

For CuO films, the resistivity is quite low and the value increases slightly with thickness but decreases on annealing. The conductivity behaviour show activation process to be present. In the case of CdS films substrate temperature has remarkable effect on resistivity and annealing the film reduces the resistivity.

Thermoelectric power (TEP) measurements on CuO show a pinning character of the Fermi levels at high temperature. In the case of CdS TEP changes slightly with temperature near the room temperature range but almost remain constant at higher temperature.

Both CuO and CdS are direct band gap semiconductors with average band gap of 1.4 and 2.36 eV respectively.

All sprayed CuO/CdS heterojunctions have been fabricated and from current-voltage characteristics of the p-n junction it was found that good quality diode may be fabricated by depositing thick CuO and CdS layers of comparable thickness on SnO_2 coated glass substrate. As an usual procedure CdS is to be deposited first on the substrate and then CuO as an over layer.

CONTENTS

CHAPTER-4 RESULTS AND DISCUSSION

CHAPTER ONE

GENERAL INTRODUCTION

GENERAL INTRODUCTION

1.1 Introduction

Experimental work on thin films has been continuing in different parts of the world for successful applicants of their properties in scientific, engineering and industrial purposes. The increasing demands for microelectronic and microstructural components in different branches of science and technology have greatly expanded the sphere of thin film research. During the last four decades a great deal of research works have been carried out on the thin films of metals, semiconductors, insulators and cermet (granular metal) materials. Sufficient time has also been utilized to search for other new coating materials relevant to electro-optical properties. These comprise the spectrally selective coating, transparent conducting coating, heating elements, antistatic coating on instrument panels, and electrical contact in liquid crystal, electrochromic and electroluminescent displays, smart window coating, photochromic, thermochromic coating and solar absorbing layer etc. According to design and structure of the devices, these coating may be either a single or multilayer on a suitable neutral substrate or may be a layer forming composite structure with the substrate. Among the above varieties of layers, 'oxide and sulfide' thin films have initially figured prominently for their application in solar cells.

Thin films have been extensively studied for over a century because of their potential applications. The thin solid films were probably first obtained by electrolysis in 1838.

Grove[1] and Bunsen[2] deposited of metal films at reduced pressure in 1852 by means of glow-discharge sputtering and chemical reaction respectively. The first evaporated metal thin films were put forward by Faraday[3] in 1857. The chief application of these studies was in optics for mirror and interference filters. However free evaporation and condensation of thin films in vacuum were probably first observed by Edison and others in 1883.

The possibility of deposition thin metal films in vacuum by joule heating of platinum wires were discovered in 1887 by Nahrwold[4] a year latter adapted by Kundt[5] for the purpose of the measuring refractive indices of metal films. Chemical vapour transport methods for deposition of thin and thick coating have developed from the early observations of Bunsen[2] on chemical reduction of FeCl, by steam to produce Fe_2O_3.

Thomson[6] in 1901 was the first to propose a 'size effect' theory to explain the observed high electrical resistivity of thin specimen as compared with that of the bulk metal. The size effect theory for a free electron model was worked out by Fuchs[7] in 1938 for a spherical Fermi surface. Lucas in 1965 generalized the Fuchs calculations to the case of scattering from the two film surfaces with different secularity parameters. The size effect theory for temperature of resistance was computed by compbell[8] in 1966. Since Fuchs-Sondheimer theory fails to explain with due precession the thickness dependence of transport parameter for metal films. Mayadas and Shatzkes in 1970 has proposed a conduction model taking into consideration of grain boundary scattering along with other scattering mechanism.

Between two world wars the thin film technology developed rapidly when vacuum evaporated metal and dielectric films were used in optics and the development of diffusion pump made it possible. Since then a new branch of optical technology has emerged which is based on optical interference system.

The most modern development in the field of thin film physics is that of the optoelectronic devices. Photovoltaic, photoconductive, and solid-state layer devices are now under consideration of the experimental physics of this respect.

Now-a-day extensive studies on different properties of thin films proceeded along different lines throughout the world. Recently an event greater application known as thin film microelectronics has emerged in the field of electronics and consequently a rapid development occurred in microelectronic industry.

1.2 Brief review of the previous work

1.2.1 Historical development and properties of CuO thin films

Copper oxide is a defect semiconductor of p-type conductivity and thorough work carried out in the 1920s and 1930s was one of the first semiconducting materials to be investigated[9]. To grow uniform and homogeneous thin film of CuO is highly desirable both from scientific and commercial point of view.

Copper oxide is a binary I-IV compound which have two phases: (i) cuprous oxide and (ii) cupric oxide. The physical properties of the two phases are different from each other.

Cuprous oxide:

According to W. L. Bragg,[10] F. Rinne,[11] W.P. Davay[12] and A. Gruhn,[13] the x-ray diagram of cuprous oxide (Cu_2O) is typical of a face centered cubic lattice with the heavy copper atoms arranged in a face-centered lattice, with the shortest distance between the atoms of 1.84Å. The oxygen atoms are so light that they make comparatively little difference to the intensities of the spectra and they lie on a cube centered lattice, which intersects the face-centered lattice of the copper atoms.

The specific gravity (by J. F. Persoz)[14] varies from 5.375 to 5.34. F. Gaud's[15] sample reduced from Fehling's solution had a specific gravity 5.881.

S. Mayer[16] found cuprous oxide to be paramagnetic. The magnetic susceptibility is 0.73×10^{-7} mass unit at 17°C. Cuprous oxide has rather a low electrical conductivity. K. Badeker[17] gives the specific resistance of cuprous oxide as 40 Ω-cm when that of copper is 1.7×10^{-6} Ω-cm.

Cupric oxide:

Cupric oxide (CuO) usually appears as a brownish black powder which is zet black when hot or else in brownish black brittle scales or granules. The measurements by N. S. Maskelyne[18] show that the crystals of Cornish melaconite are pseudo monoclinic and belong to the triclinic system; they have the axial ratio a:b:c=1.4902:1:1.3604 with $\alpha=90^\circ$; $\beta=99^\circ32'$; $\gamma=90^\circ$.

E. Kalkowsky[19] showed that these measurements agree with those of G. Jenzsch's[20] for versavian tenorite. J. A. Hedvell[21] has studied the x-ray diagram and he concluded the all the different forms of the oxide artificial and natural have the same x-ray diagram.

L. Wohler and A. Foss[22] found the melting point to be 1064°C. According to S. Mayer[23] cupric oxide is paramagnetic, magnetic susceptibility are about 3.1×10^{-7} mass unit at 17°C.

The reported values for the specific gravity of cupric oxide range from 6.13 of P. F. G. Boully and J. F. Persoz[24] to 6.451 of G. Jenzsch.

F. Streintz[25] said powdered cupric oxide is a nonconductor of electricity, but it conducts much better when it has been fused. According to K. Badeker[9], the specific resistance is 400 Ω-cm when that of copper is 1.7×10^{-6} Ω-cm.

Recently the use of CuO materials in the high T_c superconductors has emphasized the need of a renewed study of this material. It is known from the past that Cu_2O and CuO materials are p-type semiconductors and therefore their use in the field of fabrication of solar cells[26-30], specially heterojunctions, is equally

interesting[31]. CuO materials also have gas-sensing capability and can defect a variety of inflammable gases[32]. Researches in this line are also going on with equal strength in many places.

There are various methods of preparation of copper oxide thin films, such as chemical vapour deposition, electrodeposition, thermal oxidation, sputtering, plasma evaporation and laser-assisted deposition[26,33-37], in which chemical deposition techniques are very attractive due to the simplicity in the process and cost effectiveness. Chemical spray methods have been used by many workers to grow thin films of Cu_2O, CuO, ZnO etc.[38,39].

V. F. Drobny and D. L. Pulfry [40] prepared copper oxide thin films by thermal oxidation and optical constant were investigated. The phases of $Cu+Cu_2O$, Cu_2O+CuO and CuO were identified and each phase exhibited characteristic values of resistivity and optical constants. Cu_2O thin film prepared in this manner have a high refractive index in the visible range (n=2.8 to 3.4), low value of extinction co-efficient below 2.5 eV and readily controllable resistivity over the approximate range 25 to 104 Ω-cm.

Oxidized copper was studied by A. Ross and B. Westerstrandh[41], prepared by chemical oxidation of copper in a solution of copper chloride and sodium hydroxide heated to 70°C. Various copper alloys with different structures and pretreatment were investigated in order to produce the best possible values of the solar absorptance α and thermal emittance ε. In combination with the long range stability α and ε were calculated from measurements of the reflectance versus the wavelength in the range 0.35 to 15μm. The best surfaces investigated have of α values greater than 0.9 and ε values less than 0.2. Surface analysis shows that the oxide layer form in the chemical bath is mainly Cu_2O, which is also confirmed by X-ray diffraction.

N. Ozer and F. Tepehan[42] prepared copper oxide thin films by thermal evaporation method. XRD patterns of the films indicate no peaks, which means that the films are amorphous to XRD examinations. The optical transmittance of the films varies from 72% to 89% in the visible region. The refractive index of the samples was between 2.9 to 3.1. Absorption co-efficient data indicate a band gap 2 eV. The extinction co-efficient values are approximately $4x10^{-2}$.

A.E. Rakhshani et al.[43] prepared copper oxide thins films by electrodeposition method. XRD shows that these were crystalline Cu_2O. From a knowledge of the crystal structure of Cu_2O, cubic with a lattice constant of 0.427nm. $(\alpha h\nu)^{1/2}$ versus $h\nu$ curve shows that electrodeposited Cu_2O film have a band gap 1.95 eV. The resistivity of these films was in the range 106 to 108 Ω-cm.

B. Karlson et al.[44] studied the optical properties of metal oxide in solar absorbers. The samples were prepared by thermal oxidation of thin metallic films in air at atmospheric pressure. The thickness of the film ranged from 0.05 to 0.5 μm. Cu_2O and CuO were obtained by oxidation of copper films at 150°C to 180°C and 450°C to 600°C respectively. The optical band gap obtained for Cu_2O and CuO films are 2.2 eV and 1.5 eV respectively.

Locquett[45] studied the growth of CuO films employing an atomic oxygen source. They have reported the growth of [111]- and [020]- oriented CuO films respectively, on MgO(100) and YSZ(100) substrates.

Kawaguchi et al.[46] have studied the growth of study the growth of CuO/Cu_2O films using oxygen ions o energy 50 eV. This stuty has shown that the growth of Cu_2O and CuO films could be achieved by maintaining $[O^+]$/Cu flux ratios of ~1.7 and 10, respectively.

K. P. Muthe et al.[47] have also studied the growth of CuO phase formation during thin film deposition (by molecular beam epitaxy). He reported Cu_2O films could be grown with relative to maintaining atomic oxygen flux of 1.6 times the stoichiometic value. In contrast, the kinetics of CuO formation has been found to the quite slow. For atomic oxygen to copper flux ratio of ~80, only ~95% of the copper was found to be in fully oxidized state.

1.2.2 Historical development of CdS thin films and its properties

Cadmium sulphide (CdS) polycrystalline films have been extensively investigated in the past because of their uses in semiconductor devices and solar cells.

In the last three decades a large amount of work has been devoted to the study of CdS thin films in view of their potential application in the field of optoelectronic devices. Wide band gap CdS (E_g=2.4 eV) has been used as the window material in heterojunction solar cells together with several narrow band gap semiconductors such as Cu_2S (E_g=1.2 eV)[48], InP (E_g=1.35 eV)[49], $CuInSe_2$ (E_g=1.01 eV)[50], CdTe (E_g=1.45 eV)[51] etc.

From the late 1950, a period almost 20 years, the only thin film photo voltaic cell available were the heterojunction between p-type Cu_2S and n-type CdS. In spite of its complexities this system is one of the prominent contenders for photo voltaic solar energy conversion. Curiously, it is commonly referred to as the 'CdS cell'.

Other than solar cell CdS has found extensive application in various optical, electronic and opto-electronic devices and therefore has been subject of considerable research interest.

CdS has a direct band gap, giving a transparent, sunny yellow appearance. It usually has the wurtzite hexagonal structure, although the zincblende cubic structure is found for preparation near room temperature. The material is polar with respect to the hexagonal c-axis and shows markedly greater chemical reactivity on the Cd-side a-face than on the S-side b-face [52].

CdS is easily doped n-type with In, Sn, Al. Cl or Br, all of which form shallow donors. Sulfur vacancies, induced by the presence of excess Cd during film or crystal growth, acts as dondrs and resistivities below 0.1 Ω can be achieved with no intentional impurity introduction. Deep acceptor states are formed by Cu, Ag, and Au impurities and readily compensate the native donors. Although many workers have attempted to prepare p-type CdS, its existence has never been established beyond questions: the tendency toward self compensation is very strong in CdS.

Films of CdS has been deposited by perhaps a wider variety of methods than any other semiconductor material: Viz vacuum evaporation[53], chemical bath deposition[54], chemical vapour deposition[55], molecular beam epitaxy[56], anodization[57], spray pyrolysis[58-60] etc. CdS can be deposited by vacuum evaporation using the 'three temperature' method in which S and Cd evaporation sources are held at a suitable temperature while substrate is held at a third temperature. In vacuum deposition CdS usually prefers to grow with hexagonal axis (1000) perpendicular to the substrate.

The electron mobility for CdS ranges from 100 to 400 cm^2/V-sec. at 300 K for single crystal. In thin films the mobility is commonly dominated by grain boundary potential barrier and mobility from well below 1 up to over 100 cm^2/V-sec. are commonly seen depending on the carrier density. Resistively ranges from 0.001 to over 10^8 (-cm can be achieved for films deposited on amorphous substrates.

B. F. Shirreffs et al.[61] reported electrical properties of CdS film grown by spray pyrolysis in an N_2 ambient. The resistivity was found to be 453 Ω-cm. The results for the Hall effect measurement on slow cooled films were that ($_H$=66 cm^2/V-sec. and n=2.1x10^{14} cm^{-3}.

I Martil et al.[62] prepared thin films of CdS by R. F. Sputtering and studied their electrical properties. The resistivity from 10 to 10^8 (-cm and mobility in the range 2-6 cm^2/V-sec. were obtained depending on the production conditions.

A.C. Pande et al.[63] in 1984 studied the properties of electrophoretically deposited layers of CdS and D. M. Uzagare et al.[64] in 1984 used the film of CdS as electrolyte cells.

In 1985 I. Jimenez et al.[65] prepared polycrystalline CdS thin films for photoelectrochemical applications. The presence of electronic states in the band gap of the material was investigated by means of several optical techniques. The thickness of the CdS layers estimated from the weight, were a few microns and the electrode resistance was of the order of 10 (. Optical data give an energy gap of the order of 2.1 eV to 2.3 eV.

In 1986, M. Krunks et al.[66] prepared the CdS films by spray pyrolysis of neutral aqueous solution of $CdCl_2$ and $SC(NH_2)_2$. It was established that the process passes through the state of the intermediate complex compound $Cd(SCN_2H_4)_2Cl_2$ for various molar ratios of the initial components. The complex compounds are characterized by IR spectroscopy, X-ray diffraction and chemical analysis. The thermal decomposition of $Cd(SCN_2H_4)_2Cl_2$ to cadmium sulphide was studied.

In 1986, J. Ebothe et a.[67] observed the electro-optical properties of thin CdS films by photo current analysis at solid liquid junction. S. Achour et al.[68] observed the effect of the thermal annealing on the cathodo luminescence of evaporated CdS films.

Pyare Lal[69] observed the temperature variation of the thermoelectric power (TEP) of vacuum deposited CdS films. They reported that, the TEP of polycrystalline CdS films varies with the temperature (it initially decreases and then increases with a rise in temperature) and depends on the polarity and strength of the longitudinal electric field. Variation in the TEP depends on the conductivity, which is due to the non-stoichiometry of the film.

In 1966, R. R. Chamberlin et a.l[58] studied the X-ray diffractro graph of CdS film deposited at different temperature.

In 1988, M. T. S. Nair et al.[70] observed the effect of bath temperature of opto-electronic characteristics of chemically deposited films. Systematic variations in the opto electronic characteristics were also observed as functions off bath temperature: transmission T above the absorption edge was 10%-80% photoconductivity, $\sigma_{Ph}=2x10^{-3}$-2.0 $\Omega^{-1}cm^{-1}$; photoconductivity to dark conductivity ratio $\sigma_{Ph}/\sigma_d=10^6$-$10^9$ and photo current decay time, $\tau=20$-10^3 sec.

In 1990, C. De. Blasi et al.[71] observed the characterization of CdS epitaxial films by high energy reflected electrons. Photoconduction and thermo-optical hysterisis was measured in thin CdS films C. Bovchenaki et al.[72]. They got

information about the crystal structure, the absorption edge, the photoconductivity gain the free carrier life time and the surface recombination time and they also showed the thermo-optical bi-stability in transmission and photo conduction.

In 1990, F. J. Espinoza et al.[73] have calculated the reflectivity of a thin film of CdS in the spectral neighbourhood of the B (n=1) exciton. K.S. Balakrish et al.[74] studied the structural and growth kinetics of electro deposited CdS thin films for solar cell applications. Using the X-ray diffraction technique, the growth and texture of R. F. Sputtered CdS thin films were investigated by A.Bennouna et al.[75].

Basol et al.[50] have reported that chemically prepared CdS films are better as the window material in thin film solar cells. They have used very thin (~50nm) CdS as the window material in CdS/$CuInSe_2$ solar cells and have reported that this structure of solar cell leads to high efficiency[57]. The main objective of this study was to identify the conditions for the preparation o polycrystalline CdS films (using the chemical method of spray pyrolysis) with better electrical and optical properties in order to increase the efficiency of solar cells prepared using these films.

A. Ashour et al.[76] have observed the electrical and optical properties of CdS films thermally deposited. They have reported the resistivity decreases as the substrate temperature and deposition rate decrease. The films exhibited a direct transition in the range 2.23 to 2.30 eV. K. K. Nanda et al.[77] also have reported, from the optical absorption, the band gap for bulk CdS was 2.405 eV and was increased to 3.97 eV for nanocrystalline samples.

O. Trujillo et al.[78] have reported cumulative results on CW Nd:YAG laser deposition of CdS thin films. Films were characterized by X-ray diffraction, scanning electron microscopy, energy dispersive X-ray analysis, transmission electron microscopy, ultraviolet through visible light transmission, and Raman measurements. Films deposited at 400°C or higher manifest a pure hexagonal CdS phase, and films deposited at 200°C or lower remain both cubic and hexagonal phases.

1.2.3 Historical development of heterojunctions, CuO/CdS

A junction formed between two semiconductors having different energy band gaps is termed a heterojunction. If the conductivity type is the same in the two semiconductors, the heterojunction is called an isotype heterojunction. An anisotype heterojunction is one in which the conductivity type is different in the two semiconductors. Some of the requirement for forming a good quality heterojunction are[79]

(i) the lattice constant of the two materials should be nearly equal,

(ii) the electron affinities should be compatible, and

(iii) the thermal expansion coefficients should be close.

Heterojunction have a various applications such as solar energy conversion. Becquerel[80] first discovered the photovoltaic effect in 1839 with the detection of a photovoltage between illuminated AgCl and Pt electrodes immerged in an electrolyte. About 40 years later Adams and Day[81] observed the effect in a solid (selenium) in1877. Since that time the first one hundred years of sporadic solar cell research was dominated almost exclusively by non–silicon materials. During this period research was carried out on such materials as Selenium, metal oxides and metal sulfides. This work eventually resulted in the photoelectric exposure meters. These cells while exhibiting a strong photovoltaic effect would not provide better than 1% efficiency in converting solar energy. It was not until 1954 that practical solar conversion efficiencies of about 6% were reported in silicon[82] and Cadmium Sulphide[83]. Within next two years, silicon solar cells were fabricated with good yield and 8-10% conversion efficiencies; a few cells were made with efficiencies of 11%[84]. The CdS cells could not keep pace with silicon in the development of higher efficiencies, and for this reason as well as reliability considerations, lost out to silicon in the battle for the space market. The space market has continued, until recently, to provide the major impetus for solar cell development, and silicon has continued to dominate the commercial solar cell picture. In part, this is because the solar cell industry has been able to borrow from the technological advances made by the silicon-based microelectronics industry, to increase the efficiency. The enormous growth in solids state technology utilizing silicon has put that material in the unique position of currently being the most extensively studied material for photovoltaic applications. Silicon has the added advantage of being one of the most abundant elements occurring in nature. Silicon has been developed for the entire semiconductor industry and considerable money has been invested for other than solar cell purposes. On the other hand, the other materials had to be developed only for solar cells.

Atomic absorption spectroscopy combined with controlled chemical etching and Auger electron spectroscopy profiling with ion beam etching have been used to obtain composition versus depth analyses of Cu_2S/(Zn,Cd)S heterojunction solar cells formed by an aqueous cation exchange, or chemiplating, process by Uppal and Burton[85]. Chemiplated Cu_2S/(Zn,Cd)S heterojunctions were compositionally graded over very wide regions with measurable Zn and Cd concentrations observed throughout the Cu_2S layers. In all cases, the film growth rate R on either

polycrystalline CdS or (Zn,Cd)S substrates was found for a given substrate composition, to be approximately constant with time.

Optical and scanning electron microscopy observations of as-deposited Cu_2S/(Zn,Cd)S cells showed distinet topographical features indicating nonuniform film growth rates R over the substrate surface area.

Y. Aparna et al.[86] polycrystalline thin film n-CdS/p-$CuGa_xIn_{1-x}Se_2$ heterojucntions were also fabricated with a back-wall configuration and the junction characteristics were evaluated in terms of current density-voltage, capacitance-voltage and spectral response measurements. The electrical conversion efficiency obtained for cells with an active area of 1 cm^2 under a solar input of 85 $mWcm^{-2}$ was 7.6%, 6.7% and 6.5% respectively for $CuGa_xIn_{1-x}Se_2$ cells with x=0.25, 0.50 and 0.75.

J. Touskova et al. [87] were prepared thin polycrystalline layers of CdS and CdTe by a spray pyrolysis method and electrochemical deposition respectively. Electroplating was performed at deposition potentials from –500 to –600 mV (SCE). The thickness of the layers, namely tenths of a micrometre for CdS and 1-1.5 (m for CdTe, and their good optical quality were deduced from optical transmissin measurements. The study of the films by X-ray diffraction confirmed a hexagonal phase of CdS with ‹002› texture and a cubic structure of CdTe with expressive texture ‹111›. Measurement of dark I-U and C-U characteristics was used to study the charge transport in n-CdS-p-CdTe heterojunctions.

Hyeong Soo Kim et al.[88] observed that the sintered CdS/CdTe and the $Cd_{0.94}Zn_{0.06}S$/CdTe solar cells with various cell widths, the following conclusions can be drawn;

(i) Cell parameters and efficiency of the sintered $Cd_{1-x}Zn_xS$/CdTe solar cell degrade with increasing cell width.

(ii) The degradation is mainly caused by the increase in the series resistance of the solar cells.

(iii) Sintered CdS/CdTe and $Cd_{0.94}Zn_{0.06}S$/CdTe solar cells with cell widths of 4 mm show the maximum module efficiency.

(iv) A sintered CdS/CdTe and a $Cd_{0.94}Zn_{0.06}S$/CdTe solar cell with an active area of 10 mm x 4 mm showed solar efficiency of 10 and 11%, respectively, under solar illumination with an intensity of 85 mW cm^{-2}, and the estimated values of the module efficiencies were 6.7% and 7.3% respectively.

Hai-Ning Cui et al.[89] reported that, dipped CdS and sputtered ITO bilayer has a wider transmission range and a higher transmittance than that of a single CdS

layer. Of the different kinds of solar cell structures in a substrate, the one with the ITO/CdS bilayer window had better electrical and optical properties. In addition, the bilayer does not need a thick CdS film and reduces the potential toxicty by reducing the amount of cadmium compounds used.

With such formidable technology behind silicon, it is reasonable to ask why non-silicon materials should be explored for solar cell applications. The answer is that, in spite of its high technological development, silicon has several disadvantages for solar cell applications. Firstly, silicon with a band gap of 1.1 eV is not the optimum photovoltaic material based on theoretical conversion efficiency. In addition, an efficient p-n junction photovoltaic device should satisfy the following two criteria: (i) the product of the minority carrier diffusion length (L) and the optical absorption coefficient (() should observe the relationship (L(3; and (ii) the product of the optical absorption coefficient (() and the semiconductor film thickness (t) should satisfy the condition (t>>1. Silicon being an indirect band gap material has low optical absorption coefficient and, therefore, cannot satisfy the condition, (L(3, as easily as direct gap semiconductor. Similarly, for indirect band gap materials, satisfying the second requirement, (t>>1, will necessitate the use of larger film thickness, which in turn implies less material economy and can lead to problems in maximizing carrier collection efficiencies and in device fabrication.

The CuO/CdS thin film heterojunction is a prime contender fo future terrestrial application due to its relatively high efficiency and projected low cost. In a solar cell, two basic requirements for the window material are low electrical resistivity and high optical transmittance. Basol et al.[57] have reported that chemicaly prepared CdS film are better as the window material in thin film solar cell. Fabrication of solar cell needs a narrow band gap semiconductor as an absorber, CuO thin film (E_g=1.4 eV) may be used for their high optical absorption co-efficient. Studies on various heterojunction have been reported from various laboratories[80-89].

1.3 The aim of work

Use of a simple and low cost deposition technique like spray pyrolysis to grow technologically important thin films can be interesting for many reasons. There has been efforts of preparing varieties of p-type and n-type semiconducting samples in our laboratory for the last few years. Cupric oxide (CuO) and cadmium sulphide (CdS) are two such materials which are known to have p and n type conductivities respectively, and they can be applied as solar selective coatings, to prepare p-n junction or solar cells, and to prepare other photosensitive devices. These types of electronic devices are physically not very straight forward to form. Moreover

simplification of the deposition process demands a details procedure for the process optimization and control of system variables. The aim of our present work is therefore to prepare CuO and CdS thin films asserting the deposition variables to obtain good quality p and n-type semiconducting samples. After preparation their structural, electrical and optical properties are to be studied as a routine characterization work. Modern and advanced disposition systems have been used by many workers in the recent past for preparing these samples but the transport properties are still not well understood when simpler deposition methods are employed. Hence renewed investigation along this line would be interesting. As a part of these processes the possibility of forming heterojunctions of these materials has also been explored with a view to preparing all sprayed p-n junction on glass substrates.

1.3 The structure of the thesis

Some experimental work on the deposition and characterization of CuO, CdS thin films and CuO/CdS heterojunction has been presented in this thesis. It contains five major chapters in which the second and third chapter consists of two parts.

The first chapter contains an introduction to CuO, CdS thin films and CuO/CdS heterojunction.

The theoretical background of the film growth process, the apparatus design consideration and various analytical techniques, for analysis of film properties, have been given in chapter-2.

Detail description of the design of a spray apparatus, film deposition process and various experimental work (as a two part, film preparation and their properties) for the preparation of samples, characterization process has been given in chapter-3.

Chapter-4 contains a systematic analysis of different structural, electrical and optical properties of the samples and also I-V characteristics of the CuO/CdS heterojunction. The interpretations and possible implications of the obtained results have been discussed in this chapter.

The conclusions of the present work and a few suggestions for future work have been given in chapter-5.

Relevant references or bibliography for the respective chapters have been given at the end of each chapter. At the end of the thesis a list of research publications made from the text of the thesis has been given.

Reference

1. W. R. Grove, Phil. Trans., Roy. Soc., London, 147 (1851) 345.
2. R. Bunsen, J. Prakt. Chen., 56 (1852) 53.
3. M. Faraday, Phil. Trans., Roy. Soc., London, 174 (1957) 145.
4. R. Nahrwold, Ann. Physik, 31 (1887) 487.
5. R. Kundt, Ann. Physik, 34, (1888) 473.
6. J. J. Thomson, Proc. Cambridge Phil. Soc., 11 (1901) 120.
7. K. Fuchs, Proc. Comb. Phil. Soc., 34 (1938) 100.
8. D. S. Cambell, "The Use of Thin Film in Physical Investigations, New York, Academic Press, 1966.
9. L. O. Grondahl, Rev. Mod. Phys., 5 (1933) 141.
10. W. L. Bragg, Phil. Mag., 28 (1914) 355.
11. F. Rinne, Ber. Sachs. Ges. Wiss., 67 (1915) 303.
12. W. P. Davey, Phys. Rev., (2) 18 (1921) 102.
13. A. Gruhn, Centr. Min., 85(1918).
14. J. F. Persos, Jour. Prak. Chem., (1) 47 (1849) 84.
15. F. Gaud, Compt. Rend., 119 (1894) 863.
16. S. Mayer, IB. (4), 1 (1900) 664.
17. K. Badeker, Ann. Physik, (4) 22 (1907) 749.
18. N. S. Maskelyne, B. A. Rep., 33 (1865).
19. E. Kalkowsky, Zeit. Krys., 3 (1879) 279.
20. G. Jenzsch, Prog. Ann., 107 (1861) 647.
21. J. A. Hedvell, Zeit. Amorg. Chem., 120 (1922) 327.
22. L. Wohler and A. Foss, Zeit., Elektrochem., 12 (1906) 784.
23. S. Mayer, Wied. Ann., 68 (1899) 32564.
24. P. G. F. Boully J. F. Persoz, Ann. Chim. Phys., (2) 43 (1830) 266.
25. F. Streints, Ann. Physik, (4) 9 (1902) 857.
26. A. E. Rakshani, "Solid-State Electron., 29 (1986) 7.
27. P. Luzeau, Z. Xu, M. Lagues, N. Hess, j. P. Coutor, M. Nanot, F. Queyroux, M. Touzeau and D. Pagnon, J. Vac. Sci. Technol. A, 8 (1990) 3938.
28. T. Tanakai, T. Ibarak, I. Saito, H. Sindo, M. Fujnaka, Thin Solid Films, 189 (1990) 9.

29. H. Maeda, Y. Tanako, M. Fukatomi, T. Asama, Jpn. J. Appl. Phys., 27 (1988) 209.

30. J. Herion, E. A. Niekish and G. Scharl, Sol. Energy Mater, 4 (1990)*

31. J. N. Shive, "Semiconductors Devices" D Van Nostrand, Princton (1959).

32. K. Hikita, M. Miyayama and H. Yanagiba, J. Am. Ceram. Soc., 78 (1995) 865.

33. M. Fujinaka and A. A. Berezin, J. Appl. Phys., 54 (1983) 3582.

34. H. Wieder and A. W. Czanderna, J. Phys. Chem., 66 (1962)

35. Cathcart, Petersen and Sparks, J. Electrochem. Soc., 116 (1969) 664.

36. K. Santra, C. K. Sarkar, M. K. Mukherjee and B. Ghosh, Thin Solid Films, 213 (1992) 226.

37. C. Ortiz, F. Vega and J. Solis, Thin Solid Films, 218 (1992) 182.

38. S. A. Nasser, H. H. Afify, S. A. El-Hahim and M. K. Zayed, Thin Solid Films, 315 (1998) 327.

39. W. DeSisto, B. T. Collins, R. Kershaw, K. Dwight and A. Woid, Mat. Res. Bull.,24 (1989)1005.

40. V. F. Drobney and D. L. Pulfry, Thin Solid Films, 61 (1972) 89.

41. A. Ross and B. Westerstrandh, Thin Solid Films, 90 (1982) 411.

42. N. Ozer and F. Tepehan, Sol. Energy Materials and Sol. Cells, 30 (1993) 13.

43. A. E. Rakhshani et al, Thin Solid Films, 148 (1987) 191.

44. B. Karlson et al, Physical Scripta, 25 (1982) 826.

45. J. P. Locquett, J. Less Common Mct. 164-165 (1990) 300.

46. K. Kawaguchi, R. Kita, M. Nishiyama and T. Mosishima, J. Cryst. Growth 143 (1994) 221.

47. K. P. Muthe, J. C. Vyas, Savita N. Narang, D. K. Aswal, S. K. Gupta, D. Bhattacharya, R. Pinto, G. P. Kothiyal and S. C. Sabharwal, Thin Solid Films, 324 (1998) 37.

48. S. R. Das, P. Nath, A. Banerjee and K. L. Chopra, Solid State Commun., 21 (1977) 49.

49. L. M. Fraas and Y. Ma, J. Crys. Growth, 39 (1977) 92.

50. B. M. Basol. V. K. Kapur and A. Halani, Conf. Rec. 22nd IEEE Photovoltaic Specialist Conf., Las Vegas, NV, 1991, IEEE, New York, 1991, p.893.

51. T. L. Chu, S. S. Chu, C. Ferekidel, C. Q. Wu, J. Britt and C. Wang, Conf. Rec. 22nd IEEE Photovoltaic Specialist Conf., Las Vegas, NV, 1991, IEEE, New York, 1991, p.952.

52. N. Miya, Jpn. J. Appl. Phys., 9 (1970) 768.

53. N. Romeo, G. Sberreglieri and L. Terricone, Thin Solid Films, 55 (1978) 413.

54. I. Kaur, D. K. Pandya and K. L. Chopra, J. Electrochem. Soc., 127 (1980) 9433.

55. M. Aricnzo and J. J. Loferski, in R. Van Overstraeten and W. palz (eds.), Proc. 2nd EC Photovoltaic Solar Energy Conf., Berlin, 1979, Dordrecht, Netherlands, 1979, p.361.

56. J. L. Shay, S. Wangner, K. Bachman, E. Buchler and H. Kaspor, Proc. 11th Photovoltaic Specialist Conf., Phoenix, AZ, 1975, IEEE, New York, 1975, p.503.

57. Moore et al., Proc. 1st DC Photovoltaic Solar Conf., Luxemburg, 1979, p.1278.

58. R. R. Chamberlain and H. S. Skarman, J. Electrochem. Soc., 113 (1966) 86.

59. B. K. Gupta and O. P. Agnihotri, Solid State Commu., 23 (1977) 295.

60. M. Muhibbullah, M. G. M. Choudhury and M. O. Hakim, The Nucleus, 37(1-2) (2000) 95.

61. B. F. Shirreffs, C. H. Cheng, K-Geib and K. A. Jones, J. Elec. Soc., "Solid State Science and Technology", 131(2), (1984) 441.

62. I. Martil, G. Gonzlez-Diaz and F. Sanchez, Thin Solid Films, 114 (1984) 327.

63. A. C. Pande, G. J. Russell and J. Woods, Thin Solid Films, 121 (1984) 85.

64. D. M. Uzagare, G. N. Bhandari and S. B. Tyyer, Thin Solid Films, 117 (1984) 233.

65. I. Jimenez, F. Decker and P. Salvador, Thin Solid Films, 127 (1985) 305.

66. M. Krunks, E. Mellikov and E. Sork, Thin Solid Films, 145 (1986) 105.

67. J. Ebothe, P. Chartier and H. Nguyen Cong, Thin Solid Films, 138, (1986) 1.

68. S. Achour and G. H. Talat, Thin Solid Films, 144 (1986) 1.

69. Pyare Lal, Thin Solid Films, 143 (1986) 217.

70. M. T. S. Nair, P. K. Nair and J. Campos, Thin Solid Films, 161 (1988) 21.

71. C. De Blasi, A. M. Mancini, D. Manno, L. Vasanelli, J. Crys. Growth, 101(1-4), (1990) 185.

72. C. Bovchenki, B. Ullrich and J. P. Zielinger, J. Crys. Growth (Netherland), 101(1-4) (1990) 797.

73. E. J. Esplnoza-Bltran and P. Halevi, Phys. Abs., no. 95264, Vol. 93, no. 1381 (1990).

74. K. S. Balakrishnan and A. C. Rastogi, Phys. Abs. no. 133872, Vol. 93, no. 1387 (1990).

75. A. Bennouna, E. L. Ameziane and A. Haouiro, Phys. Abs. no. 133776, Vol. 93, no.1367-1390 (1990).

76. A. Ashour, N. El-Kadry and S. A. Mahmoud, Thin Solid Films, 269 (1995) 117.

77. K. K. Nanda, S. N. Sarangi, S. Mohanty and S. N. Sahu, Thin Solid Films, 322 (1998) 21.

78. O. Trujillo, R. Moss, K. D. Vuong, D. H. Lee, R. Noble, D. Finnigan, S. Orloff, E. Tenpas, C. Park, J. Fagan and X. W. Wang, Thin Solid Films, 290-291 (1996) 13.

79. K. L. Chopra, "Thin Film Solar Cells", (Mc Grow Hill Book Co., New York, 1971) Sec. 3.2, P. 83.

80. E. Becquerel, Compt. Rend., 9 (1839) 561.

81. G. W. Adams and R. E. Day, Proc. Roy. Soc., A25 (1877) 113.

82. D. M. Chapin, C. S. Fuller and C. L. Pearson, J.Appl. Phys., 25 (1954) 676.

83. D. C. Reynolds, G. Leies, L. L. Antes and R. E. Marburger, Phys. Rev., 96 (1954) 533.

84. D. H. Smith, Comm. And Electron, 1959, p.530.

85. P. N. Uppal and L. C. Burton, J. Appl. Phys., 54(2) (1983) 982.

86. Y. Aparna, P. S. Reddy, B. Srinivasulu Naidu and P. Jayarama Reddy, Thin Solid Films, 236 (1993) 32.

87. J. Touskova, D. Kindl and J. Kovanda, Thin Solid Films, 214 (1992) 92.

88. Hyeong Soo Kim and Ho Bin Im, Thin Solid Films, 214 (1992) 207.

89. Hai-Ning Cui and Shi-Qu, Thin Solid Films, 288 (1996) 325.

CHAPTER TWO

THEORETICAL CONSIDERATIONS

THEORETICAL CONSIDERATIONS

Part 1 (Theoretical aspect and film growth processes in a chemical method)

2.1 Introduction

Fabrication of films by vacuum and non-vacuum techniques yield films of different nature but the basic principles of condensation and nucleation of the films from its vapour phase (in the initial film growth stage) are the same. Since chemical spray deposition method is a non-vacuum technique and can operate in open atmosphere, and to have a good quality film therefore a stern quality requirement is imposed on the films prepared by this method. Beside this, one should have a thorough knowledge of the principles that are associated with this method. In the first part of this chapter, a brief description of nucleation and film growth aspects is presented. The second part includes the methods of analysis of various properties of semiconducting thin films.

The thin films Cu_2O and CdS deposition techniques and their properties have been given in the literature. Brief accounts of these have been presented in this chapter.

2.2 Deposition techniques

1. Thermal or vacuum evaporation method
2. Sputtering method
3. Glow-discharge method
4. Epitaxial growth
5. Dip method
6. Chemical spray deposition method.

In this chapter some of the commonly used techniques are described briefly. But our aim is to prepare films in chemical (spray pyrolysis) method, so chemical method has been discussed in some details.

2.2.1 Thermal or vacuum evaporation method

The thermal evaporation is the simple, convenient and most widely used method for the preparation of thin films. In this method materials are vaporized by heating it to a sufficient high temperature and then condensation of the vapour on to a relatively cooler substrate yielding thin solid films.

Thermal evaporation may be performed directly or indirectly by variety of physical method. Several variants are (i) resistive heating (ii) exploding wire technique, (iii) flash evaporation, (iv) arc evaporation, (v) laser evaporation, (vi) R.F. heating and (vii) electron bombardment heating.

A simple arrangement of thermal evaporation chamber is shown in fig.2.1. The martial to be evaporated lies in a high melting point metallic boat, 'B' through which a heating current is passed and the evaporated martial is deposited on the substrate, S, attached to a heater H. This arrangement is located in a vacuum chamber and the chamber is pumped to a high vacuum, through V.

2.2.2 Sputtering

The ejection of atoms from the surface of a martial (target) by bombardment with energetic particles is called "sputtering[1]. If ejection is due to positive ion bombardment, it is referred to as 'cathode sputtering'. The ejected or sputtered atoms can be condensed on a substrate to form a thin film. The sputtering technique has been known since 1852[2] and exploited for deposition of films. Because of the high pressure of gas used and high sensitivity to contamination is commonly used glow discharge sputtering, the technique has generally been termed dirty. But improved technology and new variants of sputtering arrangements have now revived low-end high pressure sputtering as a versatile and powerful deposition technique for both research and production purposes.

A schematic illustration of an r.f. sputtering apparatus is shown in fig. 2.2. The r.f. field is applied between the target T, and the substrate, S, electrode. A sputtering gas, e.g., Ar is introduced into the chamber, a plasma, P, is struck. The gas is pumped away by a vacuum system, V. The substrate may be heated by an electricaly insulated heater, H.

Sputtering, particularly using r.f. fields can produce amorphous samples of most materials of interest, Si, Ge, SiO_2, chalcogenide glasses and amorphous metals. Sputtering is superior to evaporation for the production of multi component system.

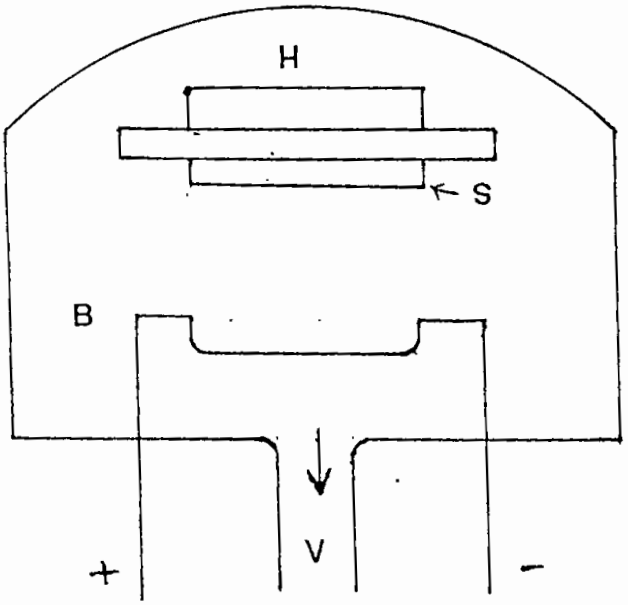

Fig. 2.1 Schematic diagram of thermal evaporation coating system.

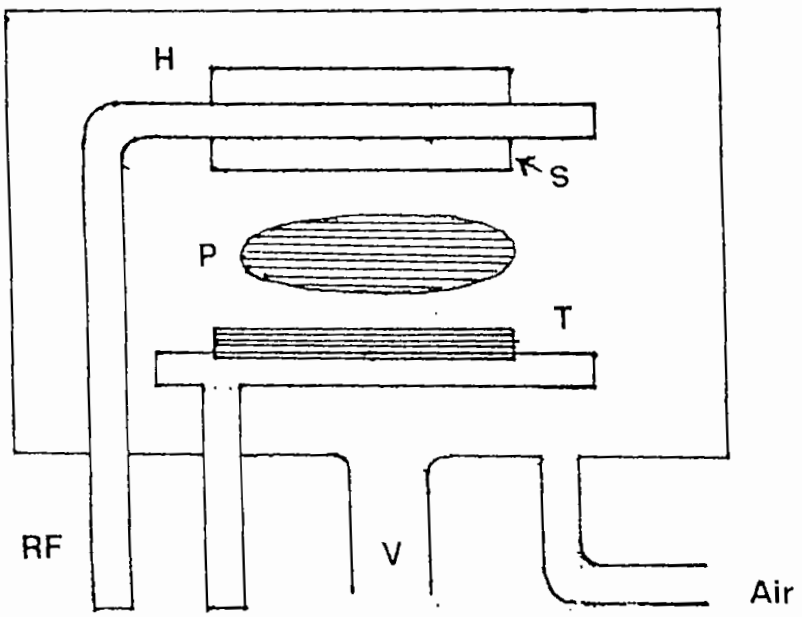

Fig. 2.2 Schematic diagram of a r. f. sputtering apparatus.

2.2.3 Epitaxial growth

Epitaxial or the oriented growth[3] of films on monocrystalline, substrate is a very interesting phenomena from a theoretical point of view and very important from a practical point of view. The evolution of these methods for the growth of very thin but very high quality epitaxial layers has resulted largely from the need for such layers of semiconductors and magnetic garnets.

The term epitaxy denotes formation of monocrystalline films usually on monocrystalline substrates either of the same substrate, when we speak of homoepitaxy or of other substrate, which we term heteroepitaxy. Formation of regularly oriented reaction layers growing upon a substrate by chemical reaction between the basic material and a substance which may be a gas, liquid or a solid is called chemoepitaxy. There is also special case of growth over an amorphous material or a liquid surface, which is, called rheotaxy. Oriented growth on amorphous specially shaped substrates is termed graphoepitaxy.

Studies of epitaxial phenomena deal mostly with the types:

(a). Metal on metal,

(b). Metal on alkali halide or mica,

(c). Alkali halide on alkali halide and

(d). Semiconductor on semiconductor.

The development of high speed, high frequency of to electronic devices as well as their integrated modulus and circuits shows the necessity and active layers. Epitaxial film of III-V compounds is grown by three techniques.

(a)Liquid phase Epitaxy (LPE)[4]

(b)Vapor phase Epitaxy (VEP)[5-7]

(c)Molecular beam Epitaxy (MBE)[8]

2.2.4. Dip technique

The dip technique[9] consists essentially of inserting the substrate into a solution containing hydrolystable metal compounds and pulling it out at a constant speed into an atmosphere containing water vapor. In this atmosphere hydrolysis and condensation process take place. Finally the films are hardened by a high temperature cycle.

2.2.5 Chemical method

Chemical-vapor-transport method for deposition of thin and thick coating have been developed from the early observations of Bunsen on chemical reduction of $FeCl_3$ by steam to produce Fe_2O_3. Chemical methods may be broadly classified in two categories:

(a)Electroplating[10-12]

(b)Chemical vapor deposition (CVD)[13-15]

Both have the widespread applications of major technical and commercial value. These techniques enable coating thickness to be varied from angstroms to fraction of a millimeter in a well-controlled fashion. Although the impurities and their effects vary with the material to be deposited, most refractory metals and several non-metals are obtained chemically in a purer form than by conventional metallurgical particles.

A brief description of the various chemical methods is given in the following sections.

2.2.5.1 Electro deposition

2.2.5.1a Electrolytic deposition

The first application of the principles of electrolysis to the deposition of metal films in the subject of controversy[16] but probably took place in 1938. According to the law of electrolysis, the weight of material deposited is proportional to the amount of electricity passed 1 gram mole equivalent of the material being deposited by the charge 96,490C. The metallic ions in the electrolyte migrate toward the cathode under the influence of the applied electric field, which ca be very high ($\sim 10^7$ v/cm) between the cathode surface and the ions in the double layer.

The experimental arrangement requires a suitable electrolyte through which current is passed between two electrodes. The deposition rate is proportion to the electrolysis time and the current density and may be varied over a wide range from about an angstrom to several microns per second. The rates vary markedly on the geometry of the cathode, the temperature and the agitation of electrolyte.

2.2.5.1b Electrolysis deposition

Electrolytic action may be achieved without an external potential source by a chemical-reduction process such as that used in the well-known technique of

silvering glass dewars. This technique, called 'electrode less deposition[11] has been employed to deposit Ni Co and Pb films by deduction of their chlorides by sodium hypophosphite. For non-metallic surfaces it may be necessary to use a sensitizer such as 0.1 percent stannous chlorides. The rate of film growth in this method depends greatly on the reaction temperature and is generally difficult to control.

2.2.5.1c Anodic oxidation

A large number of metals (called 'valve' metals) tend to form a protective oxide film of limited thickness. The anodization process involves the migration of ions of oxygen, metal, or both depending on the material, through the existing oxide film. The details of the ion-transport process, however, are still a subject of some debate[13]. Growth rate of an anodic film depends on the current density and the temperature of the electrolyte.

Anodic oxidation has been extensively utilized in producing ultra thin and thick oxide films for tunnel devices, capacitors, protective layers, etc. A serious disadvantage of anodization in aqueous solution is that it results, in some cases in the incorporation of water and OH ions into the films producing deleterious effects on their dielectric behavior[17].

2.2.5.2 Chemical vapour deposition (CVD)

When a volatile compound of the substance to be deposited is vaporized and the vapour is thermally decomposed or reacted with other gases, vapours, or liquid at the substrate to yield nonvolatile reaction products which deposited optimistically (atom by atom) on the substrate the process is called chemical vapour deposition[14,15]. Since a large variety of chemical reactions are available, CVD is versatile and flexible technique in producing deposit of pure metal, semiconductor and insulators. A very significant application of the CVD processes is the preparation of single crystal metal oxides, notably the ferrites, garnets sapphire MnO etc.

Several types of reactions are classified under the CVD heading[18]. We shall present representative examples to illustrate each type.

2.2.5.2a Hydrogen reduction

Hydrogen reduction may be thought of as a pyrolysis reaction, which is facilitated by the removal of one or more of the gaseous products of decomposition. The reaction temperature is lowered by several hundred degrees below that needed

in the absence of hydrogen. Hydrogen reduction of metal halides is frequently used for depositing metal films. Hydrogen may also be used in other types of deposition reactions such as pyrolysis of organometallic compounds where reduction is not the primary objective but improves the deposit characteristics.

2.2.5.2b Halide disproportion

The basis of this process is the control of the equilibrium that exists between Si (or Ge), the tetraiodide, and the diiodide. At 1100°C, SiI_4 attacks the source Si to put SiI_2 into the vapour phase. At 900°C, the reverse reaction takes place, resulting in the deposition of the epitaxial Si on the substrate by disproportionation of the SiI_2 vapors. Both open-tube[19] (dynamic) and closed-tube[20] (static) system have been used. The former in not studied for a controlled equilibrium process, and the latter makes it difficult to clean the substrate.

2.2.5.2c Polymerization

The polymerization process probably results in the loss of hydrogen or dislocation by breaking the carbon chain in a hydrocarbon. The process can also be accomplished by a high temperature electron bombardment, or exposure to ionizing radiation, e.g., ultraviolet light in which case it is called a 'photolytic process'. Several workers have used electron beam bombardment to produce and to study properties of polymer films of DC 704 pump fluid, siloxanes[21-23], styrene[24] and related monomers, and butadyne[25]. White[26] studied polymer films of vapours of butadiene styrene, acrylontrile, and methyl isopropenyle ketone by electron bombardment as well as by photolytic process and found them to be essentially similar for both preparation techniques.

2.2.6 Spray pyrolysis

The thermal decomposition of a compound to yield a deposit of the stable residue is called pyrolysis. Schematic diagram of spray pyrolysis technique is shown in figgure 3.1. Spray pyrolysis, which is the main concern of this work, involves spraying of solution usually aqueous, contained soluble salts of the constituent atoms of the desired compounds on the heated substrates.

It is already known that the process of spray deposition is one of the simplest and least expensive one of all the film deposition methods available to date. Because of this extreme simplicity one has to face a number of difficulties in controlling the process variables. Moreover the qualities of the deposited films are

relatively inferior to those films obtained in other complex methods. It is needed to improve the process of deposition and to reduce the cost of production, since for solar cell and other device technology the low cast production of semiconducting thin films has become a necessary precondition.

2.3 General considerations of spray pyrolysis technique

To form a qualitative as well as quantitative background of the method one has to know the chemistry, the thermodynamics and possible chemical kinetics of the method. Relative usefulness of these studies is briefly described below.

2.3.1 Chemistry of pyrolytic deposition

Chemical pyrolysis method can be defined as a material synthesis, in which the constituents of the vapor phase react to form a solid film at some surface thus, the occurrence of the chemical reaction is an essential characteristic of the pyrolysis method.

To understand the process, one must know which chemical reactions occur in the reactor and to what extent. Furthermore, the effects of process variables such as temperature, pressure, input concentrations and flow rates on these reactions must be understood. The nature and extent of chemical reactions can be deduced, if one knows the composition of solid and vapor phases in pyrolysis system. The composition of the solid product can be analyzed after the deposition but that of the vapour phase must be determined in situ at the particular reaction condition, otherwise high temperature species may disappear or change on cooling to room temperature. Several experimental methods are employed for this purpose such as mass spectrometry, Raman spectroscopy, absorption spectroscopy, gas chromatoghraphy etc.

2.3.1.1 Chemical reaction

There are several types of chemical reactions which may take part in the film formation process in a chemical method, e.g.,(1) Pyrolysis, (2) Hydrolysis, (3) Oxidation, (4) Reduction, (5) Synthesis reaction, (6) Disproportionation, (7) Carbide and Nitride formation, (8) Combined reaction etc. Among these various types of reactions the first four types are very important and have roles in spray pyrolysis method.

Pyrolysis is the process of chemical decomposition of a substance by the reaction of heat and hydrolysis is the chemical decomposition caused by the action of water. In hydrolysis reaction water itself also decomposes. We are presently interested with these two types of reactions for the preparation of CuO and CdS films. The formation reactions are given in the below:

(a) For CuO

It consists essentially of reducing or decomposing a solution upon a heated substrate. For the practical employment of this method the solution must be easily decomposed or converted into stable reaction product. This method has some similarity to the chemical bath deposition method[27,28]. However, the process is unique from the start point that all of the necessary elements are contained in the solution, which is being sprayed.

CuO films are formed by spray pyrolysis of $CuCl_2$ solution on to heated surfaces. Best results are obtained with the substrate temperature above 150°C. Following reaction takes places during deposition

$$CuCl_2 + H_2O = CuO\downarrow + 2HCl\uparrow \quad .....(2.1)$$

The technique is very simple and is adaptable for production of large area coating for industrial applications.

(b) For CdS

The starting materials generally used to prepare CdS were an equimolecular ionic solution of $CdCl_2$ 0.1M, 0.1M dimethyl thiourea[29]. This solution was sprayed over a heated substrate around 150 to 350°C with an optimum spray rate fixed up in between .5 ml/min. to 2 ml/min., depending of course on the nature of the material required.

The formation of the thin film layer of CdS over the heated substrate was assumed[30] to be formed by decomposition of intermediate complex ion $CdCl_2$, SCN_2H_4, formed in the solution, according to the basic reaction,

$$CdCl_2 + SC(NH_2)_2 + 2H_2O = CdS + 2NH_4Cl + CO_2 \quad .....(2.2)$$

A various starting materials involved in the spray technique along with the influences of various spraying parameters like substrate temperature carrier gas

flow, spraying rate and of the chemical reactions involved in the decomposition of the complex $CdCl_2(SCN_2H_4)$ has been reported by Tomar and Gracia[30].

In latter reports, however, the authors demonstrated that an intermediate reaction path was involved to form the final product. As seen in the reaction, an aqueous solution of cadmium chloride and a sulpho-organic compound is sprayed onto a heated substrate.

2.3.1.2 Spray pyrolysis reactor systems

General requirements:

A reactor system for depositing thin film materials must provide equipment that accomplishes the following function.

1. Transport and reactant gases entering the reactor;
2. provide heat to the site of reaction, namely, the substrate material being coated, and control this temperature,
3. Remove the by-product exhaust gas from the deposition zone and safely dispose of them.

The reactor should be designed to fulfil these three primary functions with maximum effectiveness and simplicity of construction. It must consistently yield films of high quality, good thickness and compositional uniformity from run to run and high purity with a minimum of structural imperfect ions such as pinholes, cracks, and particular contaminants.

2.3.1.3 Transport phenomena in pyrolytic deposition

There are two basic reasons for studying transport phenomena:

The requirement of thickness and semiconductor doping uniformity which can be fulfilled only when equal amounts of reactant gases and dopants are delivered to all substrates in the system.

The requirements of high chemical efficiency to achieve satisfactory growth rates and utilization of input chemicals; this means that sufficient amount of reactants must be delivered to growth surfaces.

Transport phenomena in fluids (i.e., gases and liquids) are related to the nature of the fluid flow. The following parameters affect the nature of gas flow in reactors:

1. velocity of flow,

2. temperature and temperature distribution in the system,
3. pressure in the system,
4. geometry of the system,
5. gas or vapor characteristics.

For two basic reasons the study of transport phenomena is important.

(1) The requirement of thickness and semiconducting doping uniformity which can be fulfilled only when equal amounts of the reactant gases and dopants are delivered to all the substrates in the system.

(2) The requirement of high chemical efficiency to achieve satisfactory growth rates and utilization of input chemicals; this means that sufficient amount of reactants must be delivered to the film growth surfaces.

All the above points should be brought under consideration at the time of designing the reactor.

2.3.2 Thermodynamics of pyrolytic deposition

The main function of thermodynamics in relation to pyrolytic technique is to predict the feasibility of the process under some specified conditions and to provide quantitative information about the process. Properly performed thermodynamic calculations give the theoretically obtainable amount of a deposit and partial pressures of all species under specified experimental conditions, such as the temperature and pressure in the reactor and the input concentrations of the reactants.

Thus, thermodynamics can be used as guide line for establishing general process parameters. One of the first steps in considering a pyrolytic deposition process is to perform the necessary thermodynamic calculations to obtain the general conditions the process requires. In order to perform the calculations, one needs reliable thermodynamic data. The most useful data are free energy of formation of all vapour and condensed constituents of the system:

If $G°_f$ is the standard free energy of formation of a compound and

$\Delta G°_f = 0$ for all elements in their standard state.

The free energy of some chemical reaction ($\Delta G°_f$) can be calculated if the $\Delta G°_f$ values is known [31]

$$\Delta G°_f = \Sigma \Delta G°_f \text{ products} - \Sigma \Delta G°_f \text{ reactants} \quad \ldots\ldots\ldots\ldots\ldots (2.3)$$

In pyrolytic deposition, one usually deals with multi component and multiphase system. Most often, there are only two phases, the vapor and the solid; although more than one condensed phase may be present. There are several ways, to calculate thermodynamic equilibrium in multi component system. One of the most important methods is the optimization method.

2.2.3 Optimization method

Let us suppose a system in which a chemical reaction proceeds to some degree of completion. This is denoted by ε:

(1-ε) (reactants) → ε (products) ..... (2.4)

If one plots the free energy of the system versus ε, one sees that the energy curve has a minimum at some value of ε. This value of ε, is the equilibrium concentrations of reactants and products.

2.3.4 Kinetics of pyrolytic deposition

The situation in spray pyrolysis reactors might differ from the prediction of thermo-dynamical equilibrium calculations. The deposition reaction is almost always a heterogeneous reaction. The sequence of events in the usual heterogeneous processes can be described as follows:

1. diffusion of reactants to the surface;
2. absorption of reactants at the surface;
3. surface events, such as chemical reaction, surface motion, lattice incorporation, etc.;
4. deposition of products from the surface;
5. diffusion of products away from the surface.

The application of kinetics in film deposition process has been exemplified by Eversteijn [32]

Some of the factors that cause deviation from equilibrium are:

a. Temperature dependence of deposition rate:

For a given substrate the nature of the rates controlling step, changes with temperature. The rate controlling steps is (a) absorption of reactants on the substrate surface; (b) diffusions of reactants and products to and from the reacting surface respectively.

b. Dependence of the deposition rate on substrate orientation:

The deposition rate can strongly depend on the crystallographic orientation of the substrate[33]. There are several fundamental reasons for the variation of deposition rate with substrate crystallographic orientation, among them is variations in

(i) The densities and geometric arrangements of surface sites;

(ii)The number and nature of surface bonds;

(iii)The number of nature of surface features, such as steps, kinks, ledge vacancies, etc.

All of these factors can influence deposition by affecting adsorption, deposition, surface mobility, reactivity, etc.

Several other kinetic effects in pyrolytic deposition have been observed, e.g., the effect of dopants on the semiconductor growth rate[34,35] and the existence of metastable phases. It is important to keep in mind that while thermodynamics specifies what ought to happen in the reactor, the kinetics determines what actually will happen.

2.4 Film growth aspects

The properties of thin film depend very much on their structure. So it is important to know the factors that govern the structure of the film. A brief discussion about the nucleation and formation of polycrystalline and amorphous thin films has been given in the following section.

2.4.1 Condensation

Generally thin films are prepared by depositing the film material, atom by atom, on a substrates. The best understood process of film formation is that by condensation from the vapour phase. Condensation simply means the transformation of a gas into a liquid or solid. Thermodynamically, the only requirement for condensation to occur is that the partial pressure of the film material in the gas phase be equal to or larger than its vapour pressure in the condensed phase at that temperature [36].

However, this is true only if condensation takes place on film material already condensed or on a substrate made of the same material. In general the substrate will have a chemical nature different from that of the film material. Under these conditions still a third phase must be considered namely the adsorbed phase in which vapour atoms are adsorbed on the substrate but have not yet combined with other adsorbed atoms.

Condensation is initiated by the formation of small clusters through combination of several adsorbed atoms. These clusters are called nuclei and the process of cluster formation is called nucleation. Since small particles display a higher vapour pressure than the bulk material under the same conditions, a super saturation ratio larger than unity is required for nucleation to occur. The process of enlargement of the nuclei to form finally a coherent film is termed growth.

The modern theory of nucleation is based upon the atomostic nucleation concept [32], which states that not all surfaces have equal bonding characteristics. Those with strong bonds are particularly favourable nucleation sites. Again, after nuclei reach a certain size it became energetically more favourable for them to grow than to re-evaporate. The growing nuclei come into contact and finally coalesce to form continuous film.

The sequences of the nucleation and growth steps to form a continuous film as revealed by an electron microscopic observation [37,38] are;

(a) The island stage

When a substrate under impingement of condensate monomers is observed, the first evidence of condensation is a sudden burst of nuclei of uniform size. Growth of nuclei is three-dimensional. These nuclei then grow to form islands, whose shapes are determined by interfacial energies and deposition conditions.

The growth is diffusion controlled, that adatoms and subcritical clusters diffuse over the substrate surface and are captured by the stable islands.

(b) The coalescence stage

In a given distribution of immobile nuclei, the separation between neighbours is continuously decreased by their growth, when contact occurs the nuclei are said to have coalesced. The coalescence occurs in less than 0.1 sec. The character of coalescence is liquid like and enlargement of the islands occurs covering larger areas of the substrate.

(c) The channel stage

When larger islands grow together they leave channels of interconnected holes of exposed substrate in the form of a network structure on the substrate. As deposition continues, secondary nucleation occurs in these channels and forms the last stage of the nucleation viz.

(d)The continuous film:

Which then become thicker as the time passes.

2.4.2 Polycrystalline and amorphous thin films

The films deposited by spray pyrolysis are generally polycrystalline or amorphous in structure. Lower temperature and higher gas phase concentration are actually favourable in forming polycrystalline film. In these situation the rate of arrival of the aerosol (spray particles) at the surface is high, but the surface mobility of adsorbed atoms is low. A large number of differently oriented nuclei are formed, after coalesce between them the films that are obtained possess grains of different orientation. Further decrease in temperature and increase in super saturation result in even more nuclei and consequently in finer grained films. When crystallization is completely stopped formation of amorphous film is favoured.

2.4.3 Incorporation of defects during growth

When the islands during the initial stages of thin film growth are still quite small, they are observed to be perfect single crystal [38]. However, as soon as the islands become large enough so that they touch, grain boundaries or lattice defects will be incorporated into the film, unless the islands coalesce to form a single grain. A large number of defects are incorporated in the film during their re-crystallization process at the early stage of film formation. The defects that are usually encountered in spray deposited films are lattice vacancies, stoichiometric excess and grain boundary. Another type of defect namely surface roughness which stems from the quality of the sprayer is especially important in the use of spray deposited films. The properties of the film are strongly affected due to surface roughness if the thickness of film is small. The most frequently encountered defects in evaporated films are dislocations, which are less important in chemical spray, deposited films.

2.4.4 Grain boundaries

In polycrystalline thin film, the grain size and the boundary regions markedly depend on the deposition variables such as (i) film thickness, (ii) substrate temperature, (iii) annealing temperature and (iv) the deposition rate. Thus the number of such boundaries are controllable parameters.

The variation of crystallite size with the parameters mentioned above are shown schematically [39] in figure 2.3. From this figure the dependence of grain size on film thickness is that the larger grains are expected as the new grains are nucleated on the top of the old ones after a certain film thickness has been reached. Another possibility of getting larger grain size are expected for increasing substrate or annealing temperature because of an increase in surface mobility. Thus

allowance is made to the film to decrease its total energy by growing large grains and thereby decreasing its grain-boundary area. Annealing at temperatures higher than the deposition temperature increases the grain size, but the growth effect is significantly different from that obtained by using the same temperature during deposition[40]. The dependence of grain size on deposition rate is less obvious but can be understood on the basis that film atoms just impinged on the surface, although they may possess a large surface mobility, become buried under subsequent layers, at high deposition rates, before much diffusion can take place[39]. In order for this effect to operate, however, a certain minimum rate must be expected. Rather than this threshold rate, grain size is limited by temperature alone and above it the grain size is decreased more and more for higher and higher rate.

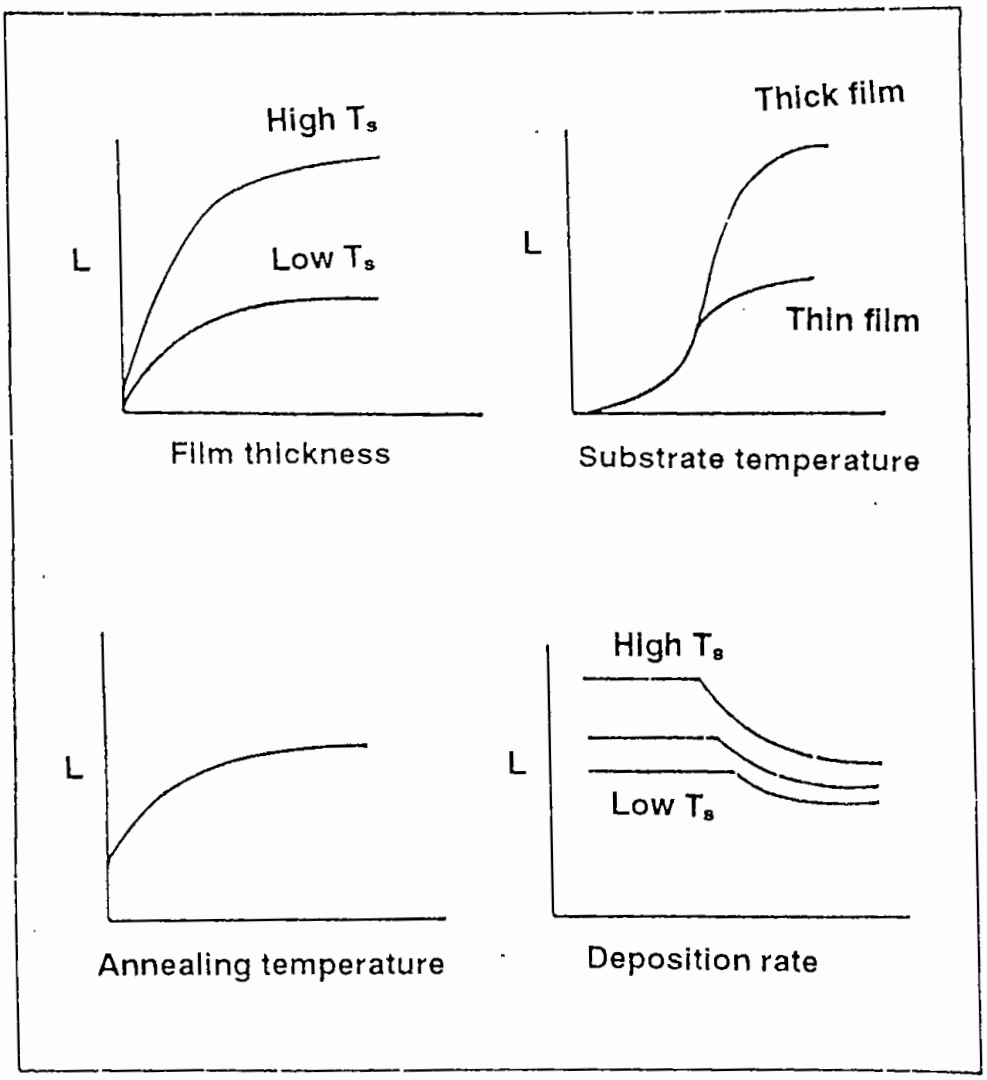

Fig. 2.3 Dependence of grain size L on film thickness, substrate temperature T_s, annealing temperature and deposition rate

Part II (Analytical methods for the study of film properties)

2.5 Introduction

Statistical methods are generally employed for analyzing the structural, electrical and optical properties of semi conducting materials. Undoped CuO and CdS thin films deposited with spray pyrolysis are found in both the non-degenerate and degenerate condition. Therefore, in this part of the chapter different theoretical principles of the various analytical methods on the properties of semi conducting materials have been briefly discussed with both non-degenerate and degenerate models.

2.6 Degenerate and non-degenerate semiconductor

Fermi level in most of the semi conductor lies in about $2K_BT$ below the bottom of the conduction band edge. In that case the electrons in conduction band follow closely Boltzmann statistics, and the electron gas is said to be non-degenerate. In some cases of an n-type semi conductor, when the Fermi level enters into the conduction band or goes close to the band edge from the mid gap the electron gas may become degenerate. The conditions that are in favour of such a situation are-

i) Relatively high donor density ($\sim 10^{19}$ cm^{-3}) for n-type material.

ii) Small donor ionization energy and

iii) Low density of states near the bottom of the conduction band i.e. small effective mass of the electrons.

Under these conditions all the statistical calculations should be performed by using the Fermi-Dirac statistics.

When the temperature increases from absolute Zero, the donors begin to ionize and the lower energy states in the bottom of the conduction band become completely occupied due to its low density of states. The position of the Fermi level relative to the bottom of the conduction band is then given by [41]

$$E_F = \frac{h^2}{8m_e^*}\left(\frac{3n}{\pi}\right)^{\frac{2}{3}} \quad \text{.....(2.5)}$$

Where n is the density of electrons in the conduction band. If $E_F >> K_BT$, the electron gas is degenerate. It is observed that degeneracy may occur at electron concentrations ($\sim 10^{18}$ cm^{-3}) with the reduced electron effective mass m_e^*. As the

temperature is increased further the degeneracy may be removed and Fermi levels enters the forbidden gap again. The approximate conduction for degeneracy is that the Fermi level be no lower than K_BT (at T=300 K) below the conduction band-edge and the temperature T_{deg} at which this condition is satisfied can be obtained from equation (2.5)

$$T_{\deg} = \frac{h^2}{8K_B m_e^*}\left(\frac{3n_{\deg}}{\pi}\right)^{\frac{3}{2}} \quad \text{.....(2.6)}$$

Where T_{deg} is the temperature at which degeneracy starts and is termed as degeneracy temperature and n_{deg}, the carrier concentration at T_{deg} is called degeneracy concentration (Concentration for the onset of degeneracy). This concentration is the demarkation line between degenerate and non-degenerate semiconductors.

2.7 The hall constant, electrical conductivity and mobility

When a magnetic field is applied at right angle to the direction of current in a conductor, Hall effect is produced as shown in figure 2.4. In presence of a magnetic field, a magnetic force eB acts on the electrons having on average velocity v due to the current I. The force acts in the direction perpendicular to both B and v causes the electrons to deflect (for n-type materials) toward the surface of one side of the conductor. As a result of this an additional electric field E_H is produced. Under equilibrium condition, the sideways force on the moving carriers due to this field just balance that arising from the magnetic field.

The magnitude of the transverse Hall field E_H, is found by equating the sideways forces.

$eE_H = ev\,B$ ..... (2.7)

Expressing v in terms of current density J and the conduction electron density n from the relation J = nev, we have E_H,

$$E_H = \left(\frac{JB}{ne}\right) = B_H JB \quad \text{.....(2.8)}$$

Where the Hall constant

$$R_H = \frac{1}{ne} \quad \text{.....(2.9)}$$

gives the carrier concentration directly. The experimental observed quantity is the Hall voltage V_H, which is obtained form the equation (2.8) since

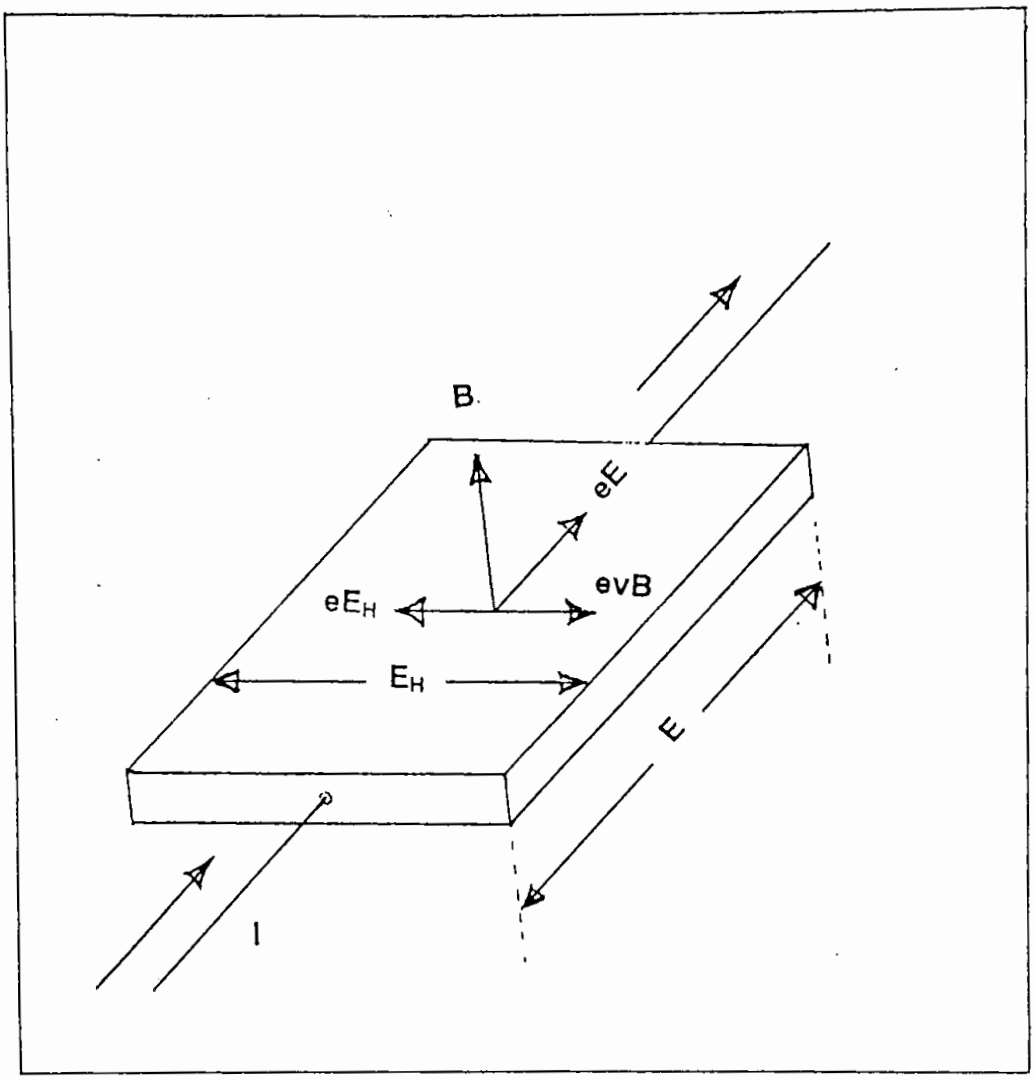

Fig. 2.4 The forces acting on a current carrier in a conductor placed in a magnetic field leading to the observable Hall field E_H.

$E_H = V_H/W$, and $J = I/wt$

Where w is the sample width and t is thickness. Therefore equation (2.8) becomes

$$R_H = \frac{1}{ne} = \frac{V_H t}{IB} \quad \text{.....(2.10)}$$

In equation (2.10), e is the magnitude of electronic charge and the algebraic sign of the Hall voltage indicates whether the carries are holes or electrons. This treatment of Hall effect is very simple and is applied for specimens with a constant energy surface. But a more regroups treatment for multivally semiconductors with ellipsoidal constant energy surfaces leads to the expression for the Hall constant [42]

$$R_H = \frac{r}{ne} \cdot \frac{3K(K+2)}{(2K+1)^2} \quad \text{.....(2.11)}$$

Where r is a constant equal to 1 for degenerate semi conductors and K is the ratio of the longitudinal to transverse effective masses of the carriers.

When the charge carrier is moving in an electric field E with the average velocity V then the Hall mobility μ is defined as the velocity of electrons per unit electric field, i.e.

$$\mu = \frac{V}{E} \quad \text{.....(2.12)}$$

combining this with Ohm's law σ = J/E, using J = nev, the expression for conductivity is –

$\sigma = ne\mu$

or $\mu = R_H\sigma$ ..... (2.13)

Due to thermal energies the electrons and holes in a semiconductor are set to rapid random motion and collide among themselves. If τ is the average time between such collisions then the rate of change of velocity is $-v/\tau$. In steady state condition this rate of change must be equal to the acceleration due to the field $-eE/m^*$. Therefore

$eE/m^* = v/\tau = \mu E/\tau$

$$or, \mu = \frac{e\tau}{m^*} \qquad and, \sigma = \frac{ne^2\tau}{m^*} \quad \text{.....(2.14)}$$

In this expression τ has been assumed to be free from the electron's velocity v for simplicity.

For semiconductor with spherical constant energy surface it has been found that over a considerable range of energies[43]

$$\tau = aE^{-r} \quad \text{.....(2.15)}$$

where r is a constant and may vary with temperature. The value of r is generally derived from the observed variation of mobility with temperature and is dependent on the scattering processes, So it is a fundamental problem in semiconductor physics to determine the exact nature of the dependence of τ on energy of the electrons.

2.8. Variation of carrier concentration with temperature

The variation of electron concentration n or hole concentration p with temperature in extrinsic semiconductor has been considered in the following manner. We suppose that the donor centers are partially ionized so that $n<N_D$(or $p < N_A$) Where N_D s the donor density. In the case of n-type material, ($N_D>N_A$), the rate of loss of electrons from donor centres to the conductor band is proportional to the number of filled donors $[N_D-(N_A+n)]$ and to the number of empty conduction bands states N_C thus it is given by

$K_1N_C(N_D- N_A-n)$

Where K_1 is a constant of proportionality. The rate of return of electrons to the donors is proportional to the number of electrons in the conduction band n and to the number of empty donor states, (N_A+n) each of which must be counted twice, however, as there are two possible ways for the electron to enter it (spin up or spin down). This rate, is

$K_2n\ [2\ (n+N_A)]$

At equilibrium these ratios are equal, so that

$$\frac{n[2(n+N_A)]}{N_C(N_D-N_A-n)} = \frac{K_1}{K_2} = K \quad \text{.....(2.16)}$$

Where K is the equilibrium constant, a function only of temperature. In the classical approximation it is given by

$$K = \exp\left(-\frac{E_C - E_D}{K_B T}\right)$$

Where (E_C-E_D) is the donor ionization energy, E_C is the conduction band edge and

$$N_C = 2\left(\frac{2\pi m_e^* K_B T}{h^2}\right)^{\frac{3}{2}}$$

is the effective density of states. For degenerate case, N_C given by

$$N_C = \frac{4\pi}{h^3}\left(2m_e^* K_B T\right)^{\frac{3}{2}}$$

considering the approximation to equation (2.16). If $n << N_A$, (2.16) reduces to

$$n = \frac{N_D - N_A}{N_A} \cdot \frac{N_C}{2} \exp\left(\frac{-(E_C - E_D)}{K_B T}\right) \quad \text{.....(2.17)}$$

In a second approximation to (2.16) when $n >> N_A$ (2.16) reduces to

$$\frac{2n^2}{N_C N_D} = \exp\left(\frac{-(E_C - E_D)}{K_B T}\right)$$

$$or, n = \left(\frac{N_C}{2N_D}\right)^{\frac{1}{2}} \exp\left(\frac{-(E_C - E_D)}{2K_B T}\right) \quad \text{.....(2.18)}$$

The pre-exponential term of equation (2.18) slightly depends on temperature and is usually neglected. Equation (2.17) and (2.18) operate so long as the sample is extrinsic and remain outside the saturation or exhaustion range. In the exhaustion

region, the supply of electrons to the conduction band is stopped because all the donor atoms are completely ionized and the electron concentration remains, approximately constant with the temperature. In that case the concentration where the (n vs. T) plot is horizontal equals the donor concentration N_D.

2.9 Annealing effect

Annealing is a process by which crystals of varying composition may be homogenized i.e. heating to a sufficient high temperature for sufficient length of time to allow diffusion to occur followed by a slow cooling procedure.

A theory of resistivity changes associated with the annealing of defects specifically aimed for films has been presented by Vand[44]. In general resistivity of the film decreases on annealing. In certain instances, however, heat treatment may lead to an increase in resistivity because of the effect of the oxidation and for agglomeration. Unless a great deal of special care is taken during their deposition, films will in general contain a lot of structural defects.

2.10 The activation energy

The activation energy which is related to the electron transport process can be expressed by a conventional Arrhenius type relation -

$$\sigma = \sigma_o \exp\frac{-E_a}{K_B T} \quad \text{.....(2.19)}$$

Where, E_a is the activation energy and σ is the electrical conductivity. For semi conductors the following two distinct cases may arise.

Case - I

For intrinsic semiconductor

The carrier concentration for n-type conductivity in intrinsic semi conductor is expressed as

$$n = (N_V N_C)^{\frac{1}{2}} \exp\left(\frac{-E_g}{2K_B T}\right) \quad \text{.....(2.20)}$$

Where, N_v and N_C are the carrier concentration in the valence and conduction bands respectively, and E_g is the band gap. At constant mobility, σ is directly proportional to the carrier concentration, n

$\sigma = ne\mu$

So the activation energy can be obtained by comparing equation (2.19) and (3.18ii) and is given by

$E_a = E_g/2$ = half the band gap ..... (2.21)

Case II

For Extrinsic Semiconductor

Extrinsic semiconductor contains impurity atoms which create an additional impurity or trap level in the regular band gap. In this case, the activation energy can be obtained by comparing equation (2.17) and equation (2.18) with the equation (2.19). Two cases may arise -

(a) For Uncompensated Semiconductor

In this situation $N_D > n >> N_A$ and the activation energy is obtained from equation (2.18)

$E_a = (E_C - E_D)/2$ = half the trap depth ..... (2.22)

(b) For partly compensated semiconductor

In this case $n << N_A < N_D$ and the activation energy is

$E_a = (E_C - E_D)$ = the trap depth

(c) For compensated semiconductor

In this regime the activation energy is compared with half the band gap because the semiconductors behave like intrinsic material.

Depending on the temperature a sample of one category may change to other one. An intrinsic conduction may set in an extrinsic sample when its temperature is high enough. It is clear from the above discussion that great care should be taken in the study of the activation energy determination for semiconductor sample.

2.11 Thomson coefficient and thermoelectric power

It has been seen that even in the absence of current, there must be an electric field if a temperature gradient is present in conductor. This indicates the elementary concept of thermoelectric effect in conductors. Phenomenologycally one may define the Thomson coefficient as the coefficient of proportionality relating the electric field and the temperature gradient as follows:

$$E_X = T_h\left(\frac{\delta T}{\delta X}\right) \quad \text{.....(2.23)}$$

Practically, this effect arises as a result of increased energy of electrons at the hot end of the material causing a diffusion of electrons towards the cold end; the charge imbalance due to diffusion sets up an electric field (Seebeck back e.m.f) in the material and this field strongly opposes further flow of charge in this direction. A quantity commonly used to describe the effect is thermoelectric power Q_{ab}. This refers to two materials denoted by 'a' and 'b'. If the junctions are at temperature T_2 and T_1, the material is being open at a point which is assumed to be at temperature T_o, then the open circuit voltage V_0 at that point is given by

$$V_o = \int_{T_1}^{T_2} Q_{ab}(T)dT$$

If $T_2 = T_1 + \Delta T$, When ΔT is small, we have

$V_0 = Q_{ab}\,\Delta T$

$$or, Q_{ab} = \frac{V_o}{\Delta T} \quad \text{.....(2.24)}$$

Where Q_{ab} is the thermoelectric power of the material "a" with respect to material 'b' and indicates specific thermoelectric power.

2.11.1 Absolute thermoelectric power

If T_h (a), T_h (b) are the thomson coefficients for the two materials then from thermodynamical argument [44] we have

$$T_h(a) - T_h(b) = T\frac{dQ_{ab}}{dT} \quad \text{.....2.25}$$

If we choose the material b as one for which T_h (b) =0 (usually lead, Pb) the thermoelectric power relative to this material we write $Q_{ab} = Q_a$, then Q_a is sometimes called the absolute thermoelectric power. In this case we have

$$T_h(a) = T\frac{dQ_a}{dT} \quad \text{.....(2.26)}$$

2.11.2 Degenerate case

When the semiconductor is extrinsic and degenerate then the situation is more complex and the formula for Q may be given by[45]

$$Q_{(n,p)} = \pm\frac{K_B}{e}\left\{\frac{(r+2)}{(r+1)}\left[\frac{F_{r+1}(\eta^*)}{F_r(\eta^*)}\right] - \eta^*\right\} \quad \text{.....(2.27)}$$

Where $\eta^* = E_F/K_BT$ .....(2.28)

is the reduced Fermi energy, and

$$F_r(\eta^*) = \int_0^\infty x^r \left\{\frac{1}{1+\exp(x-\eta^*)}\right\}dx \quad \text{.....(2.29)}$$

is the Fermi integral [46,47]. Here r = 0 for lattice phonon scattering and r = 2 for ionized impurity scattering.

2.11.3 The position of the Fermi level

For a p-type nondegenerate semiconductor with spherical constant energy surface under thermal equilibrium the thermoelectric power, Q, is given by[42] .

$$Q = \frac{K}{e}\left[\left(\frac{5}{2} - S\right) - \frac{E_{F'}}{KT}\right] \quad \text{.....(2.30)}$$

where E_F' is the Fermi energy for the holes with reference to the valence band edge,E_V , and is expressed by

$$E_F' = -\,(E_g + E_F) \quad \text{... ... ... (2.31)}$$

Here E_F is the conventional Fermi energy measured with reference to the conduction band edge E_C , and E_g is the optical band gap. The carrier scattering index , s , is related to the relaxation time and energy as $\tau = a E^{-s}$. In the absence of any detailed knowledge of the temperature dependence of E_g we may put for a limited temperature range

$$E_F' = E(0) - \gamma T \quad \text{... ... ... (2.32)}$$

where E(0) is the low temperature limit of E_F' and is the chemical potential. It is often interpreted as the half of the band gap but is not always true. γ is the appropriate temperature coefficient [48] . Using equation (4), and A =(5/2 – s), equation(2) can be written as

$$Q = \frac{(AK + \gamma)}{e} - \frac{E(0)}{Te} \quad \text{.....(2.33)}$$

The Peltier coefficient is then

$$\pi = (AK + \gamma)\frac{T}{e} - \frac{E(0)}{e} \quad \text{.....(2.34)}$$

For a non-degenerate n-type crystalline semiconductor with spherical constant energy surface under thermal equilibrium the thermoelectric power is given by [48]

$$Q = -\frac{K_b}{e}\left(\frac{E_c - E_F}{K_B T} + A\right) \quad \text{.....(2.30a)}$$

Here A is a constant that depends on the nature of the scattering process. When the energy is measured with reference to the bottom of the conduction band the equation (2.30a) reduces to

$$Q = -\frac{K_B}{e}\left(A + \frac{E_F}{K_B T}\right) \quad \text{.....(2.31a)}$$

Where, E_F is the position of the Fermi level in the band gap. Harry et al.[49] have pointed out that A = 5/2 -r where r is the scattering index.

According to Mott and Davis [48], for limited temperature range, the Fermi energy is

E_C-E_F=E(0)-γT .....(2.32a)

Where E(0) is the low temperature limit of (E_c-E_F) and corresponds to the activation energy equivalent to the band gap, and γ is the temperature coefficient of activation energy. Substituting equation 2.32a into 2.30a, we get

$$Q = -\frac{E(0)}{eT} + \left(\frac{\gamma}{e} - \frac{AK_B}{e}\right) \quad \text{.....(2.33a)}$$

Now, the peltier Coefficient, π=QT can be expressed as

$$\pi = -\frac{E(0)}{e} + \left(\frac{\gamma}{e} - \frac{AK_B}{e}\right)T \quad \text{.....(2.34a)}$$

From equation (2.34a) the plot of π versus T yields a straight line. From its slope γ is obtained. Using the value of γ in equation (2.34a), the value of E(0) can be found out. From the knowledge of γ and E(0) the value of Fermi energy, ($E_C - E_F$) can be obtained from equation (2.32a).

2.12 Scattering processes

When the electrons move in a real crystal, they suffer numerous collisions among themselves as well as with the lattice phonons, impurities and imperfections resulting in a phenomenon knows as scattering. The effect of any particular interaction i may be evaluated by calculating relaxation time τ_i associated with the process. The overall free time τ may then be expressed as

$$\frac{1}{\tau} = \sum_i \frac{1}{\tau_i} \quad \text{.....(2.35)}$$

It is clear from this that the Scattering process which leads to the shortest free time τ_i is the dominant one. Once the free time τ is known, the mobility may be easily determined. Process responsible for carrier scattering which in turn affect the mobility are described below briefly:

(i) Lattice scattering

The possibility of lattice scattering may either be by electronic potential resulting from optical polarization of the lattice or by acoustic lattice vibration that can create lattice deformation potential via Lattice dialation or via piezoelectric polarization field. A number of theoretical physicists dealt with optical scattering. Howarth and Sondheimer[50] have given a very useful expression of the mobility for non-degenerate semi conductors.

$$\mu_o = \left\{\frac{\hbar^2}{e(2K_B)^{\frac{1}{2}}}\right\} e_D^{-\frac{1}{2}} m_e^{*-\frac{3}{2}} \left\{\frac{\in\in_\infty}{\in-\in_\infty}\right\}\left\{\exp\frac{\theta_D}{T}-1\right\}$$

at $T<<\theta_D$ ..... (2.36)

Where θ_D is the Debye temperature, $\in$ is the dielectric constant and $\in_\infty$ is the high frequency (optical) dielectric constant. For degenerate semi conductor, similar formula may also be found [51]. Bardeen and Shockley calculated the mobility and showed that scattering due to lattice dialation caused by the acoustic lattice vibration, is

$$\mu_a = \frac{(8\pi)^{\frac{1}{2}}\hbar^4 C_{ii}}{3E_{1i}^2 m_e^{*\frac{5}{2}} (K_B T)^{\frac{3}{2}}} \quad \text{.....(2.37)}$$

Where, C_{ii} is the average longitudinal elastic constants and E_{1n} is the shift of the conduction band edge per unit dialation in eV.

(i) Impurity scattering

Impurity scattering is important in impure and non stoichiometric semi conductors in which ionized and neutral atoms are present. Both of them may scatter under specific conduction.

(a) Ionized impurity scattering

Ionized impurity scattering predominates when the concentration of ionized donors is high. The charge carriers suffer Rutherford scattering due to the presence of ions. When it is assumed that the ions are distributed throughout the lattice in a regular fashion, the average distance between the ions a_i is given by $a_i^3=1/N_i$, where N_i is the number of ions per unit volume. Thus if v is the velocity of an electron, the mean free time between collisions is $\tau_c=a_i/v$. The relaxation time is in general given by

$$\tau = \frac{\tau_C}{1- < \cos\beta >} \qquad \text{.....(2.38)}$$

Where cosβ is the average of the cosine of scattering angle. Making use of the Rutherform scattering formula, Conwell and Weisskopf[52] have calculated an approximate expression for τ as

$$\mu = \frac{e\tau}{m^*} = \frac{\in^2 m^* v^3}{2\pi N_i e^3}\left[\log\left(1+\frac{\in^2 m^* v^4}{(4e^4)N_i^{\frac{3}{2}}}\right)\right]^{-1} \qquad \text{.....(2.39)}$$

It is observed that this type of scattering leads to a mobility which varies approximately as $T^{3/2}$, in contrast with the $T^{-3/2}$ law for lattice scattering.

The Hall coefficient and Hall mobility associated with ionic scattering are found to be

$$R_H = \pm\frac{1.93}{nec}, \mu_H = 1.93\mu \qquad \text{.....(2.40)}$$

(b) Neutral impurity scattering

In this type of scattering, the scattering of charge carriers by neutral impurities is quite similar to the scattering of electron by hydrogen atoms. By using a modified theory, Erginsoy [53] calculated the mobility associated with this type of scattering alone. He found

$$\frac{e\tau}{m^*} = \mu = \frac{m^* e^3}{20N \in \hbar^3} \quad \text{.....(2.41)}$$

Where N is the density of neutral impurity and $\in$ is the dielectric constant. The relaxation time is independent of the velocity in this case, so that the Hall coefficient is the same as that for metals, viz;,

$$R_H = \pm\frac{1}{ne}$$

(iii) Scattering at dislocation

Distortions of the crystalline lattice cause scattering of electrons and holes. This form of scattering has been discussed theoretically by Dexter and Seitz [54] and shown to make a negligible contribution unless the dislocation density is in excess of 10^{18} cm^{-2}. When the density is of the order of 10^{11} cm^{-2} scattering should be comparable to lattice scattering at room temperature. Dislocation may be regarded as charged cylinder in the path of an electron and causes scattering. The relaxation time τ_d for the process is given by

$$\tau_d = \frac{3}{8RNv} \quad \text{.....(2.42)}$$

Where N is dislocation density and R is the radius of the dislocation line and v is the velocity of the electron. At room temperature this type of scattering is not important but at low temperature it may be important. For spray-deposited samples dislocations are less important.

(iv) Scattering by grain boundaries

Grain boundary scattering is very important for polycrystalline samples either in bulk or thin films form. From the theories the grain[55-57] boundary potential it is known that the boundary regions are characterized by a potential barrier of height E_μ and density of traps Q_t. These two quantities are related by

$$E_\mu = \frac{e^2 Q_t^2}{8 \in_0 \in n} \quad \text{.....(2.43)}$$

Where n is the carrier concentration. The barrier height is also dependent on the grain size. However, according to the nature of this barrier height the carrier transport that depends upon the scattering process in the sample may be influenced by all or any of the following mechanisms.

1 Thermoionic emission of carriers over the barrier

2 Quantum mechanical tunneling

3 Barrier reflection mechanism

In degenerate semi conductors a more complex situation may arise due to all these possibilities. Jones et al. [58] have pointed out that when $E_\mu << E_F$ quantum mechanical barrier reflection model would be applicable for a strongly degenerate sample with the Fermi level E_p at least $2K_BT$ above the conduction band edge. In this case, the relaxation time τ for the material with grain size L can be given by

$$\tau_B = \frac{2L\,\hbar^2 E}{m_e^* a^2 E_\mu^2 v} \quad \text{.....(2.44)}$$

Since $E = \frac{1}{2}(m_e^* v^2)$ is the energy of the electron having velocity v and $a = Q_t/n$ is the width of the square barrier of height $E\mu$, thus equation (2.14) takes the form $\tau a E^{-r}$ and yields the value of $r = -1/2$ for barrier scattering. It is to be noted that for pure lattice scattering $r = \frac{1}{2}$. For strongly degenerate case the temperature broadening of the Fermi surface will create a little change in the velocity distribution of the electrons and as a result of which barrier reflection scattering mechanism becomes almost temperature independent. On the other hand, Petritz[59] pointed out that

when the carriers predominate due to thermionic emission, the associated mobility becomes strongly temperature dependent, whereas in the case of tunneling, carrier transport is temperature independent[60]. Recently, the nature of the grain boundary scattering in polycrystalline semiconductors has become an interesting subject of research to many workers.

(v) Carrier-carrier scattering

In highly degenerate electron gas model, the scattering between carriers is important but it offers little contribution so they are generally neglected. In some cases, however, this type of scattering can play an important role in determining the band shape of the specimen. The effect of inter-electron collision on mobility has been discussed by Frohlich et al. [61]. When the effective mass of holes are larger than those of electrons, the electron-hole collision may reduce the electron mobility.

(vi) Inter-vally scattering

Inter-valley scattering[62] is accounted for semiconductors which contain multivalley conduction band. In such scattering process energetic phonons are generally involved and they become highly inelastic and strongly temperature dependent. This is however, noticed at high temperature only because at low temperature energetic phonons are not available.

2.13 Effect of inhomogeneity on mobility

Naturally thin film samples sometimes become inhomogeneous in their structure. The inhomogeneity creates a large effect on the carrier mobility. Such inhomogeneity may arise from (i) anisotropic impurity separation, (ii) impurity complex formation, (iii) formation of cluster in solid solution samples or, (iv) compositions during growth. The carriers suffer hard-sphere like collision by the space charge region which surround the inhomogeneity. The mobility is therefore given by [63].

$$\mu = \frac{e}{NS(2m_e^* K_B T)^{\frac{1}{2}}} \qquad \text{.....(2.45)}$$

Where N is the density of space charge region with effective scattering cross-section of S. This type of scattering is prominent in high resistive materials.

2.14 Optical properties

The optical behaviors of a semiconductor are investigated in term of the three phenomena namely transmission, reflection and absorption. So it is necessary to study the ultraviolet (UV), visible and infrared (IR) characteristics of the material.

2.14.1 Inter band optical transition and the band gap

When photon energy is incident on a material, the valence electron absorbs energy from incident photon and is excited. When incident energy exceeds threshold value, the electron may make a transition to the conduction band under suitable conditions. If this transition occurs between the bands at the same value of the wave vector K, the transition is considered as vertical and is allowed. Non vertical transitions are normally forbidden. For the simple case shown in figure 2.5(a) the minimum absorption of radiation occurs at $h\nu=E_g$ and it would intensify for all $h\nu > E_g$ where E_g is called the absorption edge or optical band gap. During the process of this type of transitions no phonon is involved for the conservation of energy except the creation of an electron and a hole and is termed as direct absorption process. Bardeen, Blatt and Hall [64] have given an expression for the absorption process as

$$\alpha_d = \frac{B(h\nu - E_g)^s}{h\nu} \quad \text{.....(2.46)}$$

Where $s={}^1/_2$ for allowed transition and ${}^3/_2$ for the forbidden transition, B is a constant and α_d is the absorption coefficient.

The process of indirect transition has also been treated by the same authors[64]. In this transition phonons generation are always involved. The absorption coefficient is given by

$$\alpha_i = \frac{A(h\nu - E_g \pm E_p)^s}{h\nu} \quad \text{.....(2.47)}$$

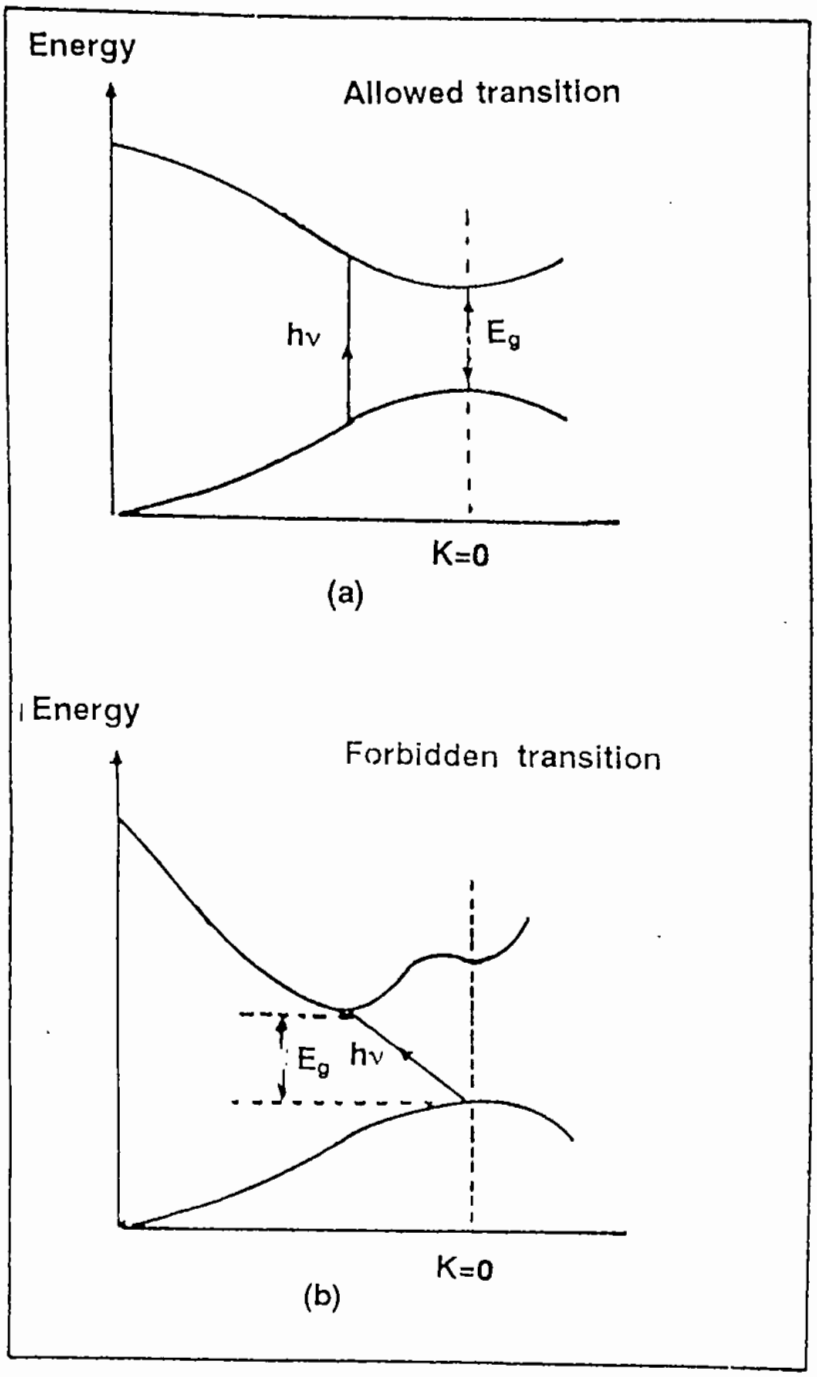

Fig. 2.5 Optical transition in semiconductor, (a) allowed transition (b) forbidden transition.

Where S=2 for allowed transition and 3 for forbidden one. The probability of allowed transition is less in indirect process. Here E_p is the energy of the phonon absorbed (+) or emitted (-).

It is clear from all these expression that a graph of $(\alpha h\nu)^s$ vs. $h\nu$ would provide the value of E_g when carefully drawn for a particular transition process.

2.14.2 Dependence of optical absorption edge on the carrier concentration

A material with a fixed carrier concentration has an unique optical absorption edge which is often found to depend on the carrier concentration for degenerate semiconductor. The effect has been explained independently by Moss[65] and Burstein[66] when they observed in InSb sample a shift of the absorption edge towards higher energy as a function of its carrier concentration.

The magnitude of this shift is determined by two competing mechanisms. One of them is a band gap narrowing which is a consequence[67] of many body interactions on the conduction and valence bands. This shrinkage is counteracted by Moss-Bursteen effect[66] which gives a band gap widening as a result of the blocking of the bottom (lowest states) of the conduction band. Either of the two mechanisms may predominate when the carrier density exceeds the Mott-critical density.

2.15 Theory of p-n heterojunction

2.15.1 p-n junction in equilibrium (no bias)

Refer to figure 2.6(a). When p-n junction is in equilibrium, the number of carriers diffusing from p side to n side is equal to the number of carriers diffusing from n side to p side. Consequently, there is no current across the junction; this can also be concluded in the following way:

The electron current from p to n is proportional to the product of electron density in p region and the probability factor. The probability of an electron sweeping from p to n region is unity because any electron which comes to the edge

of transition region on p side will definitely sweep to n side for the former is a higher potential side. The density of electrons in the conduction band of p type is proportional to the Boltzmann factor $\exp[(E_F-E_C)/K_BT]$; therefore electron current from p to n is[68]

$I_{p\to n}$ =probabilityXdensity of electrons conduction band of p type,

$$= \frac{1}{2}\left(\frac{2\pi m_e^* K_B T}{h^2}\right)\exp\left(\frac{E_F - E_C}{K_B T}\right)$$

$$= C\exp\left(-\frac{E}{K_B T}\right) \quad \text{.....(2.48)}$$

where C is the constant of proportionality and E is (E_C-E_F).

To calculate the electron current from n side to p side, we note that

$I_{n\to p}$ =probabilityXdensity of electron in conduction band of n type.

The probability of an electron to climb up the potential barrier of height $(E+E_F-E_g)$ is proportional to the Boltzmann factor $\exp[-(E+E_F-E_g)/K_BT]$. The density of electrons in the conduction band of n type is proportional to $\exp[-(E_g-E_F)/K_BT]$. Therefore,

$I_{p\to n} = \exp[-(E+E_F-E_g)/K_BT]X C\exp[-(E_g-E_F)/K_BT]$

$$= C\exp\left(-\frac{E}{K_B T}\right) \quad \text{.....(2.49)}$$

From equation (2.48) and (2.49), we note that

$I_{p\to n} = I_{n\to p}$

And, therefore, there is no net current across p-n junction. The same argument holds good for holes too.

2.15.2 p-n junction with forward bias

Figure 2.6(b) forward bias connection of pn junction is shown. p side is connected to the positive of the battery. Due to the external bias, equilibrium conditions are disturbed and therefore energy bands and the Fermi level are altered. Since in this case, negative of the battery is connected to n type side, energy of the electrons in n type region increases by an amount eV, where V is voltage applied by the battery. Consequently, as shown in figure 2.6(b) Fermi level rises by eV and the energy bands adjust their positions so as to suit the elevation of

Fermi level. Due to the increase in energy on n type side, potential barrier is reduced to $e(V_B-V)$. According to relation $X=(2\varepsilon V_B/eN_a)^{1/2}$, the space charge region width or barrier width or depletion width is also reduced. (X is the total width of space charge region, ε is the permittivity of the medium, V_B is the potential barrier, e is the electronic charge, N_a is the density of negatively charged acceptor). The net result is that the electrons crossing the junction from n side will now face a low potential barrier and small widths of space charge region. Consequently, they can easily cross the junction. Since electrons in n type side are in majority, current across the junction increases considerably as shown in fig. 2.7. The variation of junction current with different forward biassing voltages is shown in fig. 2.7.

The net current density across the p-n junction is[68]

$$I = I_o \exp\left(\frac{eV}{K_B T} - 1\right) \quad \text{.....(2.50)}$$

2.15.3 p-n junction with reverse bias

Connections are shown in fig. 2.6(c), n side is connected to the positive of battery. This lowers the Fermi level on n side by an amount eV raising the barrier height to $e(V_B+V)$ and increases the depletion width too. The electrons that are in majority in n side will now face, in crossing the junction, a greater potential barrier and larger width of space charge region. The origin of the reduce reverse bias current is due to the minority carrier.

2.16 Metal semiconductor contacts

When two substance are brought in contact, a redistribution of charge occurs, finally a new equilibrium condition is reached in which the Fermi levels of the two substances are at equal heights. This rule holds not only for contacts between two metals but also for the contact between a metal and a semiconductor. Metal semiconductor contacts play a very important role in determining the properties of most electronic devices.[69] These properties can be complex due to the presence of "surface states" and contamination. It is, however, of interest to investigate the so called "ideal" contacts. A contact may be defined as ideal if the surfaces are free from contamination and the effects of surface states are ignored. The electrodes with an ideal contact introduce a resistance to the flow of current, do not react chemically with the material and remain unaffected by variations in illumination, temperature, or applied field strength.

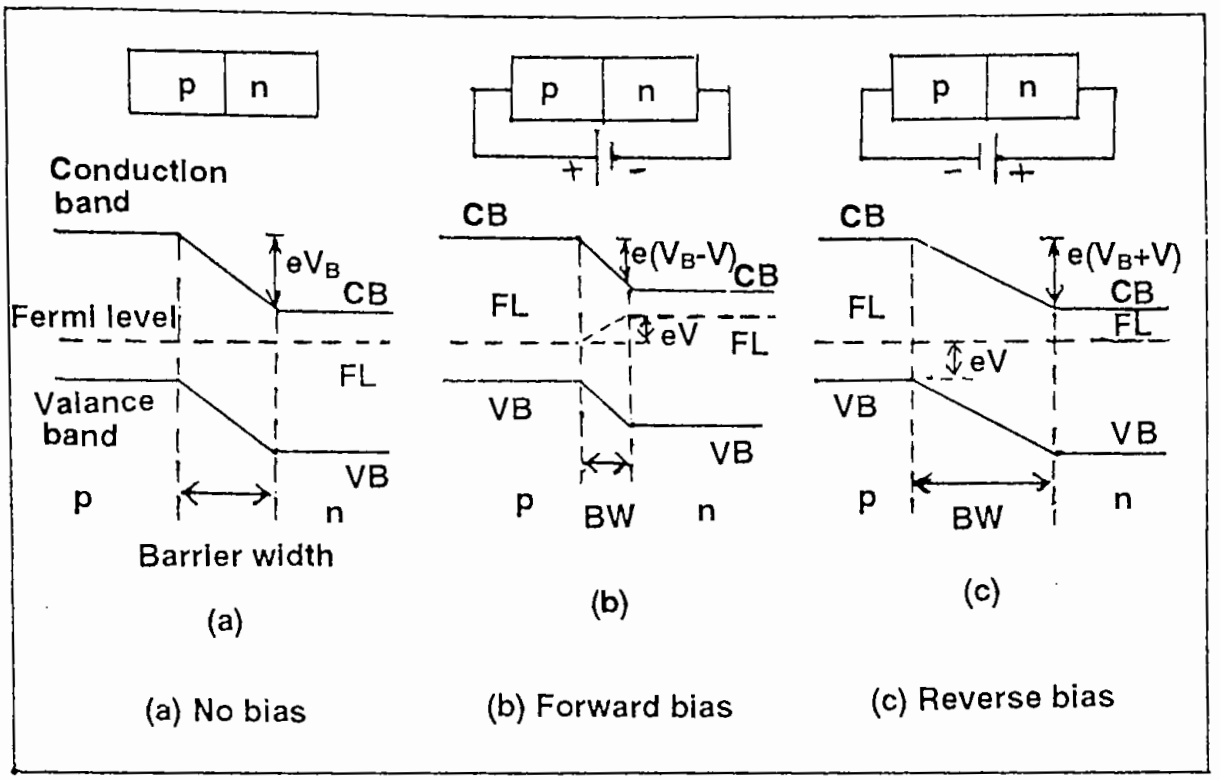

Fig. 2.6 Biasing of p-n junction

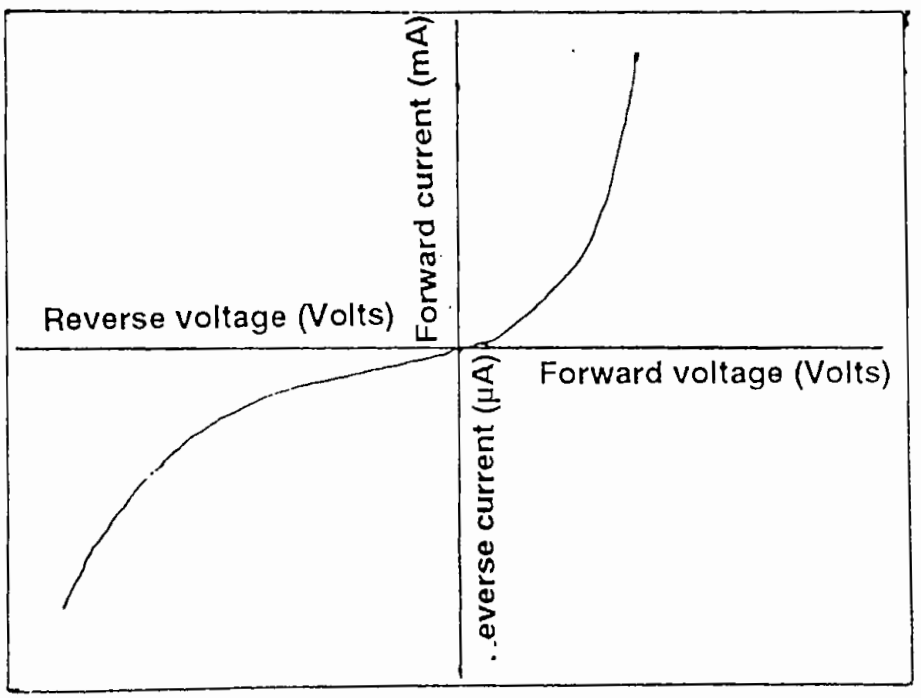

Figure 2.7 Variation of current with different biasing voltage.

In a metal-metal contact a dipole layer is always caused by surfaces charges on both sides of the contact; such a contact is an ohmic contact, since electrons can move freely from the one metal into the other. In a metal semiconductor contact, however, the contact may be either "ohmic" or "rectifying". A rectifying contact is that in which current flows much more easily in one direction than in the opposite one. Rectification effects occur due to the presence of potential barriers caused by[70] (i) improper matching of the work functions between the metal and the semiconductor, (ii)presence of surface states on the semiconductor, producing an intrinsic surface barrier, (iii) presence of a thin layer of a third material (such as an oxide) which in turn causes barriers for reason (i) or (ii) above.

Consider a contact between a metal and an n-type semiconductor as shown in fig.2.8. Let φ_m be the work function of the metal, φ_s the work function of the semiconductor, and χ_s the electron affinity of the semiconductor. If $\varphi_m > \varphi_s$ the Fermi level of the semiconductor lies above that of the metal by an amount $(\varphi_m - \varphi_s)$ before contact. After contact, electrons from the surface layer of the semiconductor enter the metal, leaving ionized donors behind in that surface layer. Electronic equilibrium is established when the Fermi levels in both materials are at the same height. This means that the energy levels in the bulk semiconductor are lowered by the amount $(\varphi_m > \varphi_s)$. As a consequence a potential barrier is formed at the surface (The contact potential). The height of this barrier on the semiconductor side is $(\varphi_m - \varphi_s)$ on the metal side, since Fermi levels are at the same height, the height of the barrier is $(\varphi_m - \varphi_s) + (\varphi_s - \chi_s) = (\varphi_m > \chi_s)$, where χ_s is the electron affinity of the semiconductor. Thus the barrier height may be expressed as

$$eV_d = (\varphi_m - \varphi_s) \quad \ldots\ldots\ldots\ldots\ldots\ldots\ldots \quad (2.51)$$

where V_d is called the diffusion potential and is the potential at the interior or the semiconductor taken with respect to metal surface.

This potential is maintained by the electric dipole layer at the contact. However the positive charge at the semiconductor side does not occur as "surface charge" but as "distributed" charge instead forming the so called space charge layer or barrier layer.

If a potential (-v) is applied to the semiconductor as in fig. 2.9, the electrons moving from left to right will face the same barrier $(\varphi_m - \varphi_s)$ and the corresponding current from right to left does not change. But since the energy levels in the conduction band have been raised by an amount eV, the barrier for electrons moving from right to left has been lowered by an amount eV. The corresponding current from left to right has changed by a factor $\exp(eV/K_BT)$. Consequently, the characteristic is $I = I_o[\exp(Ev/k_Bt)-1]$ which is a diode characteristic and the contact

is rectifying. For $V>>(K_B/e)$, the current is large and positive, and for $V<<(K_BT/e)$ the current is small and almost equal to $-I_o$. In the former case the junction is said to be forward diased and in the latter case it is reverse biased.

If $\varphi_m < \varphi_s$, the situation before and after contact is illustrated in fig. 2.8. Befor contact, the Fermi level of the semiconductor is below t5he Fermi level of the metal by an amount $(\varphi_s - \varphi_m)$. After contact, electrons will flow from the metal in to the surface layer of the semiconductor leaving a positive surface charge behind on the metal side and causing a negative "surface charge" (not distributed charge as for $(\varphi_m > \varphi_s)$ at the semiconductor side of the contact. The Fermi level in the semiconductor bulk material is thus raised by an amount $(\varphi_s - \varphi_m)$. If a voltage V is applied, this potential difference instead of being taken up in the contact area, is distributed across the bulk semiconductor. If $(\varphi_s - \chi_s)$ is relatively small, the electrons can move across the barrier without much difficulty. This type of contact may be considered as an ohmic contact, because on rectification is observed and the current passing through the contacts obey Ohm's law over a large range of applied voltage.

In the special case where the work function of the metal is the same as the work function of the n-type semiconductor, the contact formed may be called a neutral contact.[71] A neutral contact may also exhibit ohmic behaviour for sufficiently low current density that is required to supply to the semiconductor.

When contact is made on a p-type semiconductor, the very opposite effects tothose described above take place. That is an ohmic contact is produced when $\varphi_m > \varphi_s$ and a rectifying contact when $\varphi_m < \varphi_s$ as shown in fig.2.10.

2.16.1 Surface state and inversion layer

The second cause of the existence of a barrier at a metal- semiconductor contact is the presence of surface states. The surface states have been theoretically studied by Tamm[72],Shockley[73] and Othets[74,75] and have been shown to exist within forbidden gap due to the interruption of the periodic lattice structures at the surface of a crystal. At the surface of a semiconductor there are usually dangling valance bands from the valance electron sites which are not paired with electrons as they are in the bulk. The discontinuity in the electron binding gives extra states for the electrons over those in the bulk. Many of these surface states are occupied, leaving a distributed positive charge (as in fig.2.11 for n-type semiconductor) due to the ionized donors behind, in the surface layer. Making contacts with metals of different work functions then means that a different portion of the occupied surface states are emptied into the metal which does not change

the space charge barrier at the surface. The measurements on clean surfaces in an ultrahigh vacuum system have confirmed that the density of surface states is very high[76] of the order of density of surface atoms. Figure 2.11(a) shows a typical energy level diagram for an n-type semiconductor with surface states and figure 2.11(b) shows a similar scheme for a p-type semiconductor. It is frequently found that the effect of the surface is so great that actually a layer of opposite conductivity type is formed near the surface. This layer is called the "inversion layer" as has also been shown in figure 2.11.

The existence of the barrier at a metal semiconductor contact is currently being explored to create at low temperatures the electrostatic fields in the semiconductors needed for carrier separation in solar cells such as Schotky barrier, MIS, inversion layer.

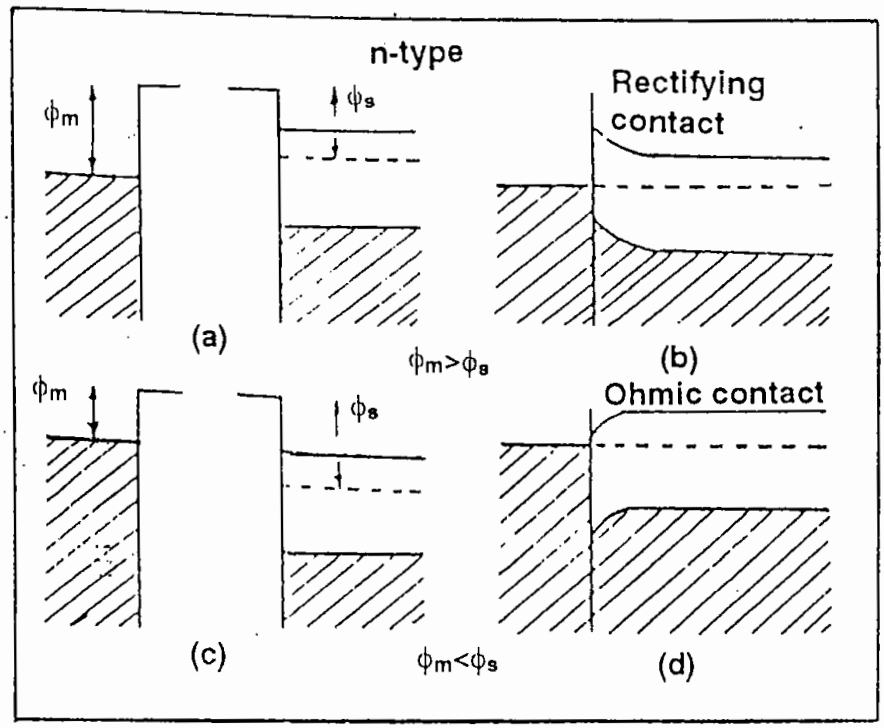

Fig. 2.8 Energy level representation of a contact between a metal and an n-type semiconductor. (a) and (c) before, and (b) and (d) after contact. ϕ_m, ϕ_s are the work functions of metal and semiconductor respectively.

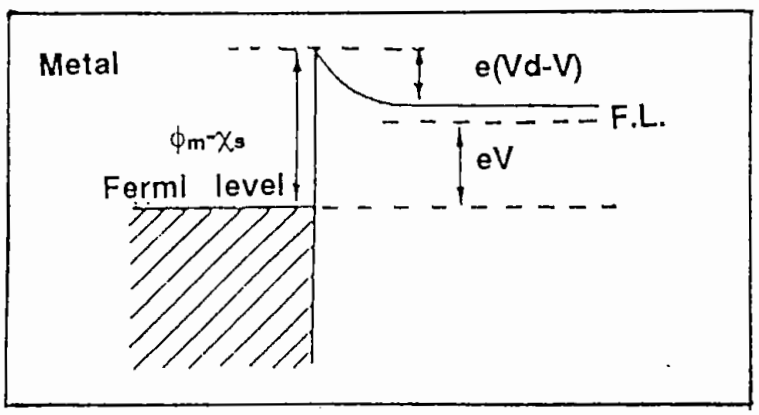

Fig. 2.9 A rectifying metal semiconductor contact. Fermi level in the bulk semiconductor has shifted by an amount eV when a voltage V is applied to the semiconductor.

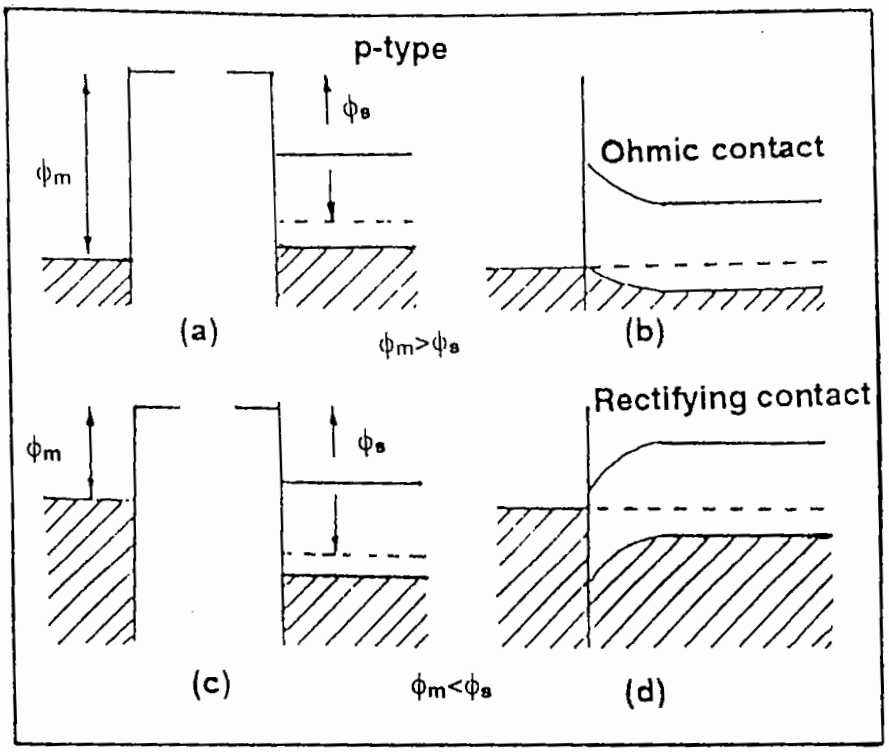

Fig. 2.10 Energy level representation of a contact between a metal and an p-type semiconductor. (a) and (c) before, and (b) and (d) after contact. ϕ_m, ϕ_s are the work functions of metal and semiconductor respectively.

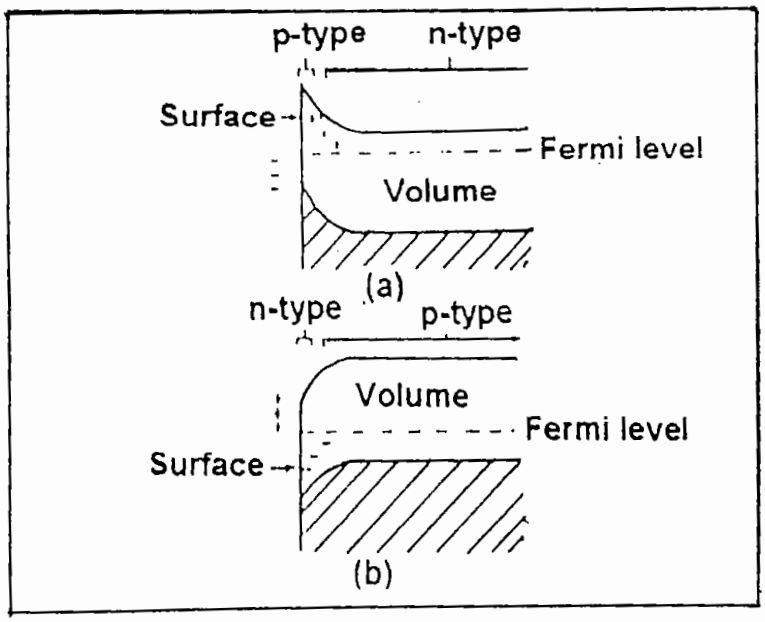

Fig. 2.11 Barrier at the surface of a semiconductor because of the presence of surface states: (a) n-type material (b) p-type material.

References

1. K. L. Chopra, Thin Film Phenomena, McGraw-Hill Bokk Co., New York, 1969.
2. W. R. Grove, Phil. Trans. Roy. Soc., London, 142 (1852) 87.
3. Ludmila Eckertova, Physics of Thin Films (Second revised Edition), New York.
4. H. C. Casyn and M. B. Panish, Heterostructure Lasers, Academic Press, Inc., New York, 1978,
5. A. Boucher and L. Hollan, J. Electrochem. Soc., 117 (1970) 932.
6. V. S. Ban and M. Ettenberg, J. Phys. Chem. Solids, 32 (1973) 1119.
7. R. D. Dupuis, P. D. Dupkus, R. K.Yingling and L. A. Moody, Appl. Phys. Lett. 31 (1978) 201.
8. A. Y. Cho and J. R. Arther, In Somorjai and J. McCaldin, eds., Progress in Solid State Chem., Vol. 10, Pergamon Press, New York, 1975.
9. H. Dislich and E. Hussmann, Thin Solid Films, 77 (1981) 129.
10. G. Milazzo, "Electrochemistry", Elsevier Pblishing Company, Amsterdam, 1963.
11. F. A. Lowenheim (ed), "Modern Electroplating", John Wiley and Sons, Inc., New York, 1963.
12. E. C. Potter, "Electrochemistry", Cleaver-Hume, London, 1956.
13. L. Young, "Anodic Oxide Films", Academic Press Inc., New York, 1961.
14. H. Schfer, "chemical Transport Reactions", Academic Press Inc., New York, 1964.
15. C. F. Powell, J. H. Oxley and J. M. Blocher, Jr. (eds.), "Vapor Deposition", John Wiley and Sons, Inc., New York, 1966.
16. G. Gore, "The Art of Electro-metallurgy", 3rd ed., Longmans, Green and Co., Inc., New York, 1877.
17. D. A. Vermilyea, in "Non-crystalline Solids" (V. D. Frechette ed.), p. 328, John Wiley and Sons, Inc., New York, 1958.
18. A. G. Baker and W. C. Morris, Rev. Sci., Instr., 32 (1966) 458.
19. J. J. Oberly and A. Adams, J. Electrochem. Soc., 109 (1962) 210.
20. E. S. Wajda, B. W. Kippenhan and W. H. White, IBM J. Res. Develop., 4 (1960) 288.

21. A. E. Ennos, Brit. J. Appl. Phys., 5 (1954) 27.
22. R. W. Christy, J. Appl. Phys., 31 (1960) 1680.
23. L. Holland and L. Laurenson, Vacum, 14 (1964) 325.
24. M. Stuart, Nature, 199 (1963) 59.
25. I. Haller and P. White, J. Phys. Chem., 67 (1963) 1784.
26. P. White, J. Phys. Chem., 67 (1963) 2493.
27. D. H. Robertz and J. E. Baines, J. Phys. Chem. Solids, 6 (1958) 184.
28. J. Starkiwicz, L. Sosnowski and O. Simpson, Nature, 158 (1946) 28.
29. R. R. Chamberlin and J. S. Skarman, J. Elec. Soc., 113 (1966) 86.
30. M. S. Tomar and F. J. Gracia, Prog. Cry. Groth., 4 (1981) 221.
31. W. Kern and V. S. Ban, "Thin Film Process", (ed. J. L. Vossen and W. Kern, Academic Press, New York, 1978).
32. F. C. Eversteijn, Philips Res. Rept., 29 (1974) 45.
33. D. W. Shaw, J. Cryst. Growth, 31 (1975) 130.
34. Y. S. Chiang, "Semiconductor Silicon 1973", Electrochem. Soc. 1973, p.285.
35. C. A. Chang, J. Electrochem. Soc., 123 (1976) 1245.
36. Lean I. Maisseel and Reinhard Ghang, "Hand book of Thin Film Technology", McGraw Hill Book Co., 1970.
37. D. W. Pashley, Proc. Phys. Soc., London, A64 (1951) 1113, A65 (1952) 33.
38. G. A. Bassett, J. W. Menter and D. W. Pashley, "Structure and Properties of Thin Films" (ed. C. A. Neugebauer, J. B. Newkirk and D. A. Vermilyea, John Wiley and Sons Inc., 1959).
39. R. Thun, "Physics of Thin Film", (ed. G. Hass, Academic Press Inc., New York, Vol. 1 (1964) 187.
40. R. B. Belser, J. Appl. Phys., 28 (1957) 109.
41. N. B. Hannay, "Semiconductors" (Reinhald Publishing Co., New York, 1959).
42. A. R. Smith, "Semiconductors" (Cambridge University Press, 1968).
43. A. R. Smith, The Physical Properties of Thermo-dynamics (Chapman and Hall, 1952) 84.
44. V. Vand, Proc. Phys. Soc. London, 55 (1943) 224.
45. C. Wood, V. Harrap and W. M. Kane, Phys. Rev., 121 (1961) 978.
46. R. W. Wright, Proc. Roy. Soc., A64 (1951) 350.
47. J. S. Blakemore, "Semiconductor Statistics" (Pergamon Press, 1962).
48. N. F. Mott and E. A. Davis, "Electronic Process in Non Crystalline Materials", 2nd edn. (Clarendon Press, Oxford, 1979).

49. H. Harry, B. Kwok and R. H. Bube, J. Appl. Phys., 44 (1973) 138.
50. D. J. Howarth and E. H. Sondheimer, Proc. Roy Soc., A219 (1953) 53.
51. E. H. Puttey, "The Hall Effect and Semiconductor Physics" (Dover, New York,1968).
52. E. M. Conwell and V. F. Weisskopt, Phys. Rev., 77 (1950) 388.
53. C. Erginsoy, Phys. Rev., 79 (1950) 1013.
54. D. L. Dexter and F.Seitz, Phys. Rev., 86 (1952) 964.
55. J. Y. W. Seto, J. Appl. Phys.,46 (1975) 5247.
56. G. Baccarani, B. Ricco and G. Spadini, J. Appl. Phys.,49 (1978) 5565.
57. A. K. Ghosh, C. Fishman and T. Feng, J. Appl. Phys., 51 (1980) 446.
58. R. E. Jones Jr. and S. P. Wesolowski, J. Appl. Phys., 56 (1984) 1701.
59. R. L. Petritz, Phys. Rev.,104 (1956) 1508.
60. M. V. Garcia-Cuenca, J. L. Morenza and J. Esteve, J. Appl. Phys., 56 (1984) 1738.
61. H. Frohlich, B. V. Paranjape, C. G. Kuper and S. Nakajima, Proc. Phys. Soc., B 69 (1956) 842.
62. C. Herring, Bell Syst. Tech. J., 34 (1955) 237.
63. L. R. Weisberg, J. Appl. Phys., 33 (1962) 1817.
64. J. Bardeen, F. J. Blatt and L. H. Hall, "Photoconductivity Conference", (ed. R. Breckenridge, B. Russel and E. Hahn, New York, John Wiley, 1956).
65. T. S. Moss, Proc. Phys. Soc., London B67 (1954) 775.
66. E. Burstein, Phys. Rev., 93 (1954) 632.
67. K. F. Berggren and B. E. Sernelius, Phys. Rev., B24 (1981) 1971.
68. S. L. Gupta and V. Kumar, "Hand Book of Electronics" (Revised and Enlarged Thirteenth Edition 1985) Pragati Prakashan, Meerut, India.
69. E. H. Rhoderick, "Metal Semiconductor Contacts", Oxford University Press,1978.
70. H. K. Henisch, Sylv. Technol., 9 (1956) 73.
71. F. Stockmann, Photoconductivity Conference, John Wiley and Sons, New York (1956) 269.
72. I. Tamm, Physik. Z. Sowjetunion, 1 (1933) 733.
73. W. Shockley, Phys. Rev., 56 (1939) 317.
74. J. Kontecky, J. Phys. Chem. Solids, 14 (1960) 233.
75. D. Pugh, Phys. Rev. Ltters, 12 (1964) 390.
76. F. G. Allen and G. W. Gobeli, Phys. Rev., 127 (1962) 150.

CHAPTER THREE

EXPERIMENTAL DETAILS

EXPERIMENTAL DETAILS

This chapter deals mainly with the design and construction of the experimental apparatus and preparation of samples (CdS, CuO thin films and CuO-CdS heterojunctions) on glass substrates. Various experimental methods which were adopted throughout the course of the work for the analysis of the structural, electrical and optical properties of the deposited films have also been described here.

Part I (Film preparation technique)

3.1 Introduction

It is already known that the process of spray deposition is one of the simplest and least expensive one of all the film deposition methods available to date. Because of this extreme simplicity one has to face a number of difficulties in controlling the process variables. Moreover the qualities of the deposited films are relatively inferior to those of films obtained in other complex methods. Experimental arrangements have been put forward by many workers [1-8] to promote ease of operation and to overcome difficulties which were often encountered at the time of film deposition. But still more work is needed to improve the process of deposition and to reduce the cost of production, since for solar cell and other device technology the low cost production of semiconducting thin films has become a necessary precondition.

Pyrosol process [8,9] is a chemical spray deposition process where an aerosol is prepared from the working solution in one section of the apparatus and simultaneously carried to the other section where pyrolysis of the aerosol takes place. We have described in the following sections a new arrangements for this process. It could be mentioned here that like the CdS and CuO thin films, several other semiconducting thin films of binary and ternary compounds such as ZnO, CdS, CdTe, $CuInSe_2$ and many oxides and sulphides can also be easily prepared by this apparatus only by adjusting some of the parameters of the process.

It was observed that in all spray deposition process common defects like the surface roughness and thickness inhomogeneities of the deposited films are often encountered. Therefore the role of the deposition process is very important in preparing good quality films free from these defects.

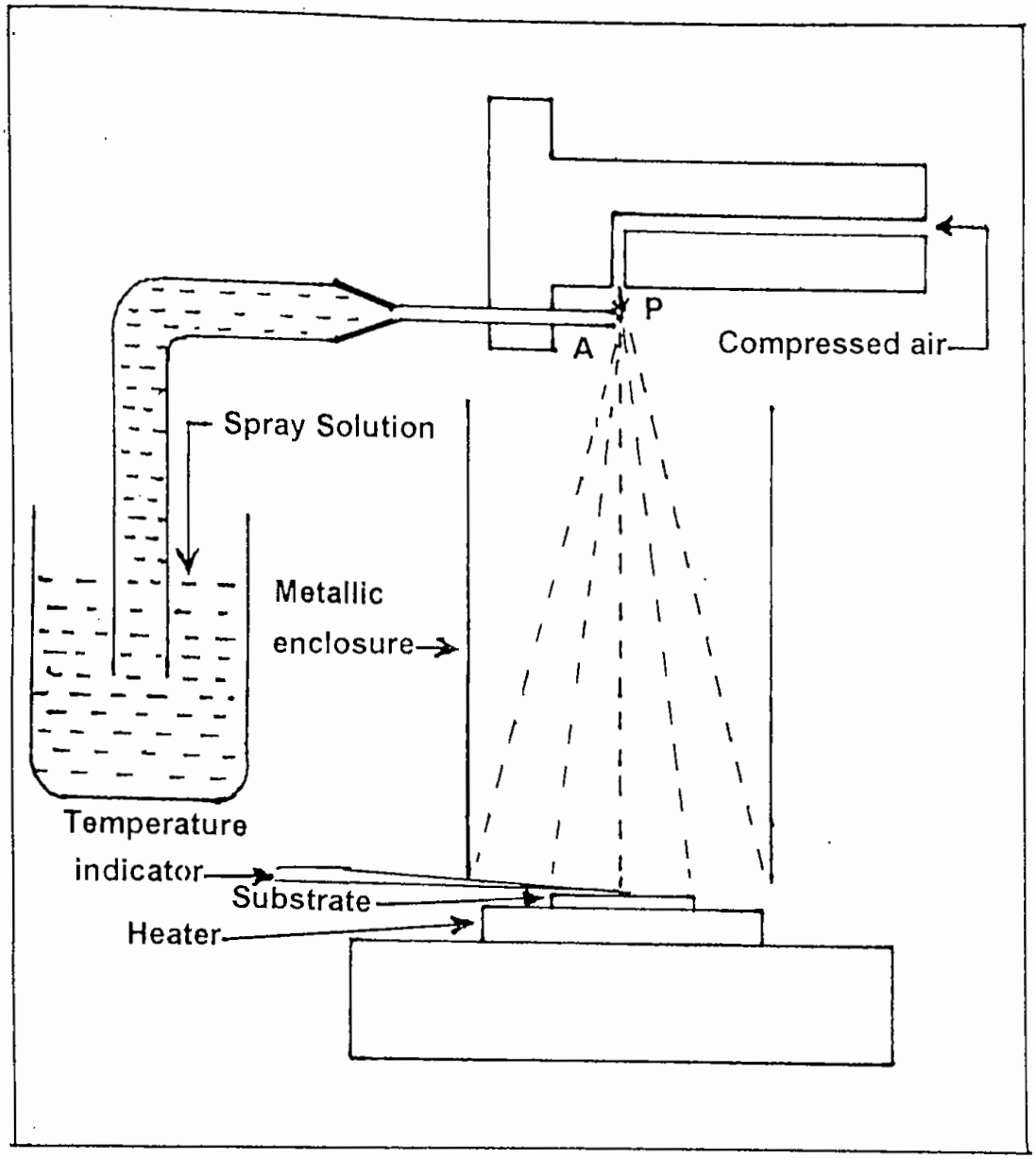

Fig. 3.1 Schematic diagram of spray pyrolysis apparatus.

3.2 Designing of spray deposition Apparatus

In this section the design and construction of different parts of the spray unit have been described. The whole setup of the system is shown in figure 3.1.

3.2.1 Heater

The heater is an ordinary hot plate 2000-watt Nichrome wire heater. The top of the plate is covered by piece of mica sheet which is used an electrical insulation. A thick stainless steel susceptor plate (fig.3.1) is then placed on a mica sheet. Substrate is placed on this suspector plate to have a uniform temperature through out the substrate surface. Normally a mica sheet is placed on the suspector plate to protect it from chemical corrosion during spraying. The heater power is controlled by an electrical voltage variac. The temperature of the heater was measured by copper-constantan thermocouple attached on the substrate surface.

3.2.2 Spray nozzles

The single spray nozzle consists of capillary tubes fitted at right angle to each other as shown in fig.3.1. When the compressed air is passed rapidly through the upper tube p in a direction tangential to the mouth of the lower tube, A, a partial vacuum is created at the front part of the tube A whose other end is kept immersed in the spray liquid.

Due to the partial vacuum the liquid rises up through the tube A and the compressed air drives it away in the form of fine spray particles (aerosol). The thinner the spray nozzle the finer would be the spray particles.

A very fine needle shaped capillary tube was used for the spray nozzle. Fine spray through the nozzle depends on the size of the bore and it may vary from nozzle to nozzle.

3.2.3 The design of the reactor

The design of the reactor is shown in figure 3.1. It is a vertical bath type reactor consists of a stainless steel enclosure and a heater. The substrate is placed on the susceptor and the substrate temperature is monitored by a copper-constantan thermocouple. The heater power is controlled by a variac.

The reactor wall is cylindrical. The chemical reactions, which occur in the reactor, are endothermic. Moreover the reaction process would be disturbed due to a rapid fall of substrate temperature. For this reason the temperature of the reactor

wall should be maintained at a level much higher than that of room temperature but lower than the reaction temperature. This temperature is maintained automatically by the metallic enclosure placed over the heater.

3.2.4 The fume chamber

It is a large box type chamber with a slanting top and is provided with a chimney. There is an exhaust fan with regulated power supply fitted at the mouth of the chimney. The slanting top and the sidewalls are made of glass. There are air tight doors in the front side. The chamber has purging facilities. The whole spray system and reactor are kept inside this fume chamber at the time of film deposition because of

a) Safety grounds and

b) To check air current disturbances at the deposition site.

These two points just stated are very important for the pyrosol process when deposition is carried out in open-air atmosphere.

3.2.5 Air compressor

It is a reservoir type electrical air compressor. A rotary pump in its suction mode draws atmospheric air and keeps it reserve in a large capacity air tank. At the out let of the tank a pressure gauge is attached which records the pressure of the air at the time of supplying it from the tank. There is a by pass control valve which can keep the output pressure constant.

3.2.6 The carrier gas

The carrier gas is selected according to the criterion of the chemical reaction-taking place. In some cases carrier gas takes active part in chemical reaction for the formation of the film, in the other cases it remains inactive with deposition material but serves only to transport the spray particles to the reactor section. For the deposition of an oxide layer air or oxygen may be used so as to supply oxygen needed for the reaction. Other gases like nitrogen, argon; helium may be used to serve this purpose. In the present work dry compressed air has been used as carrier gas. The pressure of the gas can be varied by adjusting the outlet valve of the air compressor and was maintained constant according to the requirement of the spray rate during the deposition run. The standard pressure for the spray system has been found to be 1-5 PSI.

3.2.7 Rate of deposition

In preparing the thin films, the solution flow rate of 0.5 ml/minute to 1.2 ml/minute was used for the present experiment. The rate of flow of the working solution is controlled to a better accuracy by suitably designing the nozzle A and adjusting the airflow rate.

3.2.8 Thickness control

The deposition time is the main thickness-controlling factor in the spray pyrolysis deposition process provided the other parameters remain constant. Using a calibration chart the thickness of the thin films is controlled. These curves are generally the deposition time versus thickness curves. The thickness control is therefore easy, since the rate of deposition in our setup is rather small.

3.3 Cleaning of the substrates

Cleanliness of the substrate surface exerts a decisive influence on film growth and adhesion. A thoroughly cleaned substrate is a pre-requisite for the preparation of films with reproducible properties. The choice of cleaning techniques depends on the nature of the substrate, the contaminants and the degree of cleanliness required. Since our glass substrates were ordinary sodalime microscope slides and cover slides and therefore residue from manufacturing and packaging, lints, fingerprints, oils and air borne particulate matters were supposed to be contaminations.

The following procedure was found adequate for substrate cleaning in our laboratory. The gross contamination of each of the substrates are first removed by luke warm aqueous solution of sodium carbonate. Then after washing in a stream of cold water they are dipped at first into nitric acid for some time and then into chromic acid mixture ($K_2Cr_2O_7$) for several days. Taking them out of the chromic acid bath one by one they are washed and thoroughly rinsed with deionized water several times and finally made dry by blowing hot air. They are then preserved in desecrator. During the whole process slide-holding forceps were used to held the substrate.

3.4 Shape of the sample and preparation of masks

In order to study the various properties of thin films, specific shape and size of films are necessary. The most commonly used methods of pattering thin film are (i) Physical masking (ii) Photoresist (iii) Inverse photoresist and (iv) Inverse metal making. In the present work, physical masking has been used. There are suitably shaped apertures through which deposition is made to have a desired pattern of the film. Especially for the chemical spray deposition system, the material for the masks should be selected in such a way that is remained inert to the chemical used for the deposition. Mica and stainless steel is a suitable masking material for this process because of their chemical inertness and capacity for high temperature tolerance. The film uniformity strongly depends on the dimension of mask. As the film thickness are of the order of 1000 -6000 Å so the mask should be as thin as possible. The smaller is dimension of the pattern the thinner should be the mask. In figure 3.2(a), (b) and (c), the effect of the mask thickness on the film size and uniformity has been clearly shown. In the pyrosol process it is assumed that the chemical reaction takes place in the vapour phase at the substrate surface or in its close vicinity. So the effect of mask dimension on the uniformity of film thickness is very important and should be taken into account. Preparing mask using single layer mica sheet can probably solve this problem.

For the measurement of resistivity and Hall co-efficient of our samples Vander Pouw's method[10] was followed. Specimen was prepared by using mask (mica) shown in figure 3.3(a). To keep this mask in contact with the substrate surface, a stainless steel frame is cut in the shape shown in figure 3.3(b). This frame can hold the mask with substrate surface by giving suitable pressure. Other types of mask are shown in figure 3.3(c) and 3.3(d) (for the study of thermoelectric power).

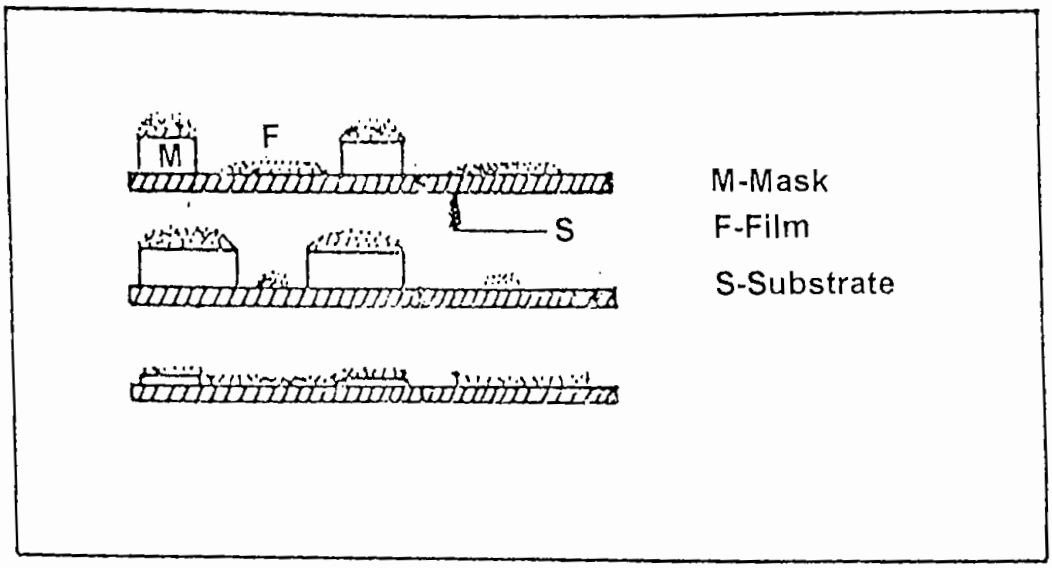

Fig. 3.2 The effect of size of mask on the deposited film in spray pyrolysis process.

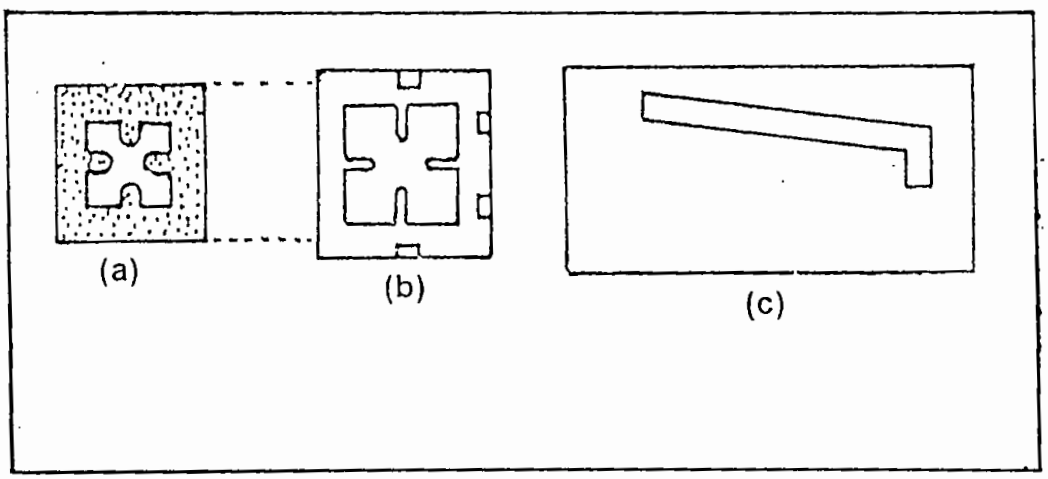

Fig. 3.3 : (a) Mica mask with the design cut on it, (b) a stainless steel frame to hold the mask and the substrate intimately in contact, (c) mask to deposited experimental sample for the thermoelectric power measurement.

3.5 Selection of spray solution

3.5.1 Source compound

The choice of the source compound must satisfy a number of essential conditions; it should be a stable compound at room temperature, it should not oxidize in air or in the presence of water at room temperature, it should have a decomposition temperature below 400°C and preferably higher than its boiling or sublimation temperature.

$CdCl_2$ and $SC(NH_2)_2$ for CdS and $CuCl_2$ for CuO thin films were used as the source compounds. All the source compounds are crystalline solid at room temperature.

3.5.2 Solvent

Different types of solvent may be used to prepare ionic solution for a single source compound. Among them the most suitable one is chosen so that it can permit a high aerosol flow rate in connection with the concentration and viscosity of this solvent. The spray system, which is used in the present experiment, has a spray nozzle of capillary bore type. The ejection of spray liquid through the spray nozzle depends on the solution concentration. Higher solution concentration causes to reduce the spray rate because it has to pass through a partial vacuum path. So the concentration of the solution prepared by the solvent should be such that the nozzle could at least draw it. Preference is given in selecting a solvent that is not easily inflammable to avoid sudden combustion in the reactor. The most commonly used solvent is water, which facilitates the hydrolysis action. In this experiment water was used as the solvent because there is no possibility of occurring any accident with it in the reaction and it acts as a powerful oxidizing agent.

3.5.3 Preparation of the ionic solution.

3.5.3.1 For CuO

The working solution was prepared by taking $CuCl_2 2H_2O$ as source compound. The most commonly used solvents are water and ethenol. As $CuCl_2$ is soluble in water at room temperature, water was taken as solvent. A typical value of solution concentration 0.2M was used in this experiment. Solution of other concentration can also be taken to prepare CuO thin films.

3.5.3.2 For CdS

For cadmium sulfide (CdS) thin films preparation, thiourea (NH_2-SC-NH_2) and Cadmium Chloride ($CdCl_2$) was used as the source compound. A working solution which is sprayed on the heated substrate will yield an optically clean and very adherent films of CdS consists simply of an aqueous solution of cadmium chloride of concentration of 0.1 Molar and thiourea which is also made with a concentration

of 0.1 Molar by arbitrary choice. It was difficult to dissolve the $CdCl_2$ in the distilled water at room temperature. So it is necessary to heat the solution at about 60^0-70^0C. Complex compounds were obtained from neutral solutions of $CdCl_2$ of 30-70% and of $SC(NH_2)_2$ of 70-30%.

3.6 Film deposition parameter

Because of the reversibility of the chemical reactions (2.1) and (2.2) the structure, composition and other characteristics of the deposited films depend on a number of deposition parameters (process variables), such as the temperature of the substrate, the flow rate of the aerosol and carrier gas, deposition time, quality of the substrate material, size of the atomized spray particles, concentration of the ionic solution and distance between the substrate and the source (mouth of the pipe supplying the aerosol). Obviously the substrate temperature is the most important factor and must be controlled with care.

In Preparing films for the present work all of the above parameters except (i) the deposition time t_d , (ii) the substrate temperature T_s , (iii) the concentration of the solution and (iv) the composition of solution were kept unchanged. To study the effect of any one of these four parameters on the film properties the remaining other should be kept reasonably constant.

3.7 Film deposition

Spray pyrolysis method for preparing CdS [1,11,12] and Copper Oxide[13] films is an economically attractive method which consist basically of spray a solution on a heated substrate. Prior to the deposition, the whole set was be cleaned properly. A considerable amount of (above 80 ml) spray solution with a desired solution composition ratio is taken in a beaker F connected with a spray nozzle. The clean substrate with a suitable mask is put on the susceptor of heater H. The distance between the tip of nozzle and the surface of the substrate was 25 cm. A copper-constantan thermocouple was attached to the substrate to monitor the temperature of the substrate. The temperature of the substrate was control by controlling the heater power by a variac. Before supplying the compressed air the heater is kept on for some time so that the substrate and the reactor wall attains the requisite temperature. The substrate temperature T_s is to keep at a level slightly higher than the required substrate temperature because at the onset of deposition a slight fall of temperature takes place.

The solution spray rate was generally maintained in the range of 0.05ml/min. to 1.2 ml/min. When compressed air is passed through P at a constant pressure (1-5 PSI) a fine aerosol is produced and falls to the reactor zone where film is deposited on the substrate. 1-40 minutes of spray produces CdS and CuO films of thickness 1000-6000Å at a substrate temperature (T_s) about 150 -350°C.

3.8 Optimization of the deposition process

To optimize the deposition process one should have to select at first the requirement with respect to which the process is to be optimized. Since there are several process variables, the optimization process would therefore be lengthy. We have selected the high stability as well as the best crystallinity of the films as our basic requirement. We have proceeded to optimize the process under certain limitations and it cannot be taken as the ultimate optimization.

First a set of films was deposited at various substrate temperatures T_s. Then at a constant temperature T_s films were again deposited by varying only the distance between the substrate and the exit of the conduit pipe (may be called source). From this set of films the best one was taken to fix the distance d between the substrate and the source. Keeping this distance d and temperature T_s as fixed the pressure (P) of the carrier gas was then varied and a third set with adequate pressure of the carrier gas was prepared and best film was selected. Since the process variables are to some extent mutually interdependent, the resulting optimization was undoubtedly a tentative one. We found that d = 25 cm and a pressure of 2.0 PSI of the carrier gas has the best results for CdS and CuO films. All the experimental samples for our present work have been prepared by taking this value of d and pressure P.

3.9 Lead attachment to thin film

Usually, two methods are used for attaching lead to thin films; (i) solid phase bonding and (ii) alloy bonding. Thermos compression and ultrasonic means form the solid phase bonds whereas, the alloy bonds are formed by soldering.

In the present work, metallic indium (without flux) was used as soldering material to make electrical contacts. Since the experimental samples were very hard, good contacts were obtained by indium. Indium dots were first soldered to the clean film surface. One end of a clean fine copper whisker was then wetted by indium and then placed in contact with the indium dot on the film and the whisker was heated with the help of a 25 watt fine tip soldering iron. The applied heat just melted the upper part of the indium dot and made a good ohmic contact with the film. Slight pressure was sometimes applied to the contact points to make it very tight.

For the measurements at high temperatures (above 100°C) the contact points were thickly covered with an insulating hard adhesive resin that can withstand high temperature unto ~300°C. Indium contacts were then found to remain operative at temperatures unto ~ 260°C without any disturbance.

3.10 Fabrication of CuO/CdS Heterojunction

Usually, there are a number of basic steps involved in the fabrication process of CuO-CdS thin film heterojunction; (i) preparation of the base, (ii) deposition of CdS, (iii) formation of CdS-CuO junction and (iv) attachment of upper electrode.

(i) Preparation of the base

All the junctions described in this thesis were fabricated on chemically cleaned glass substrates. The glass substrate was then coated with a transparent and conducting layer of fluorine doped SnO_2 by spray process.

(ii) Deposition of CdS

The CdS films were deposited using the technique described in section 2.2.5.2c. The CdS thin films have been prepared on doped SnO_2 coated glass substrate by the spray technique using aqueous solution (both 0.1M) of $CdCl_2$ and $SC(NH_2)_2$ in equal proportion and at 250°C temperature (i.e. at optimum condition). In a constant preparation condition, a set of samples was prepared with different spray time to obtain films of different thickness.

(iii) Formation of CdS-CuO junction

In the formation of CuO-CdS junction, CuO thin layer have been deposited on CdS layer by the spray pyrolysis technique using $CuCl_2.2H_2O$(aq.). In the deposition of CuO layer, the substrate temperature was kept at about 200°C using solution concentration 0.2M and spray rate ~1ml/min. Reasonably good junction was obtained with these deposition condition.

(iv) Attachment of upper electrode

The copper wires have been used as a connecting lead. Copper wire was attached on the top layer i.e. on CuO layer by the silver paste. The bottom contact was made on the base layer. Schematic diagram of CuO/CdS heterojunction is shown in figure 3.4.

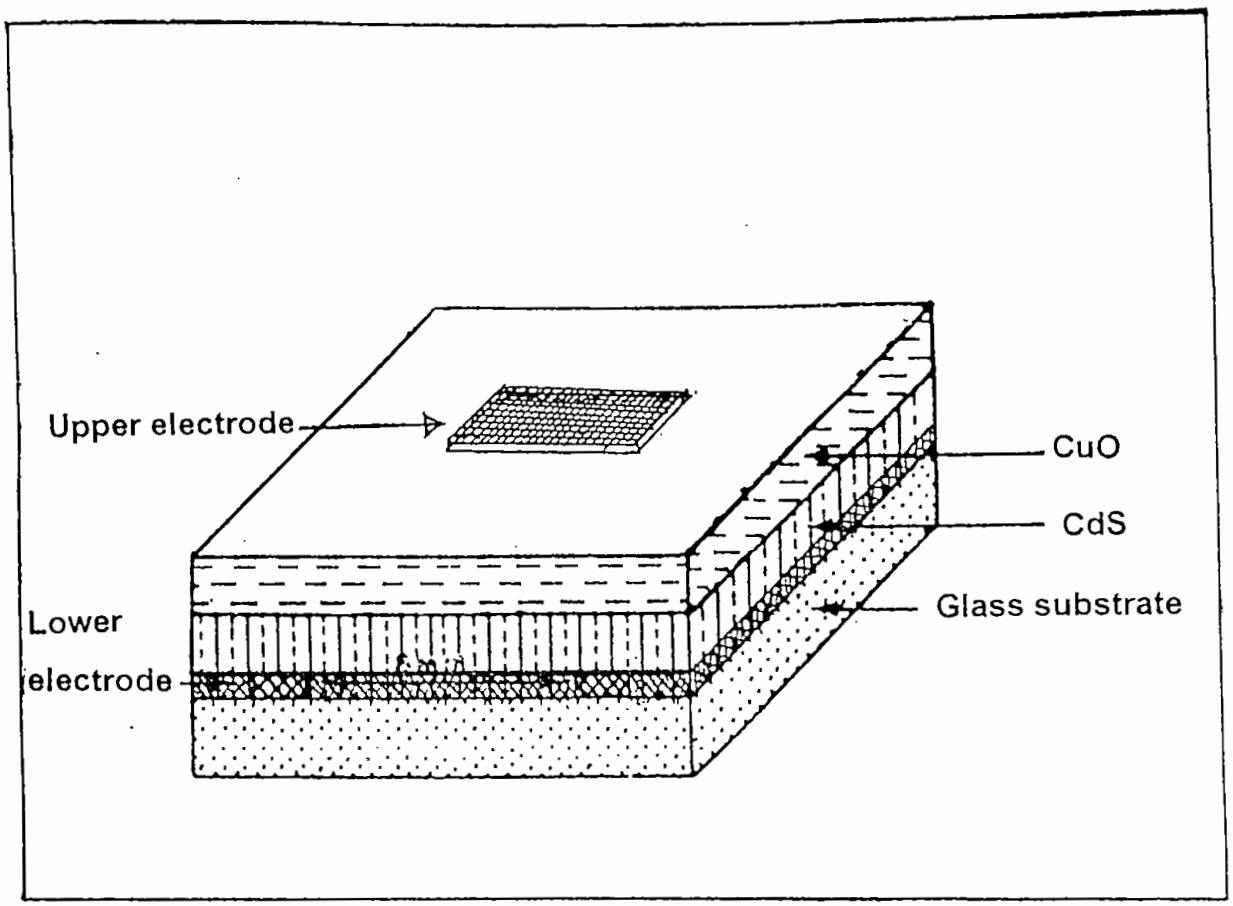

Fig. 3.4 Schematic diagram of CuO/CdS heterojunction.

Part II (Description of measuring equipment and experimental measurements)

3.11 Measurement of the film thickness

In thin film experiments thickness measurement is an essential job. All most all the electrical parameters except the Hall mobility and sheet resistance need for their evaluation the value of film thickness. Therefore thickness should be measured with precision as far as possible. There are several methods of measuring the film thickness, some of which are briefly described below.

3.11.1 Conventional method

At present there are several methods of determining thickness of transparent or semi- transparent films. A few simple methods are mentioned below.

(a) Gravimetric method

This is one of the oldest techniques for the determination of film thickness. The mass m of a film of area A is determined by a microbalance by weighing the substrate before and after deposition. The thickness is then calculated by assuming bulk density ρ of the film material. Thickness t of the film is given by

$$t = m/A\rho \quad \ldots\ldots\ldots\ldots\ldots\ldots\ldots\ldots\ldots\ldots (3.1)$$

There are several difficulties and sources of errors in this method, especially the value of ρ cannot be known with precision. This method is therefore avoided.

(b) Stylus instrument

Stylus instruments are largely used for the measurement of surface roughness and surface finishes. Here also a film step is required. In principle the instrument compares the vertical movements of the stylus travelling across the sample surface with the movement of a " shoe" or "skid" on a smooth and flat reference surface, the substrate. The mechanical signals produced by the stylus movement are converted to electrical signals, which are then amplified and recorded on a chart. From the pattern of the chart thickness of the film is evaluated. For hard films like CdS and CuO this method is very much suitable. The main advantage of this method is that it does not depend on the optical nature of the sample. If the sample can just support the load of the stylus then the method can be applied. Here the accuracy depends on the sensitivity of the stylus.

(c) Colour comparison

This is a crude but very simple and rapid method of estimation of thickness of transparent film on a reflecting substrate. Transparent films display colours when viewed through ordinary reflected light. The colour depends on the thickness of the film. First precise colour thickness gauge was made by Blodgett [14] who had deposited layers of barium stearate on a lead-glass plate producing a very colourful and useful thickness gauge.

In making colour comparison, one must be careful not to confuse different film thicknesses which give rise to similar colours but in different orders. This can be done by comparing the colours of the films while varying the angle of observation. The value of the refractive index however limits this method in some cases.

3.11.2. Fizeau fringes method (Tolansky Method)

Since the CdS samples are slightly transparent to the visible light the measurement of thickness by interferometric method would be adequate. The interferometric method for the determination of film thickness using Fizeau fringes has been developed to a remarkable degree by Tolansky [15] and is now accepted as a standard method. To make the Fizeau fringes of equal thickness visible in a multiple beam interferometer formed by a thin absorbing film on a glass substrate, generally an auxiliary reflecting coating on the film surface is required. But if the experimental sample has very smooth surface no such auxiliary coating is necessary [16].

The film to be measured is required to form a step on a glass substrate over which another plane glass plate (Fizeau plate) is placed. This forms the interferometer as shown in figure 3.5(a). When the interferometer is illuminated with a parallel monochromatic beam of light a fringe system as shown in figure 3.5(b) is produced. The displacement h of the fringe system across the film-substrate step is then measured to calculate the film thickness t, using the relation

t = (h / fringe spacing) Xλ/ 2

$$or, t = \frac{h\lambda}{2l} \quad \text{.....(3.2)}$$

The accuracy of the method depends on how accurately the fraction h of the fringe space l has been measured. Thickness measurement from 30 Å to 20,000 Å can be made with an accuracy of ±10 Å.

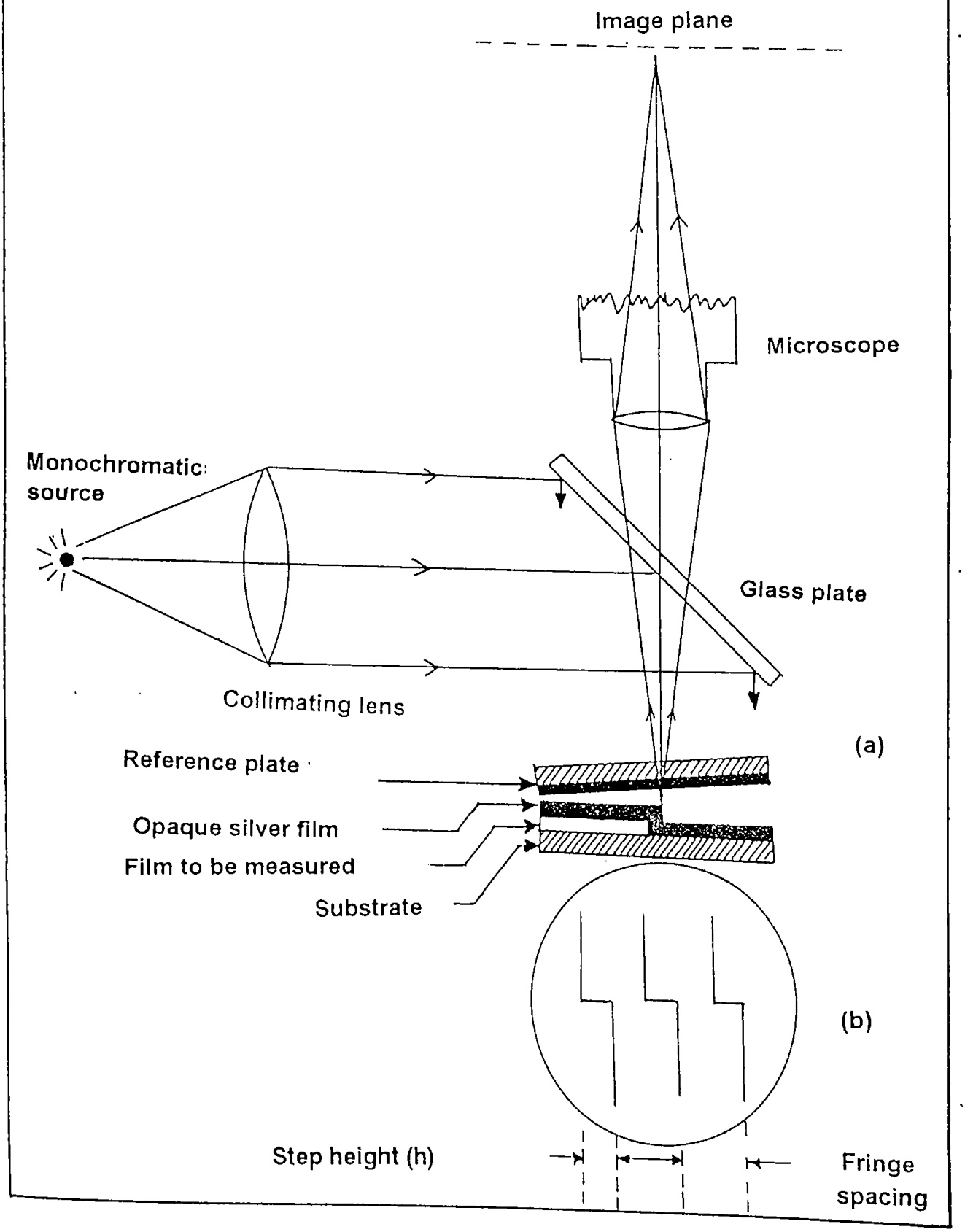

Fig. 3.5 Interferometer arrangement for producing reflecting Fizeau fringes of equal thickness.

3.11.3 Newton ring method

When a plano convex lens of large radius of curvature is placed on a plane glass plate, a thin air film of gradually varying thickness is formed. When the point of contact is viewed with monochromatic light it is found to be surrounded by alternate dark and bright rings. When it is viewed with white light it is found to be surrounded by several coloured rings with the white center as dark

The method has particularly been possible due to the facility of using white light fringes. In this case the fringes appear coloured and countable and can be identified easily for a particular order.

Let us consider a particular ring formed at a point B. The radius of the ring= PB=r_n. Let the thickness of the air film at point B is t' i.e. AB =t' as shown figure 3.6. From the right angled triangle OAE we get,

$OA^2= OE^2 + AE^2$

$OA^2=(OP- PE)^2+ PB^2$

$R^2= (R-t')^2 + r_n^2$

$R^2= R^2- 2Rt' + t'^2 + r_n^2$ .....(3.3)

But t' is very small in comparison to R so we can neglect the term t'^2. Therefore

$2Rt' = r_n^2$

$$or, t' = \frac{r_n^2}{2R} \quad \text{.....(3.4)}$$

Now if we set a thin film of uniform thickness between the lens and the glass plate as shown in fig.3.6b, then due to the film thickness t the thickness of the air film will be increased by an amount t and the ring for film thickness t will be formed at another point B' closer to the contact point P and in that case we get

$$t' = t + t'' = \frac{r_n^2}{2R} \quad \text{.....(3.5)}$$

And

$$t'' = \frac{r'^2_n}{2R} \quad \text{.....(3.6)}$$

Where r_n' is the radius of the ring at point B'. Subtracting (3.6) from equation (3.5) we get

$$t = \frac{r_n^2 - r'^2_n}{2R} \quad \text{.....(3.7)}$$

Thus measuring the radius of nth ring without film and with film we can calculate the thickness of the film using equation (3.7).

The radius of the ring of selected colour has been measured by measuring the chord length, and the perpendicular distance between the mid point of the chord to the midpoint of the arc intersected by the chord. A travelling microscope has been used for this purpose. An extra device with adequate travelling facility and micrometer has been attached to the vertical arm of the microscope so that it can move in YOY$^{/}$ direction in addition to XOX$^{/}$ direction. Movement in the ZOZ$^{/}$ direction is also kept functioning. If l is the length of the chord and h is the perpendicular distance then the radius can be measured using the relation

$$r = \frac{l^2}{8h} + \frac{h}{2} \quad \text{.....(3.8)}$$

3.12 Structural measurement

Scanning electron microscope (SEM) and X-ray diffraction measurements were made to determine the structure of CdS and X-ray diffraction was used to determine the structure of CuO thin films.

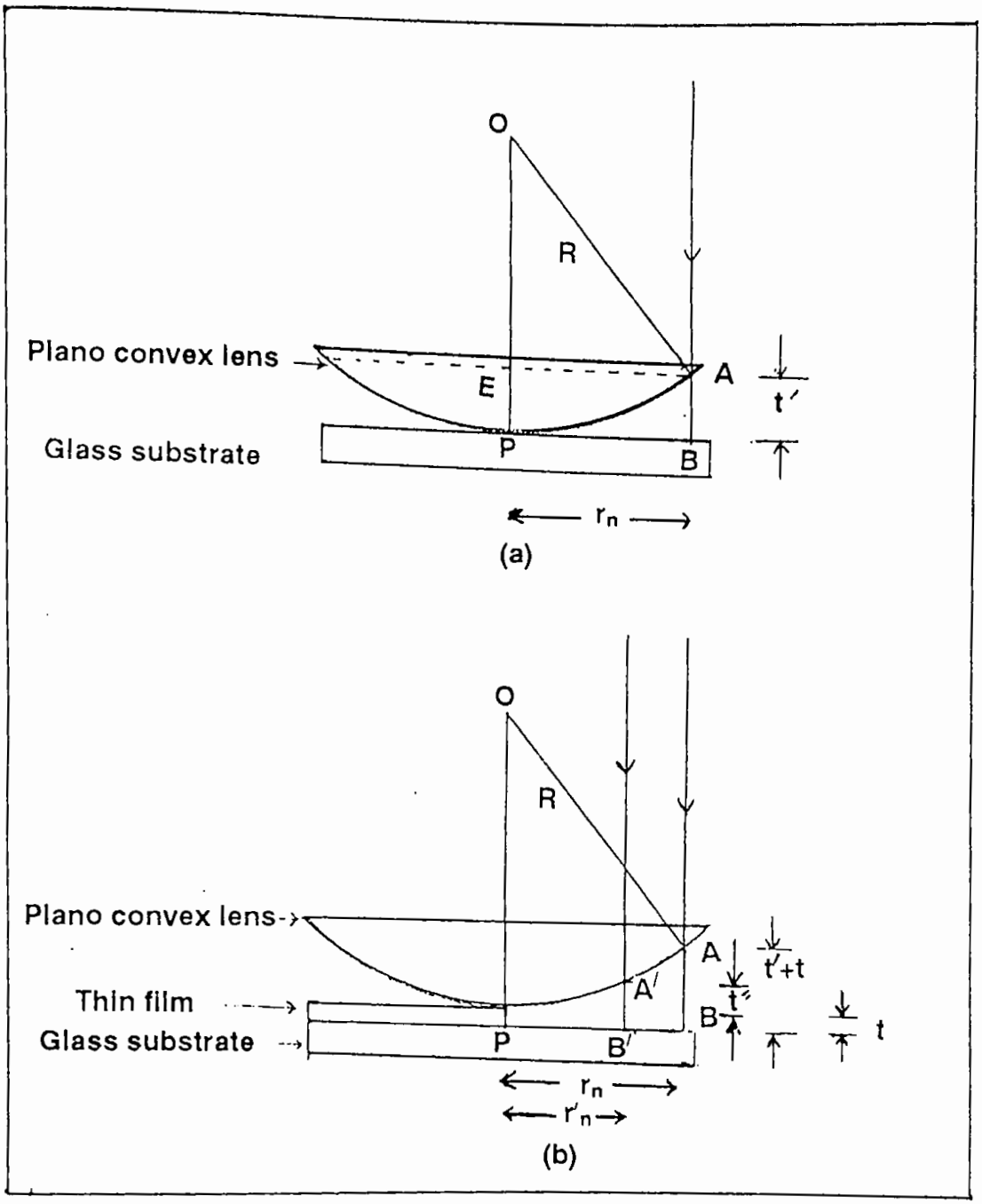

Fig. 3.6 Schematic diagram for measurement of film thickness by Newton's ring method (a) arrangement without film (b) arrangement with film.

3.13 Resistively, Hall mobility and carrier concentration measurement

For thin film samples Van der pauw's method[10] is used most extensively for the measurement of resistivity and Hall constants and we have followed this method throughout the work.

Using this method, both resistively and Hall constant can be obtained from measurement on any uniform sheet of material of arbitrary shape with four small contacts applied to the periphery. Figure 3.7 shows the Vander pauw's specimen with four smalls contacts A, B, C and D in order. 1,2,3 and 4 are terminals of the electrometers that measure voltages and currents. Digital multimeters were used for this purpose. The arrows indicate commutating switches, which can make concoctions between the film and meter terminals. If a dc current I_{AB} entering the specimen through the contact A and leaving it through the contact B produces a potential difference V_{CD} between the contacts D and C then $R_{AB,CD}$ is defined as V_{CD}/I_{AB}. Similarly, $R_{BC,DA}$ is defined as V_{DA}/I_{BC} and $R_{BD,\,AC}$ as V_{AC}/I_{BD}. $\Delta R_{BD,\,AC}$ measures the change in $R_{BD,AC}$ due to the application of magnetic field B. For a plate of arbitrary shape and of constant thickness t, the resistivity and Hall constant are given by the expression

$$\rho = \frac{\pi t}{\ln 2}\left(\frac{R_{AB,CD} + R_{BC,DA}}{2}\right) f\left(\frac{R_{AB,CD}}{R_{BC,DA}}\right) \qquad \text{.....(3.9)}$$

And the Hall constant

$$R_H = \Delta R_{BD,AC}\left(\frac{10^8 t}{B}\right) cm^3 C^{-1} \qquad \text{.....(3.10)}$$

Where the magnetic field B is in Gauss and film thickness t is in cm. The function of can be evaluated from

$$\frac{R_{AB,CD} - R_{BC,DA}}{R_{AB,CD} + R_{BC,DA}} = \frac{f}{\ln 2} arc.\cosh\left\{\frac{\exp\left(\frac{\ln 2}{f}\right)}{2}\right\} \qquad \text{.....(3.11)}$$

The function f of this equation depends only on the ratio $R_{AB,CD}$ / $R_{BD,DA}$. Figure 3.8 shows in graphical form, the dependence of f on the ration $R_{AB,CD}/R_{BC,DA}$.

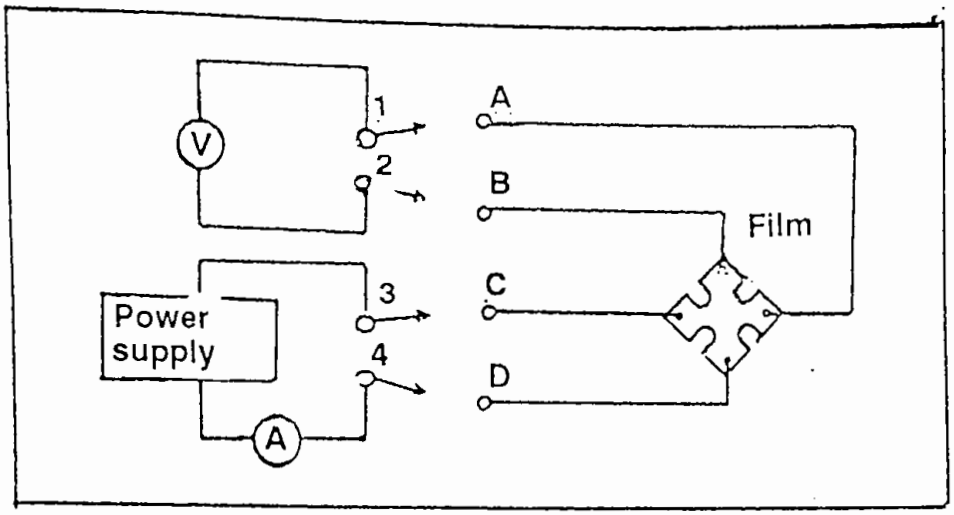

Fig. 3.7 Schematic diagram for the measurement of film resistivity. 1, 2, 3 and 4 are meter terminals and A, B, C and D are the film terminals. Arrows indicate commutating switches.

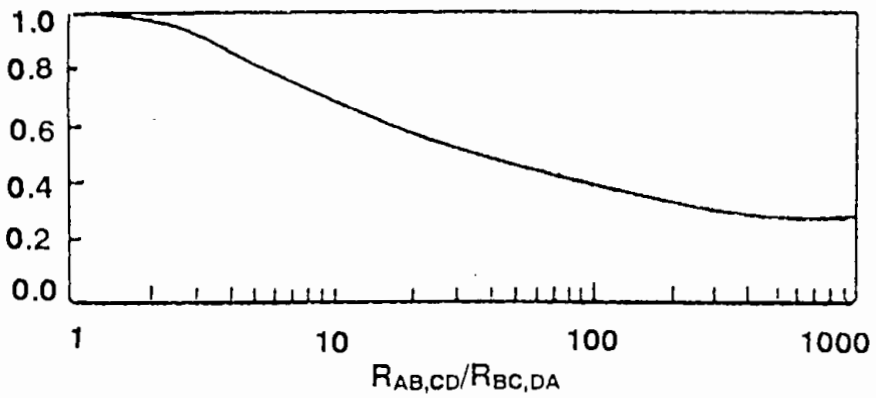

Fig. 3.8 The dependence of function f on the resistance ratio $R_{AB,CD}/R_{BC,DA}$.

The shape of the sample is taken in the form of a "quatrefoil leaf" so as to eliminate the influence of contacts and to keep the ration $R_{AB,CD}/R_{BC,DA}$ approximately equal to unity. Under this condition the resistively ρ if given by

$\rho = 2.266t\,(R_{AB,CD} + R_{BC,DA})$ ohm-cm ..... (3.12)

The magnetic field B is always perpendicular to the plane of the sample.

The Hall mobility μ and the carrier concentration n can then be calculated from the relation $\mu = R_H/\rho$ $cm^2V^{-1}sec^{-1}$ and $n = 1/R_H e$ cm^{-3}. In calculating ρ, appropriate correction factor evaluated form figure 3.8 was used where it was necessary.

3.14 Measurement of resistivity with temperature

The work presented in this thesis includes some measurements performed at temperatures ranging from room temperature upto about 250°C. For all such measurements a nichrome wire flat heater 2.5x5 cm^2 in size and properly insulated by mica sheet in conjunction with thick aluminum heat sink (4mm) has been used. The temperature of the surface of the heat sink could be kept constant for a considerable time. Applying voltages from 5 to 50 volts a.c. across the heater coil, temperature could be varied from room temperature to about 280°C. the temperature of the specimen was measured by a copper-constantan thermocouple.

3.15 Measurement of thermoelectric power

The experimental set up for the measurement of thermoelectric power of CdS and CuO thin films are given in fig. 3.9. The mask and the substrate geometry for the film preparation also showed in Fig. 3.3(c).

Integral Method[17] was used as technique for measurement of seeback co-efficient. In this method one end of the specimen was held at ice temperature and the other end is heated to a temperature T which is made to vary over the temperature range 30°C to 100°C for CdS (and upto 175°C for CuO). An appropriate heat insulating barrier E was inserted between the hot and cold ends to minimize heat radiation form the hot to the cold end. The temperature of the sample was varied by a small heater and the emf was measured by a digital multimeter (Backma Industrial, Model D.M. 10 XL). Thermocouple voltage was measure by a digital multimeter (Model 775).

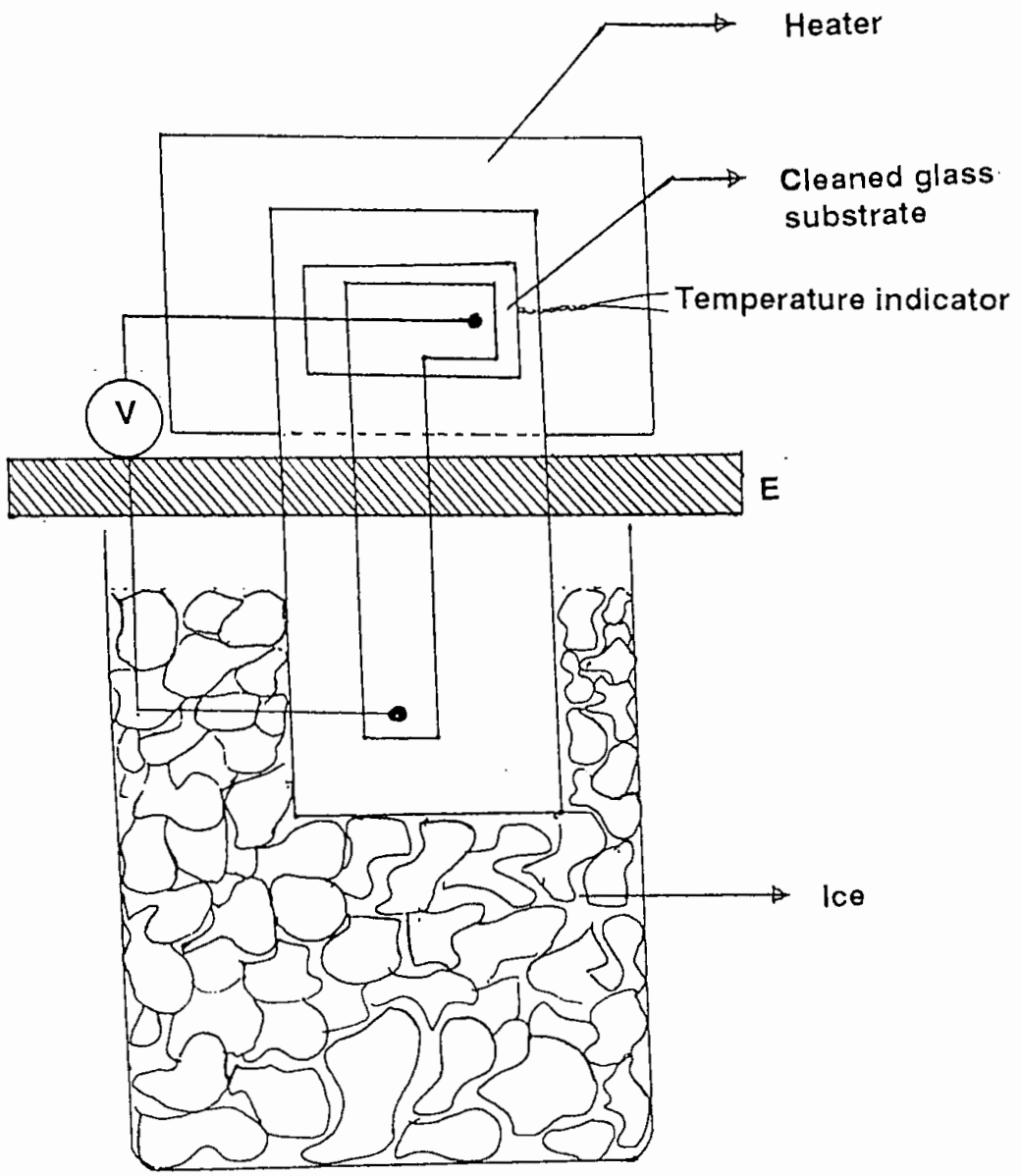

Fig. 3.9 Experimental arrangement for thermoelectric power measurement.

The temperature of the hot junction was raised slowly by definite intervals and when the temperature of each of these points become steady the thermo-emf was noted from the electrometer attached to the terminals.

3.16 Post-deposition heat treatment experiments

For thin film devices the temperature stability and reproducibility of the film properties are very important for the device operation and reliability. For the fabrication and optimization of electronic devices it has been observed that a common process of heat treatment often comes in the way. Polycrystalline CdS and CuO films deposited in the vacuum are very sensitive to post-deposition heat treatments especially in the case of films deposited by pyrosol process. Therefore studies on post-deposition heat treatment of these samples (CdS and CuO) are necessary for proper understanding of the behavior of the deposited films under thermal cycling.

For the heat treatment experiments the sample immediately after its deposition was cooled down to room temperature, and was kept in desecrator. Heat treatment operations were performed in air

(i) at normal pressure, and

(ii) In vacuum of the order of ~ 10^{-3} torr. By heat treatment we mean a heating cycle from room temperature to 250°C followed by a cooling cycle back to room temperature in the same ambient. Heating temperature was raised at an average rate of ~10°C/ min up to a maximum temperature of 250°C at which the sample was kept for an hour before the commencement of the return operation of cooling. Cooling rate was maintained almost the same as that of heating. Resistivity and Hall constants were the main objects of study in this experiment. Optical transmission of the films was also studied before and after the heat treatment operation.

3.17 Measurement of optical transmission

3.17.1 Absorption co-efficient

For optical measurement, at first transmittance was measure using a double beam spectrometer (shimadzu UV-180, Japan) in the wavelength range 312-900 nm. The sample with the substrate was placed in the incident beam and another empty substrate was in the reference beam of the instrument. The optical transmittance T

of the films with respect to glass substrate was then directly measured for different wavelength λ.

Absorption coefficient (α) was measured using the relation

$$\alpha = (\log_e T)/t \quad \text{.....(3.13)}$$

Knowing the value of film thickness t and transmittance T of the corresponding wavelength we can be determine the absorption coefficient α and band gap E_g.

3.17.2 Energy gap determination

According to Bardeen et al.[18] the relationship that exist for possible transmission across the energy gap of the semiconductor show that the absorption coefficient α is given by the following expression for conditions[19]

(1) Direct transmission:

$$\alpha h\nu = A^*(h\nu - E_g)^n \quad \text{.....(3.14)}$$

Where n=1/2 for allowed transitions and n=3/2 for forbidden transitions.

(2) Indirect transition:

$$\alpha h\nu = A(h\nu - E'_g + E_p)^n \quad \text{.....(3.15)}$$

Where n=2 for allowed transitions and n=3 for forbidden transitions. E_g is the energy for direct transitions, E'_g the energy for indirect transition and E_p the energy of photon absorbed (+) or emitted (-). By plotting graphs of $(\alpha h\nu)^{1/n}$ against $h\nu$ for various n gives above it is possible to determine which of this conditions dominate, and hence to determine the appropriate energy gap of the sample.

3.18 Measurement of current-voltage (I-V) characteristics

To obtain the current-voltage (I-V) characteristics of the heterojunction, two different methods can be used;(a) the x-y plotter for continuous recording of the I-V characteristics, and (b) the digital method of current and voltage reading throughout the observation.

The advantage of using x-y plotter is that the I-V characteristic is plotted in a relatively short time. In the digital method, the I-V characteristics of the heterojunction have to be drawn by hand and the measurement time is longer. As the facilities for the x-y plotter were not available, the digital method was used in the present work to obtain all the I-V characteristics. The current-voltage characteristics under dark were obtained.

3.18.1 Measurement of I-V characteristics using both forward and reverse bias

Figure 3.10 illustrates the experimental arrangement for the measurement of dark I-V characteristics of the junctions. A Heathkit regulated low voltage power supply unit was used as the d. c. source. A digital multimeter (Beckma Industrial digital multimeter model D.M. 10 XL) has measured the current and a digital multimeter model, DMM 775, measured the voltage. The junction was covered with black cloth during the measurement. Bias voltages from 0 to 1 volt were applied.

To obtain the reverse characteristics, the polarity of the power supply was changed to reverse bias the junction.

3.18.2 Measurement of forward and reverse resistance of p-n junction

One of the most important properties of the p-n junction is its resistance in the forward and reverse bias. An ideal junction must offer zero resistance in forward bias and infinity large resistance in reverse bias. Here we consider the two resistances i.e., one d.c. Resistance and the other a. c. resistance or dynamic resistance. The equivalent circuit for the junction is shown in fig. 3.11, where R_p and R_n are the resistance of p and n materials respectively.

The junction voltage is given by

$$V=V_1-I(R_n+R_p) \quad .....(3.16)$$

The d.c. resistance is given by

$$V_1/I=V/I+R_n+R_p$$

or, $$R_{d.c.}= r_{d.c.}+ R_n+R_p \quad .....(3.17)$$

where $r_{d.c.}$ represents the d.c. resistance of the part of the junction. The value of $r_{d.c.}$ Is given by[20]

$$r_{d.c.} =V/I=V/\{I_o[\exp.(eV/K_BT)-1]\} \quad .....(3.18)$$

The a.c. resistance ($r_{a.c.}$) of the junction is given by

$$r_{a.c} = dV/dI=1/(dI/dV) \quad .....(3.19)$$

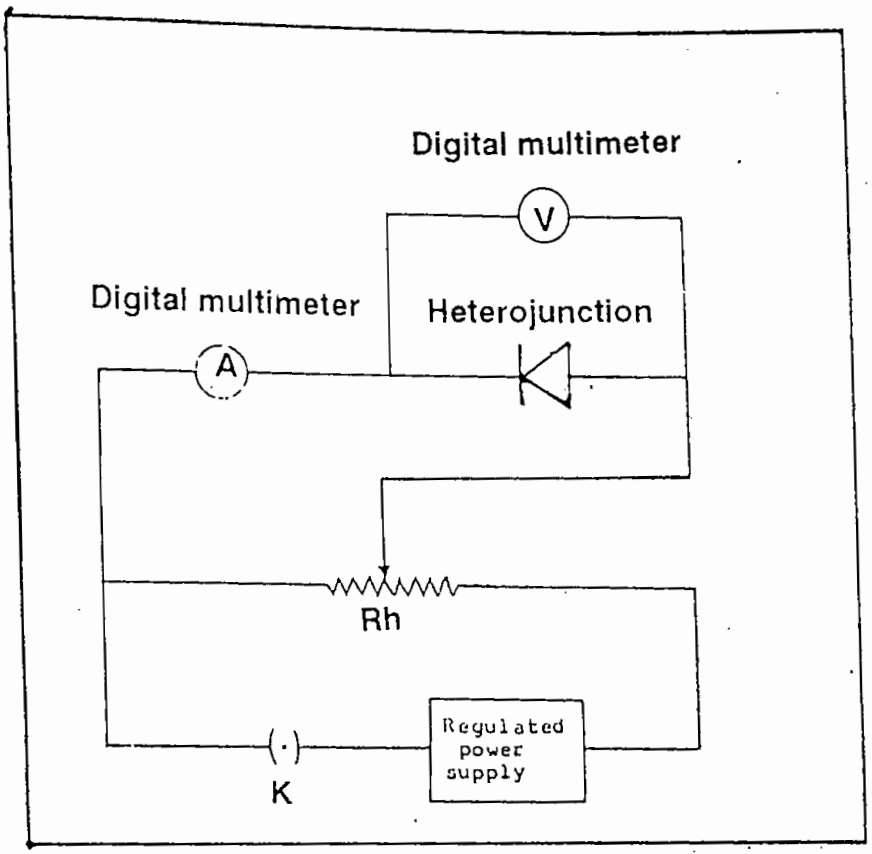

Fig.3.10 Schematic circuit diagram for the measurement of I-V chacacteristics.

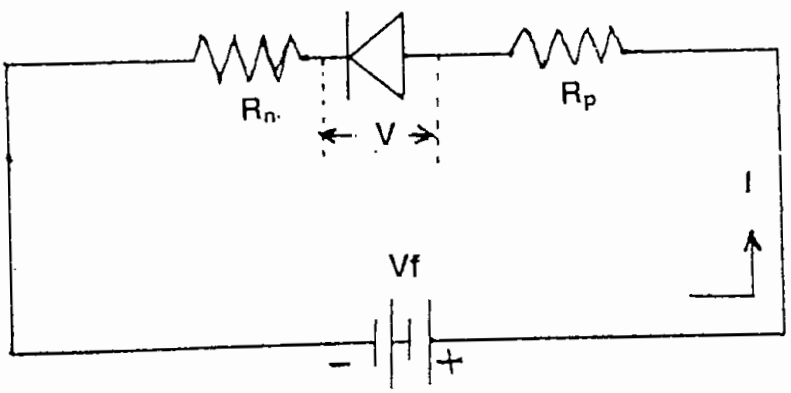

Figure 3.11 The equivalent circuit of a diode.

References

1. R.R. Chamberlin and J.S.Skarman, J. Electrochem. Soc., 113 (1966) 86.
2. B.K. Gupta and O.P. Agnihotri, Solid State Commun., 23 (1977) 295.
3. E. Shanthi, V.Dutta, A.Banerjee and K.L. Chopra, J. Appl. Phys. , 51 (1980) 6243.
4. J.C. Manifacier, N.De Nurcia and J.P. Fillard, Mat. Res. Bull., 10 (1975)1215.
5. M.S. Tomar and F.J. Garcia, Prog.Cryst. Growth Chract., 4 (1981) 221.
6. J.Aranovich, A. Ortiz and R.H. Bube, J.Vac. Sei. Techol., 16 (1979) 994.
7. S. Kulaszewicz, Thin Solid Films, 74 (1980) 211.
8. G. Blandenet, N. Court and Y.Lagarde, Thin Solid Films, 77 (1981) 8.
9. M.N. Islam and M.O. Hakim, J. Phys. Chem. Solids, 46(3) (1985) 339.
10. L. J. Vander Pauw, Philips Res. Rept., 13 (1955) 1.
11. C.H. Wu and R.H. Bube, J. Appl. Phys., 45 (1974) 648.
12. M. Savelli and J. Boughnet: Second Int. Symp. on N.G.E., TRIESTE (Italy) 124 (1977) 1430.
13. J.E. Hill and R.R. Chamberlin, United States Pat., 3 (1984) 148.
14. K.Blodgett and I. Langmuir, Phys. Rev., 51 (1937) 964.
15. S. Tolansky, "Multiple Beam Interferometry of Surfaces and Films." (Oxford University Press, 1948).
16. J.G. Gottling and W.S. Nicol, J. Opt. Soc. Am., 56 (1966) 1227.
17. A. Boyer, B. Deschacht and E.Graubert, - Thin Solid Films, 76 (1981) 119.
18. Barden, J. Blatt, E.J., and Hall, 2.H., 1965, Phot0o conductivity conference. eds. R., Breekerridge, B. Russal and E.Halmn (New Youk).
19. P.A. IEE. and G.A. Said Brit., J. Appl. Phys., 2 (1968) 837.
20. S. L. Gupta and V. Kumar, "Hand Book of Electronics" (Revised and Enlarged Thirteenth Edition 1985) Pragati Prakashan, Meerut, India.

CHAPTER FOUR

RESULTS AND DISCUSSION

RESULTS AND DISCUSSION

4.1 Studies on CuO thin films

In this part of the chapter the results of the various experimental investigations such as on growth, structural, electrical and optical properties of CuO thin films have been presented. The details of the experimental techniques for these studies have already been given in the previous chapter.

Samples were prepared under different deposition condition such as i) keeping the solution concentration and spray time fixed and varying the substrate temperature, ii) keeping solution concentration and substrate temperature fixed and varying spray time iii) keeping spray time and substrate temperature fixed and varying the solution concentrations. Results obtained on the films deposited under three conditions have been presented and discussed.

4.1.1 Physical growth rate

The effects of substrate temperature, deposition time and solution concentration on the thickness of the deposited film have been shown in fig.4.1.1, where the "film growth rate" have been plotted in place of thickness. We can observe that film growth rate decreases with the time of spray although the gross thickness of the film, t, increases with time. This implies that on a clear glass substrate films can grow more easily at the initial stage of deposition. But as the deposition progresses subsequent layers can grow with a slower rate. Film thicknesses decrease at higher substrate temperature, and increase with the solution concentration when sprayed for a constant time.

4.1.2 Structural properties

X-ray diffraction patterns of the films prepared at substrate temperature T_S=175°, 200° 225° and 275°C are given in fig.4.1.2a, 4.1.2b, 4.1.2c and 4.1.2d respectively. The XRD shows fine crystalline structure with clear characteristic peaks of CuO phase in all the samples as we find it by comparison with standard XRD patterns of the pure CuO material. Some of the peaks were common to both the Cu_2O and CuO phases but as we know chemical reaction of cupric chloride with H_2O does not favour Cu_2O formation in this spray condition ,the possibility of Cu_2O formation is thus very small. In a defect lattice however there may be a small fraction of other phases but they are nondeliberate and may be considered as crystal imperfections. Cu_2O has a prominant peak at 2θ=36.45° which we do not find in any of our samples. The CuO (111) reflection at 2θ=35.495° ,observed with the highest intensity, in addition to all the other peaks of CuO phase confirms that the crystal lattice is mainly copper(II) oxide. The structure is monoclinic with lattice parameters a=4.704Å, b=3.414Å and c=5.004Å.

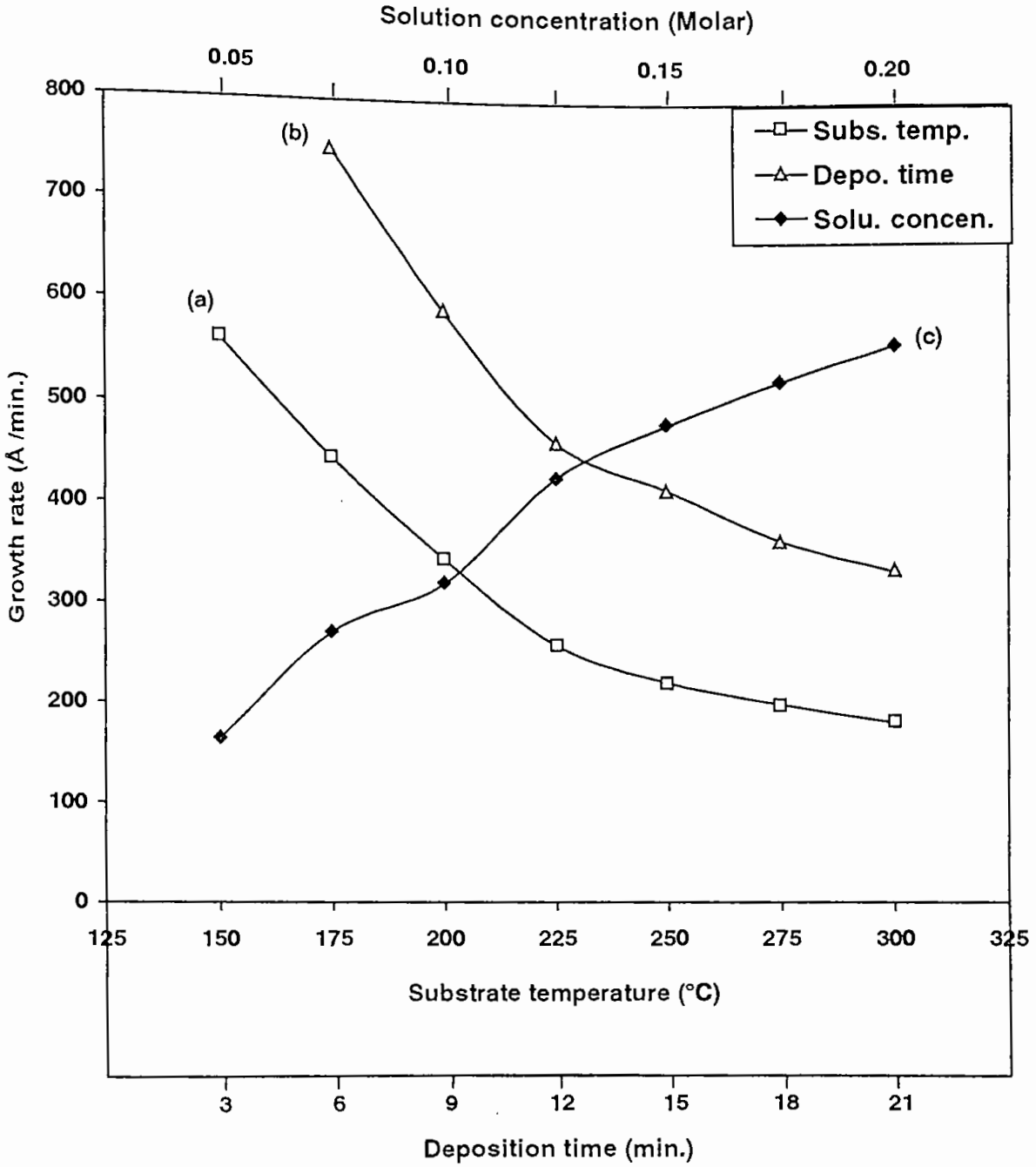

Fig. 4.1.1 Variation of film growth with (a) substrate temperature (b) deposition time (c) solution concentration .

4.1.3 Electrical properties

4.1.3.1 DC Conductivity and Hall effect

Electrical conductivity of the samples was measured both in the as-deposited and in the annealed condition. Annealing was performed in vacuum by heating the samples at a constant temperature of 150°C for an hour and then slowly cooled down to room temperature. Fig.4.1.3 shows the resistivity, ρ, versus thickness, t, and ρ versus T_S plots for a set of films at room temperature. Films deposited at higher substrate temperature have relatively low resistivity. Resistivity slightly increases with film thickness but it remains almost constant above 4000Å, and this may be the optimum thickness for bulk properties to appear in these samples. Resistivity values were between 30 to 120 Ω-cm ,and annealing only lowers this value slightly.

Variation of resistivity with temperature has been studied in the temperature range 293K to 403K in vacuum. ρ were found to decrease with the rise of temperature showing a negative temperature coefficient for all the films. Fig.4.1.4 and fig.4.1.5 show the variation of resistivity with temperature for films deposited with different thickness at constant substrate temperature and for films deposited at different substrate temperature respectively. Heating and cooling cycle did not show much discripancies. Fig.4.1.6 shows the plot of log conductivity against inverse of temperature for a set of samples with varying thickness, deposited at 200°C. The curves fitted to $\sigma = \sigma_o \exp(-E_\sigma/kT)$ show a single activation energy ,$E_\sigma \sim 0.13$ eV in the investigated temperature range, and the variation of thickness has a small effect on this energy. This is true for the annealed films as well. Values of thermal activation energy normally depends on the grain size and other defects in the crystalline phase. However similar values of activation energy, 0.14eV in the low temperature range have been reported by Drobny at al.[1] for reactively sputtered CuO films. Dc reactive ion sputtering of CuO films have activation energy higher than this while textured CuO films show activation energy of ~0.088eV [2].

Hall effect studies show a positive Hall constant at room temperature and all the samples can be considered p-type having carrier concentrations in the range $\sim 10^{15}$ to $\sim 10^{16} cm^{-3}$. Hall mobility has a very small value, μ_H=2 to20 $cm^2/V.sec$ in samples of thicknesses above 3000Å. It has been observed that when films are prepared using solutions of lower concentration and thickness is kept below 3000Å, μ_H is greatly enhanced,~120 $cm^2/V.sec$, without any substancial increase of the carrier concentration. It has been widely believed that in CuO thin film excess oxygen ions, or copper ion vacancies in the lattice site are the main sources of

acceptors which produces p-type conductivity[2,3] . On the other hand oxygen ion vacancy or excess copper ion in the interstitial position can act as donors. In addition to those centres Cl^- ions coming from the spray solution can also work as donors. In spray deposited films all types of such defects may be present, but their relative concentration depends remarkably on the physical stoichiometry of the sample and the preparation condition. Carrier concentration and Hall mobility of CuO films prepared under different physical conditions are given in table 1.

Table-1: Values of Hall mobility and carrier concentration of CuO films at the room temperature with different deposition parameter.

Thickness (Å)	Substra. temp. (°C)	Slution concen. (M)	Hall mobility (cm^3/V-sec.)		Carrier concentration x(10^{16} cm^{-3})	
			As deposited	Annealed	As deposited	Annealed
2256			2.449	2.538	7.258	7.655
4117			3.873	2.829	2.097	3.036
4224			1.016	11.77	9.416	1.070
5239	200	0.20	1.271	3.544	5.965	2.505
5484			3.297	2.173	2.513	4.057
5904			4.155	2.455	1.638	3.131
5644	150		2.481	8.142	2.221	0.763
5252	175		7.959	3.451	0.793	1.696
5103	200		31.67	16.45	0.204	0.320
4460	225	0.20	21.51	36.21	0.252	0.165
2775	250		17.53	84.30	0.888	0.234
3439	300		10.34	12.40	1.288	1.478
2152		0.05		124.3		0.102
2441		0.10	110.4	104.6	0.221	0.173
2641	200	0.15	123.9	51.71	0.108	0.164
2419		0.20	38.82	117.6	0.322	0.014

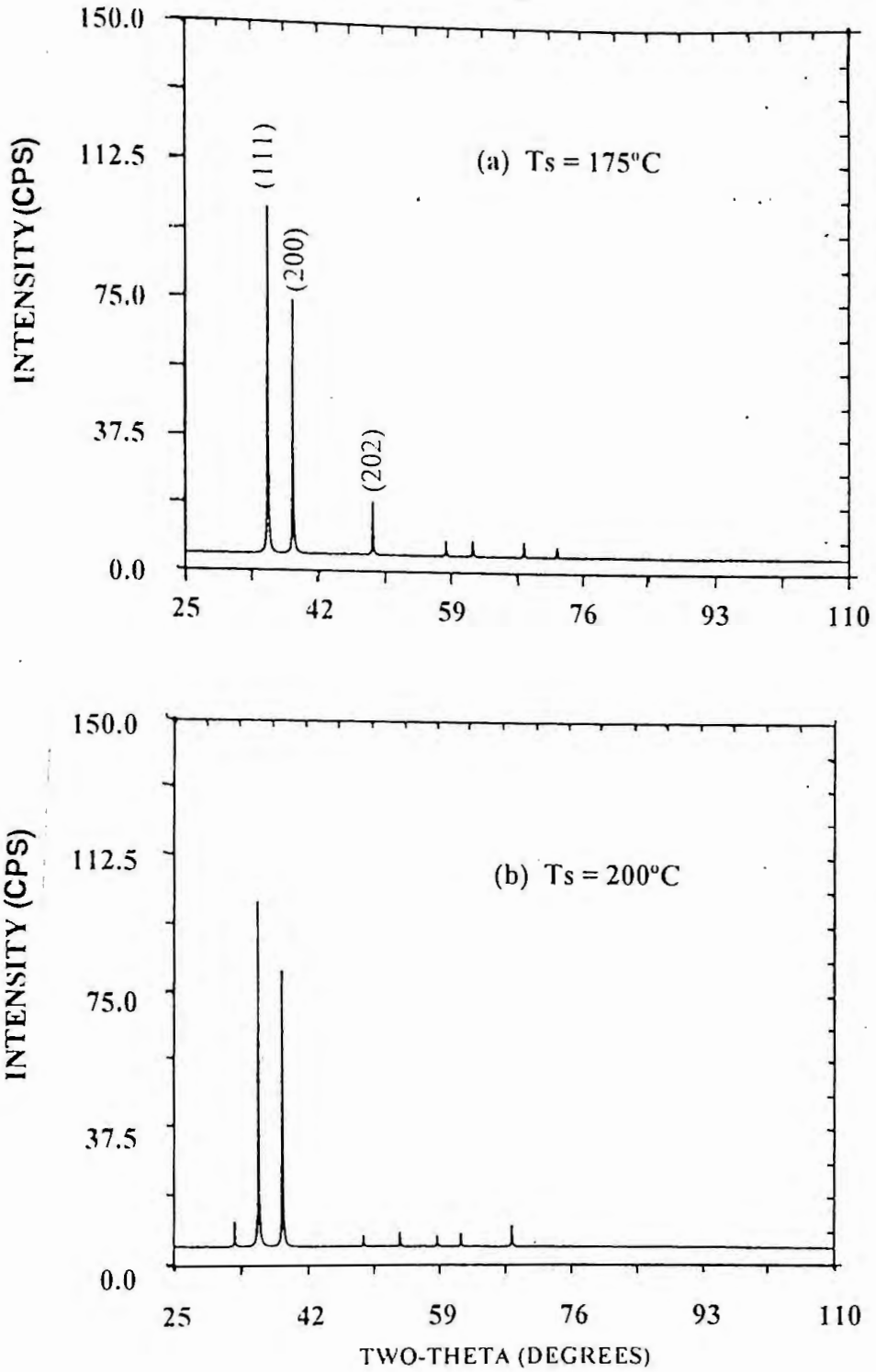

Fig. 4.1.2 (a & b) X-ray diffraction patterns of CuO films prepared at different substrate temperature: (a) Ts = 175°C (b) Ts = 200°C.

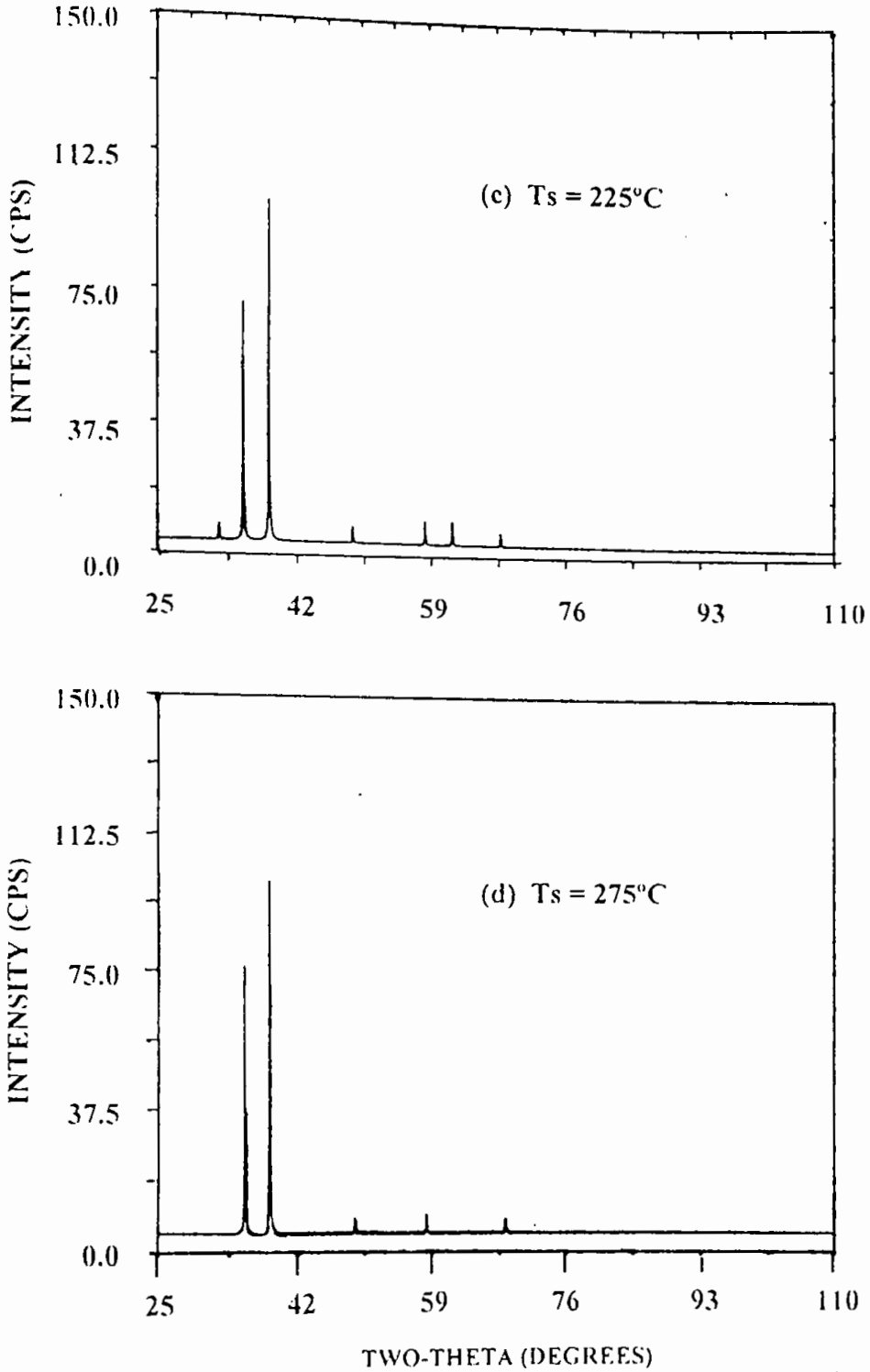

Fig. 4.1.2 (c & d) X-ray diffraction patterns of CuO films prepared at different substrate temperature: (c) Ts = 225°C (c) Ts = 275°C.

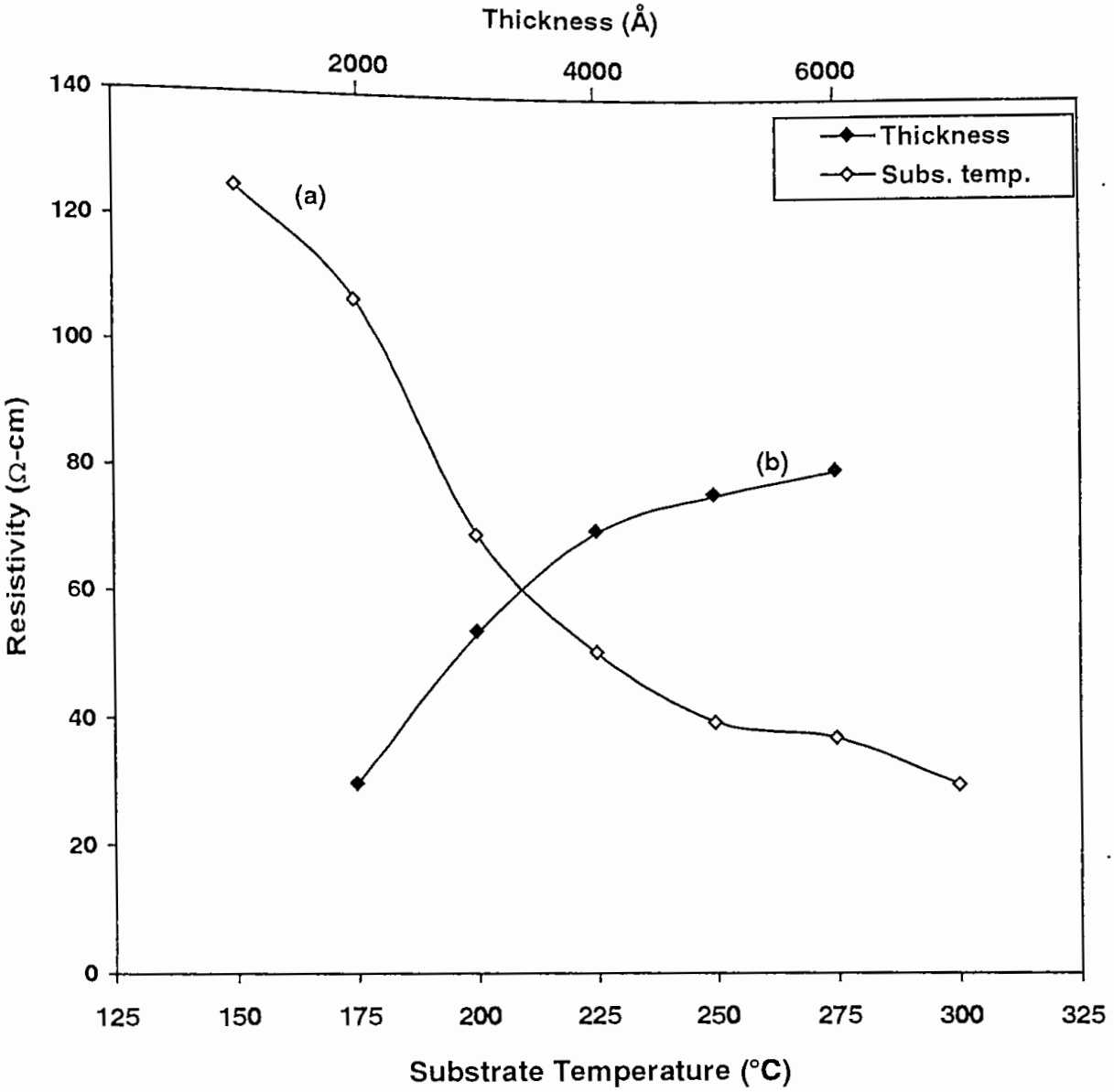

Fig. 4.1.3 Resistivity with (a) substrate temperature (b) thickness of CuO films.

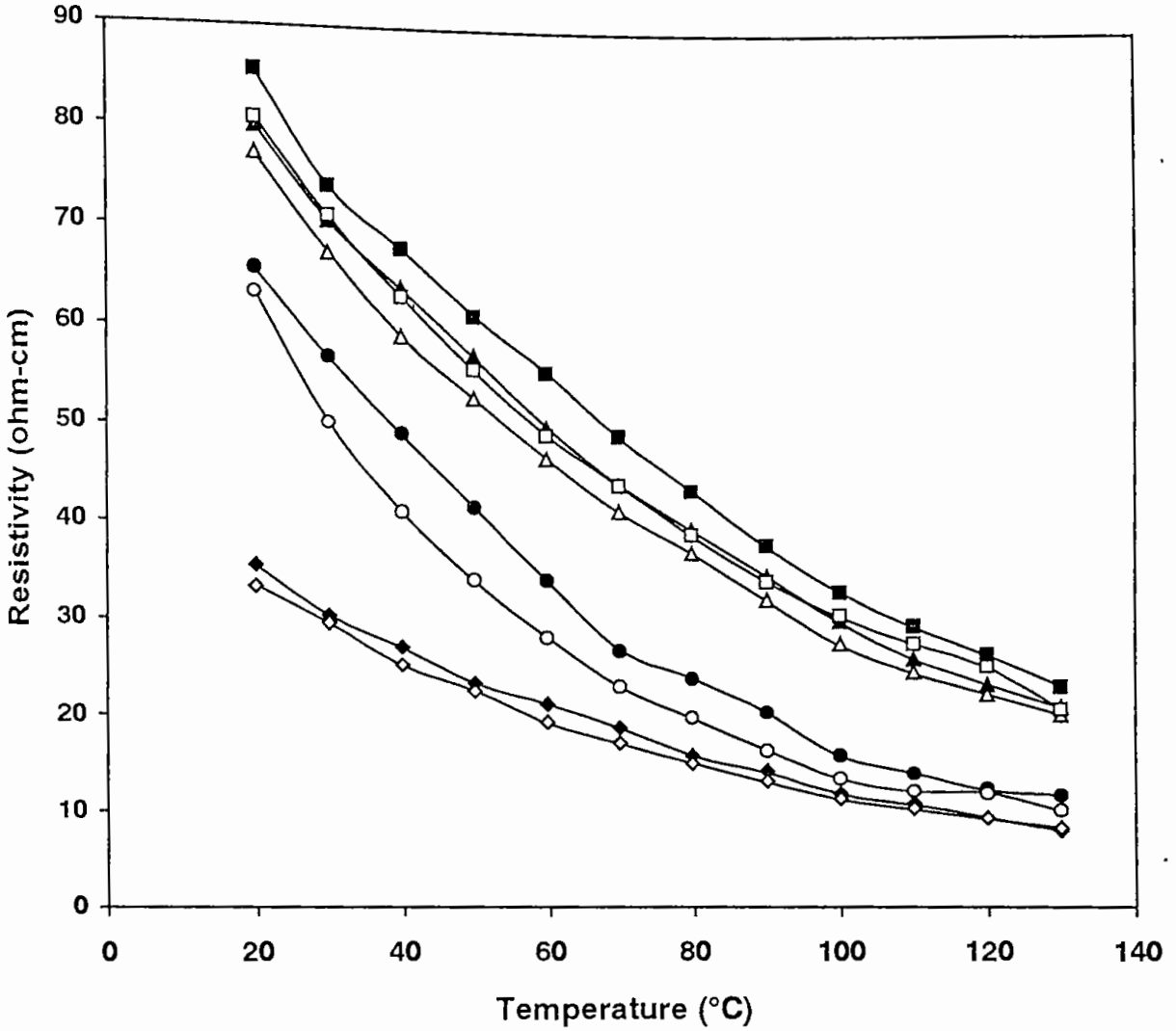

Fig. 4.1.4 Resistivity with temperature for different thickness both as deposited and annealed films of CuO.

i) t=2256Å as deposited annealed ii) t=4224Å as deposited annealed
iii) t=5239Å as deposited annealed., iv) t=5904Å as deposited annealed

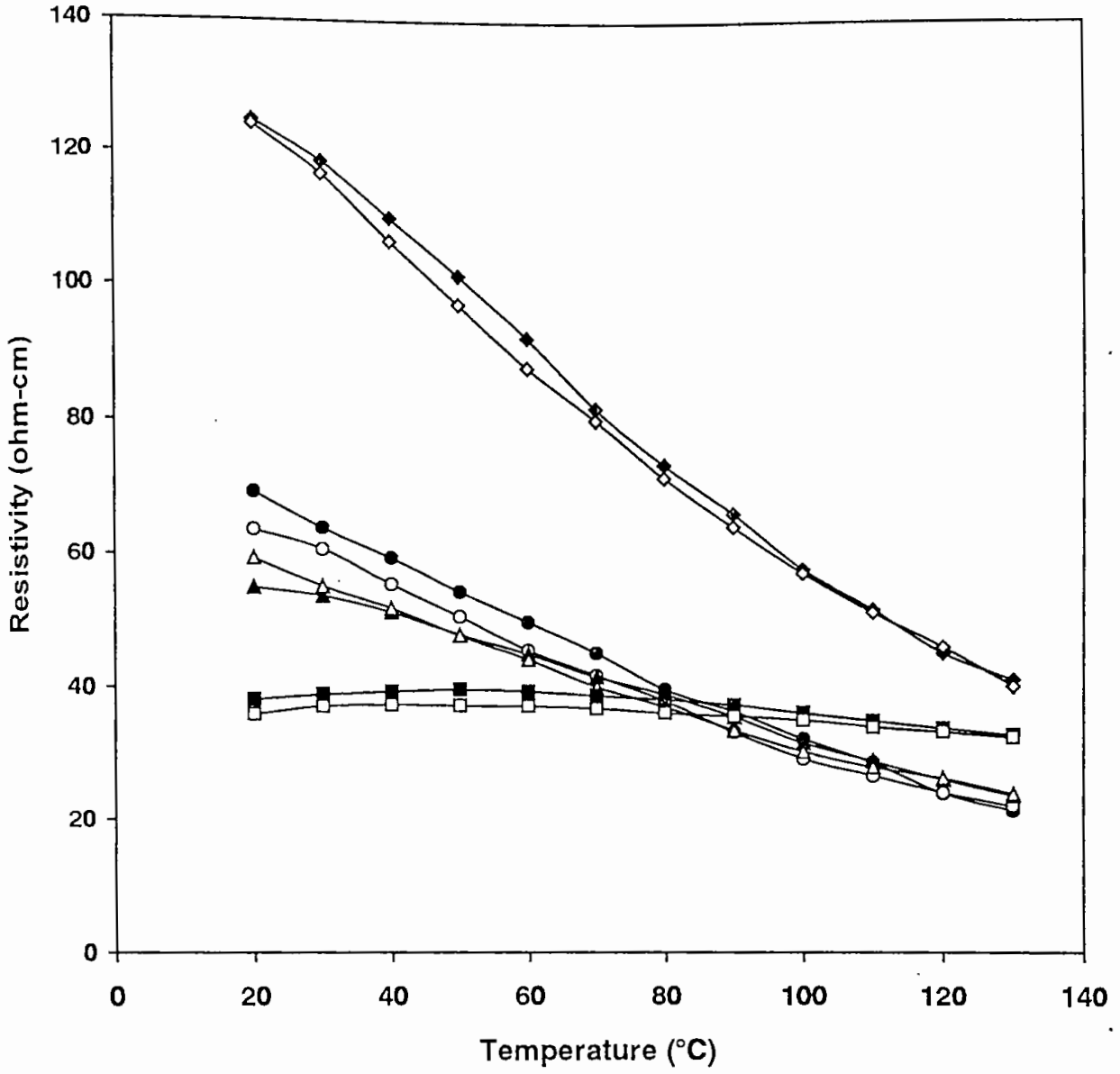

Fig. 4.1.5 Resistivity with temperature for films prepared at different substrate temperature. (as deposited and annealed films of CuO).

i) Ts=150°C as deposited annealed ii) Ts=200°C as deposited annealed
iii) Ts=250°C as deposited annealed., iv) Ts=300°C as deposited annealed

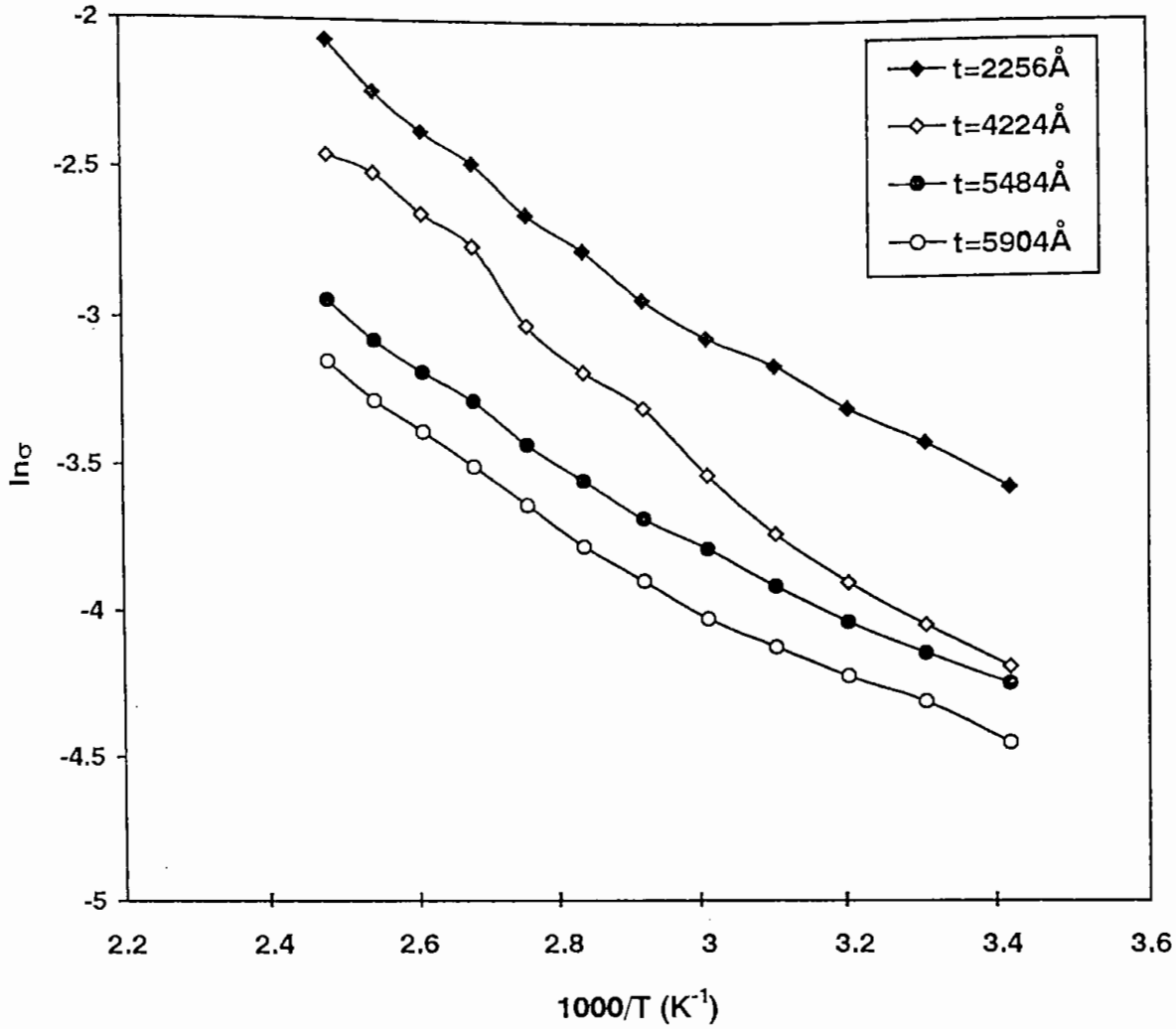

Fig. 4.1.6 lnσ versus 1/T for different thickness of annealed films of CuO.

4.1.3.2 Thermoelectic power (TEP)

Measurement of thermoelectric power was carried out by the so called integral method[4] viz holding the cold junction at a fixed reference temperature, 0°C, and varying the temperature of the other junction (upto 177°C). Reference metal was pure copper which has a negligibly low TEP value, in comparison to those of CuO samples (100 to 500 μV/K). Fig. 4.1.7 shows the thermo emf generated with temperature for a number of samples having different thickness. From figure it can be seen that thermo emf increases with temperature and also with the thickness of the films. Fig.4.1.8 shows a plot of TEP as a function of film thickness at three different temperatures. In the room temperature side strong thickness dependence is observed while at the elevated temperature only films of thickness below 4250Å show such thickness dependence.

Fig.4.1.9 shows TEP, Q versus 1/T plots for films of different thicknesses. It shows that TEP becomes almost temperature independent at higher temperature, which is a characteristic of the pinning nature of Fermi levels in these films. From fig.4.1.9 it is observed that the high temperature side of all the curves when extrapolated to 1/T = 0 give almost a common intercept on the ordinate and the value of A = 1.15 can be obtained. This shows that $s \approx 3/2$, and the predominant scattering mechanism is the lattice phonon scattering in the room temperature range, and Hall mobility $\mu_H \sim T^{-1.5}$ may be expected. From the slopes of π vs. T plot, as shown in fig.4.1.10, and using $A \sim 1$ in equation (2.34) values of γ and E(0) for the set of samples were calculated from the experimental values of π at room temperature. Now the values of Fermi levels E_F' can be calculated from equation (2.32), or E_F from relation $E_F'=-(E_g+E_F)$ by using the experimentally measured values of E_g. Obtained values of E(0), E_F', and γ for our samples are plotted as a function of inverse of film thickness,(1/t) in fig.4.1.11. From this figure we observe that the curves are almost straight line and the extrapolated values may correspond to the values of those quantities for the bulk CuO crystals having the same composition and structure as that of the films. We obtained E(0) =1.6eV, γ=- 4.15 meV/K,and E_F'=0.38eV above the valence band edge.

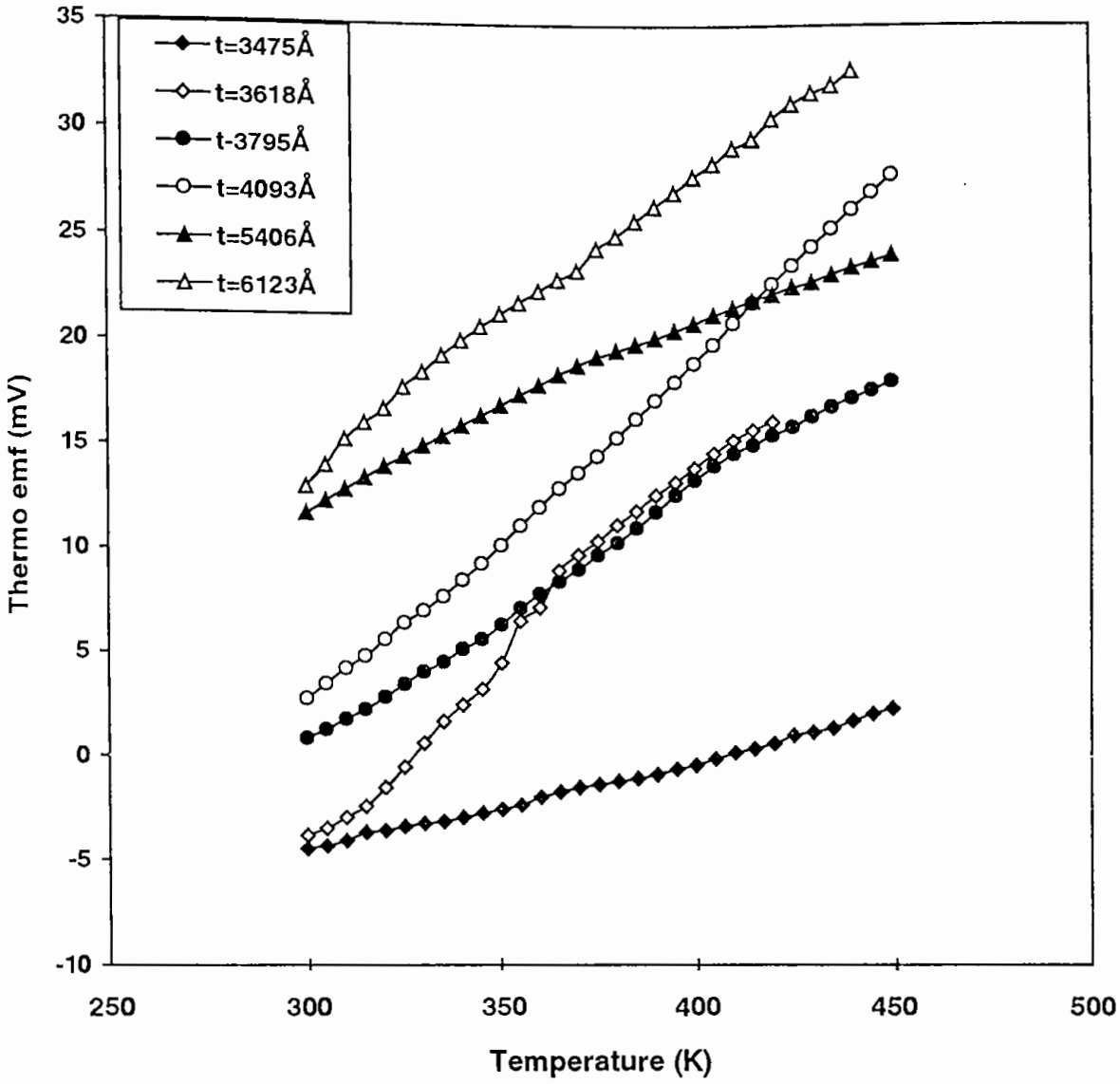

Fig. 4.1.7 Thermo emf with temperature for CuO films of different thickness.

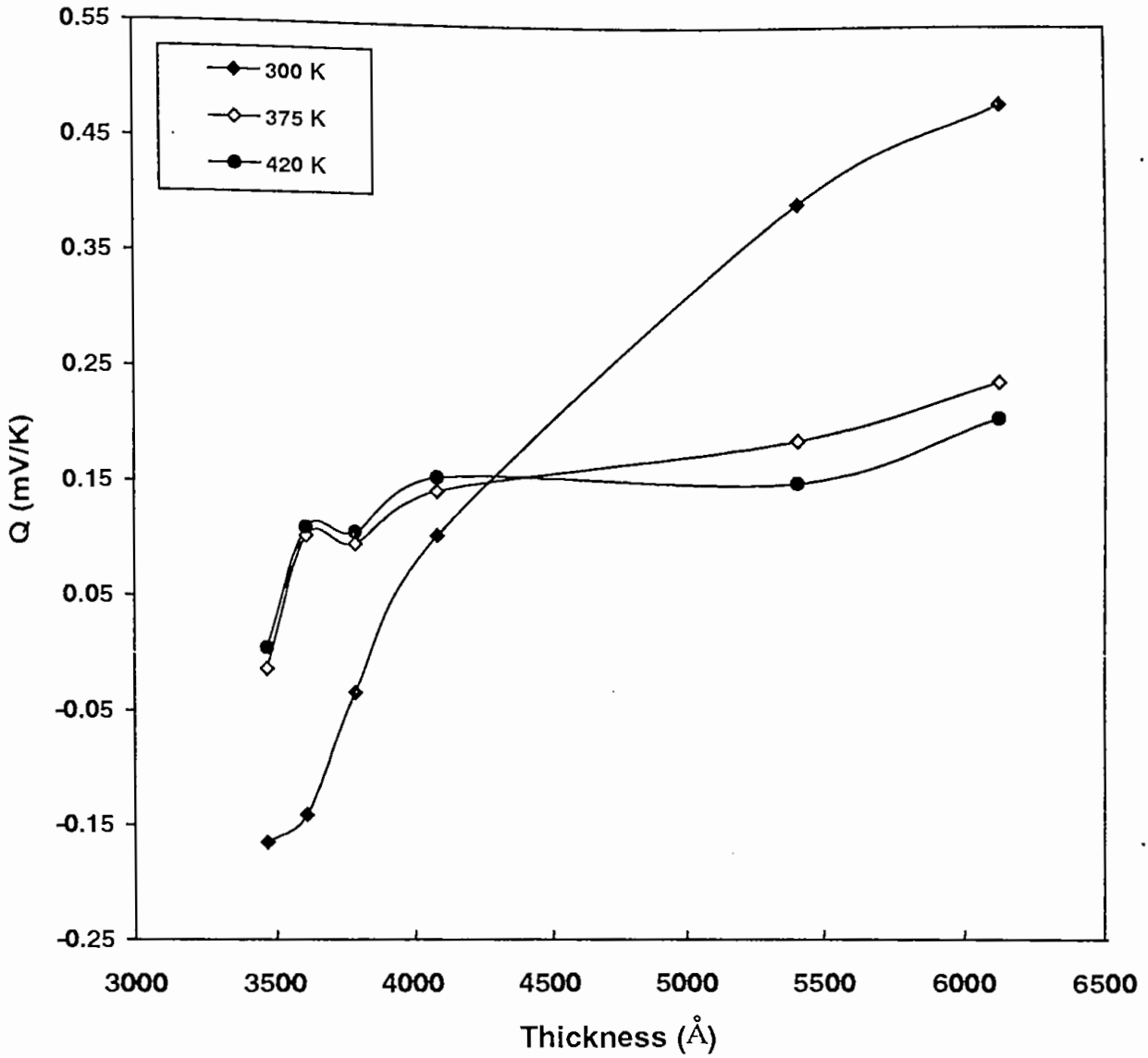

Fig. 4.1.8 Thermoelectric power with thickness at the three temperature for CuO thin films.

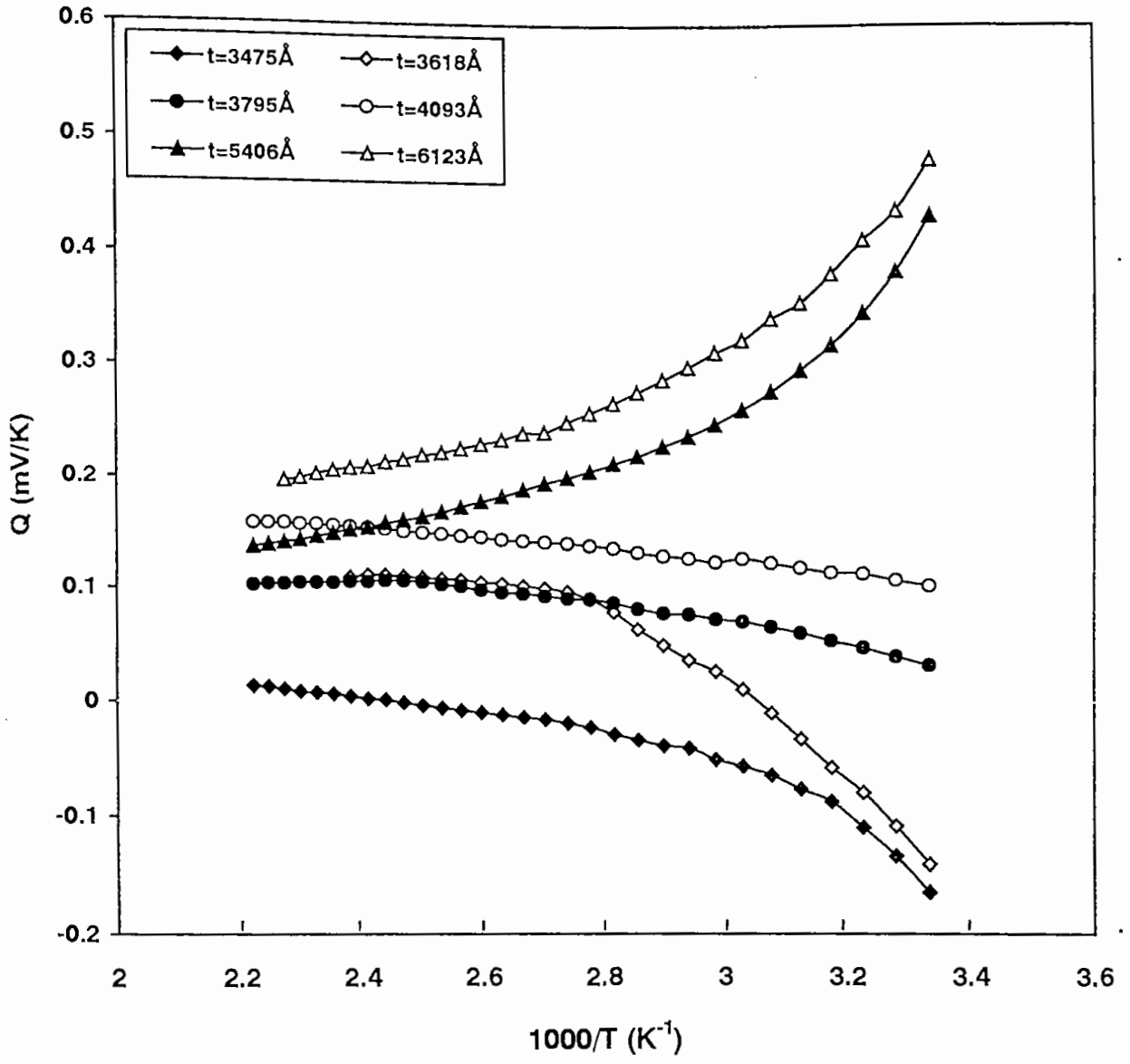

Fig. 4.1.9 Thermoelectric power with 1/T for different thickness of CuO films.

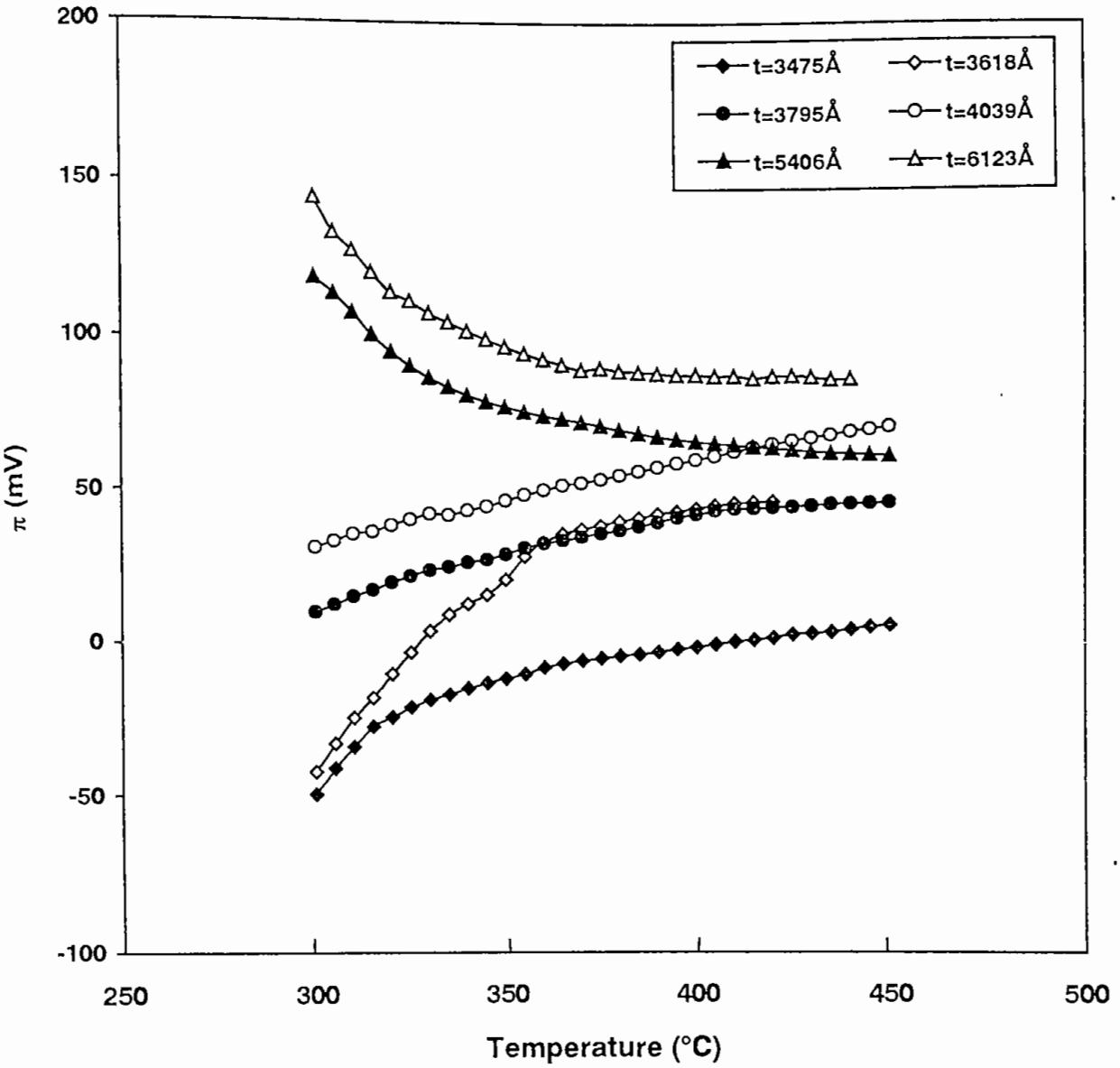

Fig. 4.1.10 Peltier coefficient with temperature for different thickness for CuO filmss.

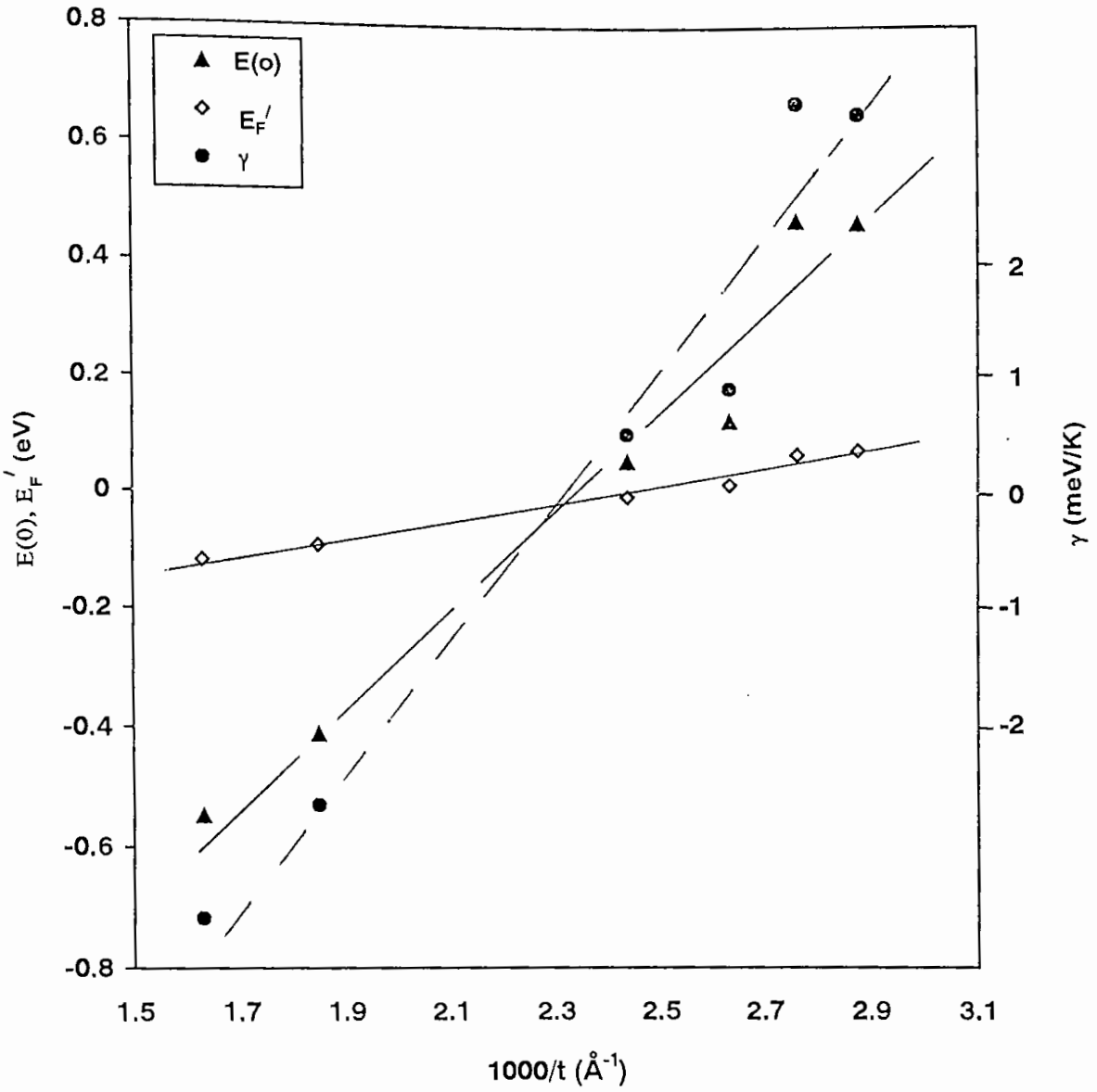

Fig. 4.1.11 Variation of E(0), E_F' and γ values with inverse of thickness for CuO films.

The values of E_F' for different film thicknesses show that Fermi levels start from 0.118 eV above the valence band edge at higher film thicknesses and move towards the band edge, and finally entered the extended band at lower film thickness. The latter situation occurs only when the density of the acceptor centres, $N_a >> N_d$, the density of donor centres , in the band gap. As we noticed in figure 4.1.1 that at the initial stage of spraying the film growth rate remains faster so that there is a big possibility of creation of Cu ion vacancy in the lattice site (or excess oxygen to be trapped) at lower film thicknesses and the condition $N_a >> N_d$ holds good . But as the film thickness gradually increases and the chemical reaction rate becomes slower while the reactant supply rate remains sensibly constant, a considerable amount of unreacted excess Cu ions got trapped in the interstitial position of the crystal lattice which enhances the donor concentration N_d ,and leads to $N_a \sim N_d$. Fermi level is then pulled out of the band edge at higher film thicknesses[5].

Regarding the conduction mechanism in these samples a few points can be noted here. (a) There is a considerable difference between the values of the activation energies obtained from the thermopower data and conductivity data, except one sample of the highest thickness, (b) during the thermal cycling of the samples a clear change in the Hall mobility values has been observed as has also been predicted above for the temperature dependence of μ_H, and (c) the pre-exponential factor σ_o in equation $\sigma=\sigma_o \exp(-E_\sigma/KT)$ was found very small , maximum of about σ_o=16 (ohm-cm)$^{-1}$. All of these facts are very much in favour of hopping type conduction in the films.

4.1.4 Optical properties

To determine the fundamental optical absorption edge, E_g , the transmission coefficient, T, and reflection coefficient, R, have been measured over the wavelength range 200 to 1100 nm. Absorption coefficients α were evaluated from a conventional formula

$$T = [(1-R)^2 \exp(-\alpha t)] / [1-R^2 \exp(-2\alpha t)]$$

where t is the film thickness. For our set of samples the values of R were found very small (max 20%). Considering a direct transition between the extended bands and following a conventional method [6] of plotting $(\alpha h\nu)^2$ against $h\nu$, the fundamental optical absorption edges for all the samples were determined by extrapolating the curves to $(\alpha h\nu)^2 = 0$. Fig.4.1.12 and fig.4.1.13 shows these plots for different thickness and different substrate temperature respectively. Obtained values were between 1.3 and 1.5 eV. The values of band gaps obtained are listed in table-2.

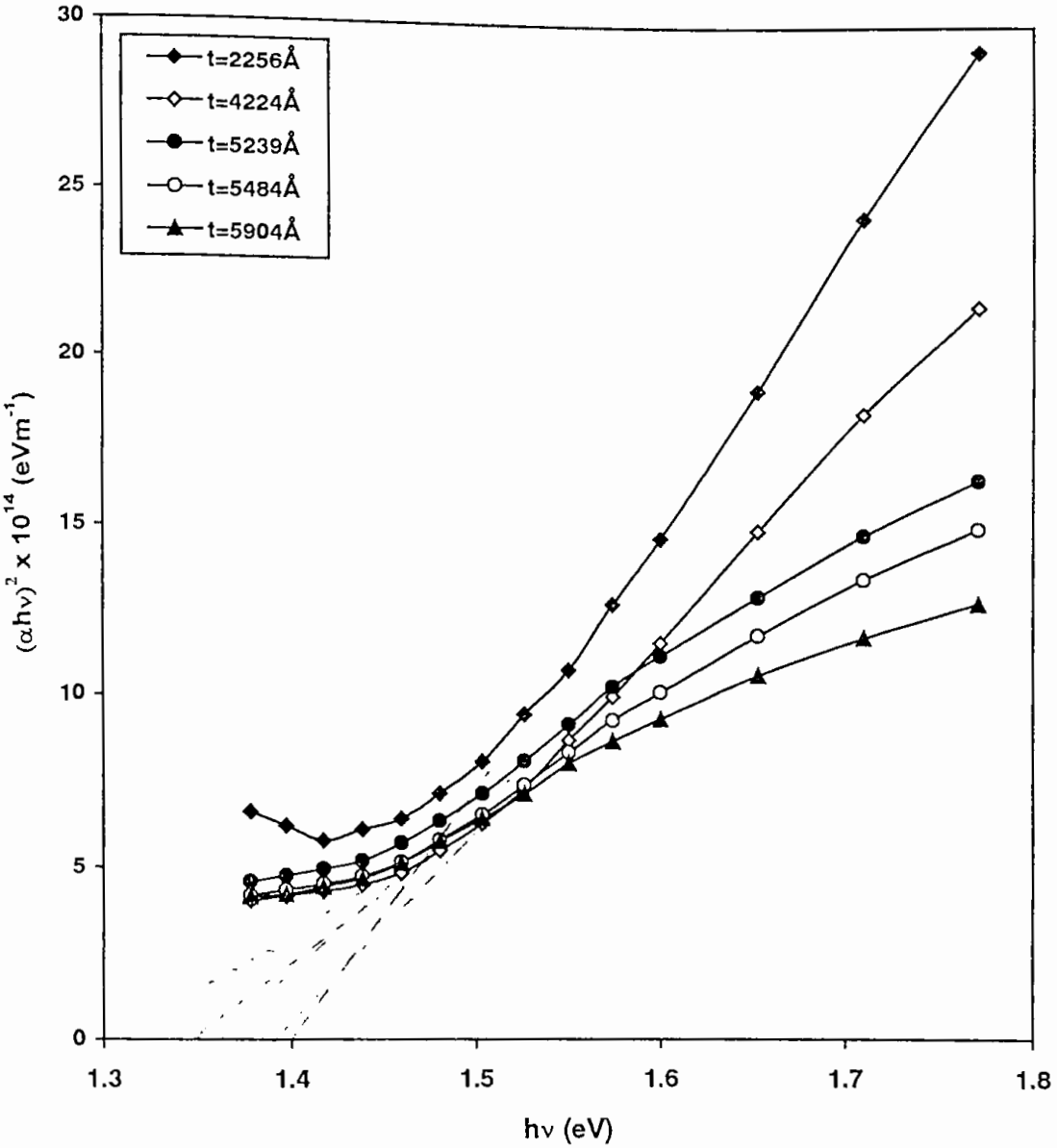

Fig. 4.1.12 Variation of $(\alpha h\nu)^2$ with $h\nu$ for different thickness.

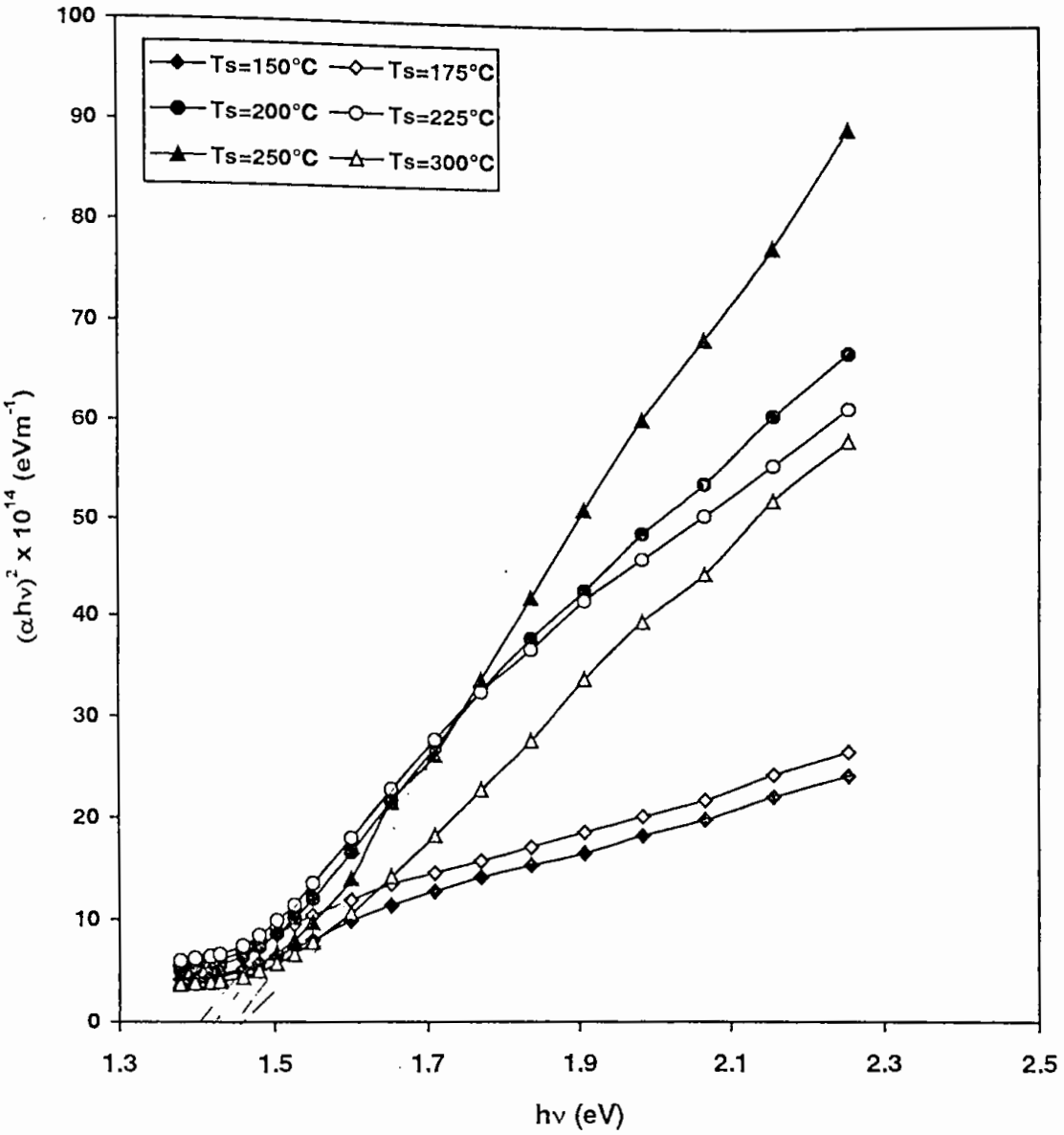

Fig. 4.1.13 Variation of $(\alpha h\nu)^2$ with $h\nu$ for different substrate temperature.

Table 2 : Values of the optical band gap of CuO films with different deposition parameters.

Thickness (Å)	Substrate temperature T_s (°C)	Solution concentration (Molar)	Band gap (eV)	
			As deposited	Annealed
2256	200	0.2	1.40	
4224			1.39	
5239			1.37	
5484			1.35	
5904			1.30	
5644	150	0.2	1.29	
5252	175		1.28	
5103	200		1.34	
4460	225		1.40	
2775	250		1.47	
3439	300		1.48	
2152	200	0.05	1.33	1.35
2441		0.10	1.49	1.48
2641		0.15	1.51	1.50
2419		0.20	1.55	1.52

The values are in good agreement with the reported optical band gap 1.5eV for the crystalline phase of CuO materials [7,8]. Thickness dependence of E_g was not very prominant and may be within the experimental errors.

In the thermopower experiment the values of E(0) obtained from fig.4.1.11 should not be compared with the optically determined E_g values at very low temperature but there are several cases in the scientific literature where these two values are compared[6] . We do not think that the present case is an exception in this regard since we find these two values to be comparable in the present case.

4.2 Studies on CdS thin films

In this part of the chapter the results of the various experimental measurements on film growth, structural, electrical and optical of CdS thin films prepared by spray pyrolysis of aqueous solution of $CdCl_2$ and $SC(NH_2)_2$ have been presented. For this study films were prepared with different thickness and at different substrate temperature. Samples were prepared under different deposition condition such as i) keeping spray time and substrate temperature fixed and varying the solution compositions. ii) keeping the solution composition and spray time fixed and varying the substrate temperature, ii) keeping solution composition and substrate temperature fixed and varying spray time. In preparing the sample the solution spray rate was maintained at ~1.2 ml/min., spray gun height was 25 cm and the carrier gas pressure was kept at 4 PSI. The thicknesses of the deposited films were measured by Fiezeau fringe's method. Possible explanations and discussions of the results are also given. The details of the experimental techniques for deposition of CdS thin films have already been given in the previous chapter.

4.2.1 The films growth rate

Variation of the percentage composition of $CdCl_2$ in the working solution and substrate temperature (T_s) has remarkable effect on the film deposition rate. Curve (a) of figure 4.2.1 shows dependence of deposition rate on solution composition. Deposition rate was found to increase of solution composition and saturates at about 45% $CdCl_2$ while the substrate temperature was constant at about 250°C. Deposition rate was found to decrease with the increase of substrate temperature as shown in curve (b) of figure 4.2.1. This is quite usual because of lower amount of available particle have a large distribution of sizes and velocities and are normally supplied from the top of the heater against the upward hot air current. As the temperature goes up this air current carries more and more reactant with it and a less amount of spray particle reach the substrate surface so long as the spray rate is kept constant.

From curve (a) and (b) of figure 4.2.1 we notice that about 50% of $CdCl_2$ and 250°C of substrate temperature can give an appreciable deposition rate ≈ 350Å/min. and results a good quality CdS film.

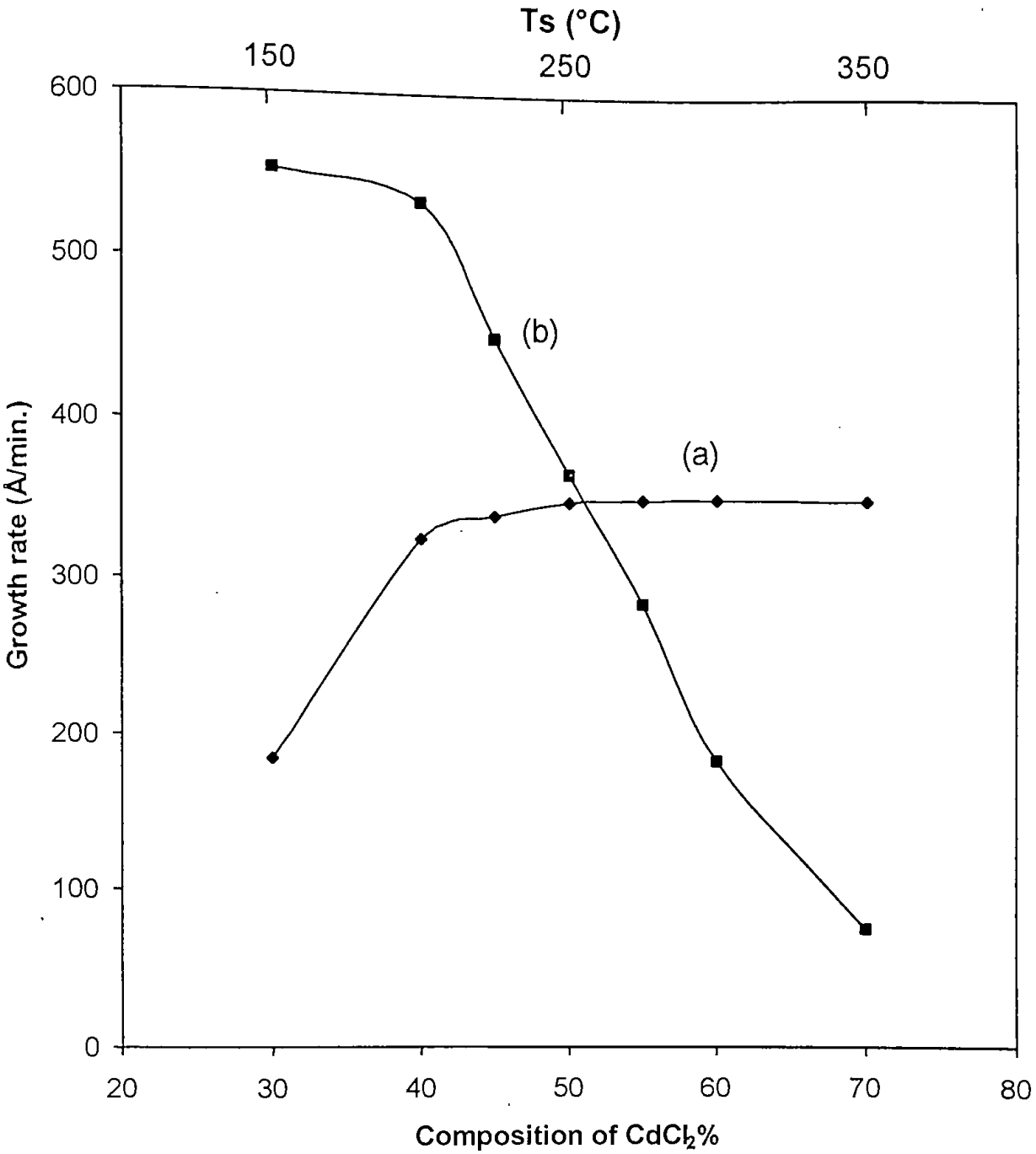

Fig. 4.2.1. Variation of growth rate with (a) $CdCl_2$ composition (b) substrate temperature Ts.

4.2.2 Structural properties

The crystallographic properties of CdS films were investigated by X-ray diffraction (XRD) analysis. It was found that the crystallinity of the films depends on the growth conditions. The X-ray patterns of CdS films on glass substrate deposited at various substrate temperatures with fixed solution concentration and different solution compositions at fixed substrate temperature are shown in figure 4.2.2 and figure 4.4.3 respectively. The intense peak at 2θ near 30° corresponds to the hexagonal (101) planes of CdS. Figure 4.2.2 shows that the intensity of this peak increases as the substrate temperature increases to a maximum at about 250°C and then decreases as the substrate temperature increased further. Also from figure 4.2.3 it can be seen that at 250°C substrate temperature if the solution concentration changes around 50% $CdCl_2$ then the intensity of this peak decreases. This is consistent with the proposition that the orientation of crystallites under goes a change when cation to anion ratio is varied. Other observed peaks correspond to (100), (102) and (103) planes are also related to the hexagonal structure of the materials. Thus XRD studies revealed that a good crystalline CdS films formed at about 250°C substrate temperature and with about 50% $CdCl_2$ solution concentration. The actual ratio of Cd and S in the deposited films was not studied. The lattice constants of the CdS structure were calculated from the XRD peaks and the values obtained a=4.136Å and c=6.713Å. These values are in good agreement with values observed by K. H. Hellwege et al.[9].

SEM studies of these films show a columnar growth of the crystal grains, 0.3-0.5 μm size, which are uniformly distributed over the substrate. Some micro cracks have been found to exist in a film deposited at 200°C but not in other samples of the group prepared at higher temperature. In other group of samples prepared by varying the composition of the working solution with T_s at 250°C, such cracks were not observed. Baranski et al.[10] have reported about such micro cracks. Their view is that either non uniform stresses in the film or the ions displacement along the lateral direction of the substrate plane compared to that along the direction of growth (normal to the substrate plane) may be the cause of these cracks. Figure 4.2.4(a) and 4.2.4(b) show the SEM of CdS films prepared in 50% of solution composition $CdCl_2$ with Ts= 200°C and 250°C respectively. Figure 4.2.4(c) and 4.2.4(d) show SEM of the samples prepared at 250°C with 40% and 60% $CdCl_2$ of solution composition respectively.

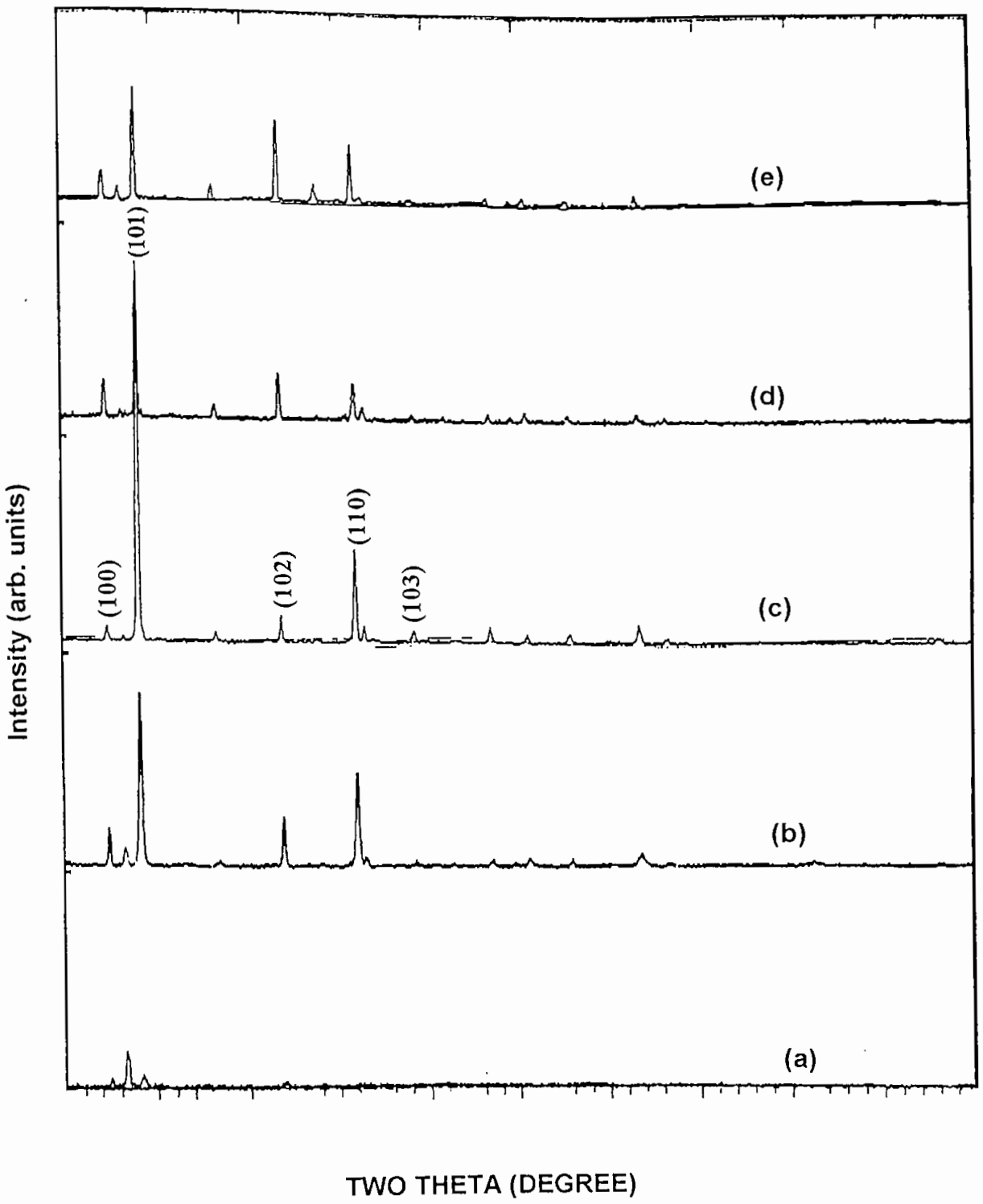

Fig. 4.2.2 X-ray diffraction patterns of CdS films prepared at different substrate temperature: (a) Ts = 150°C (b) Ts = 200°C. (c) Ts = 250°C (d) Ts = 300°C. (e) Ts = 350°C

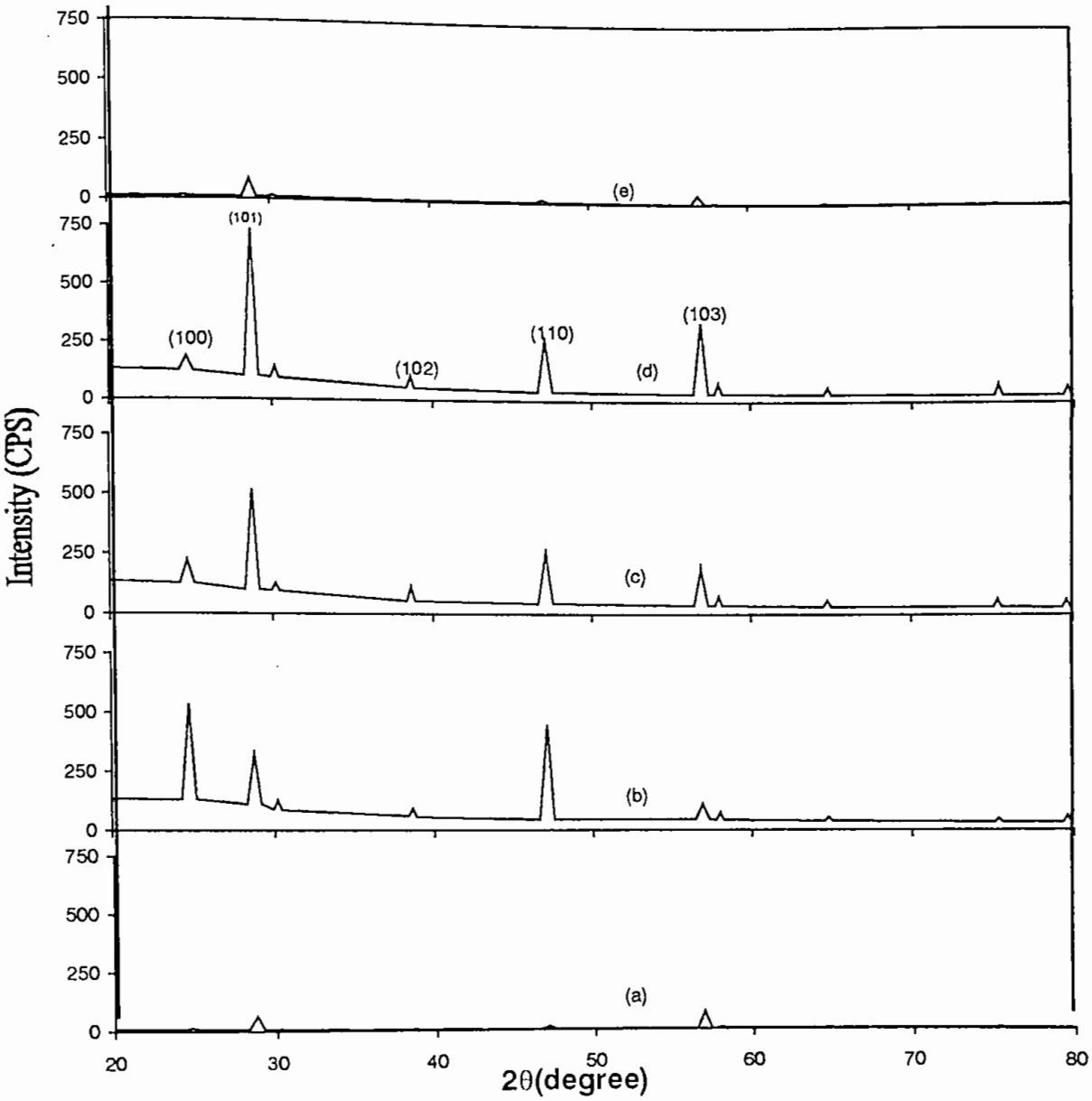

Fig. 4.2.3. X-ray diffraction patterns of CdS films prepared at different composition (a) 30% of $CdCl_2$ (b) 40% of $CdCl_2$ (c) 45% of $CdCl_2$ (d) 50% of $CdCl_2$ (e) 55% of $CdCl_2$.

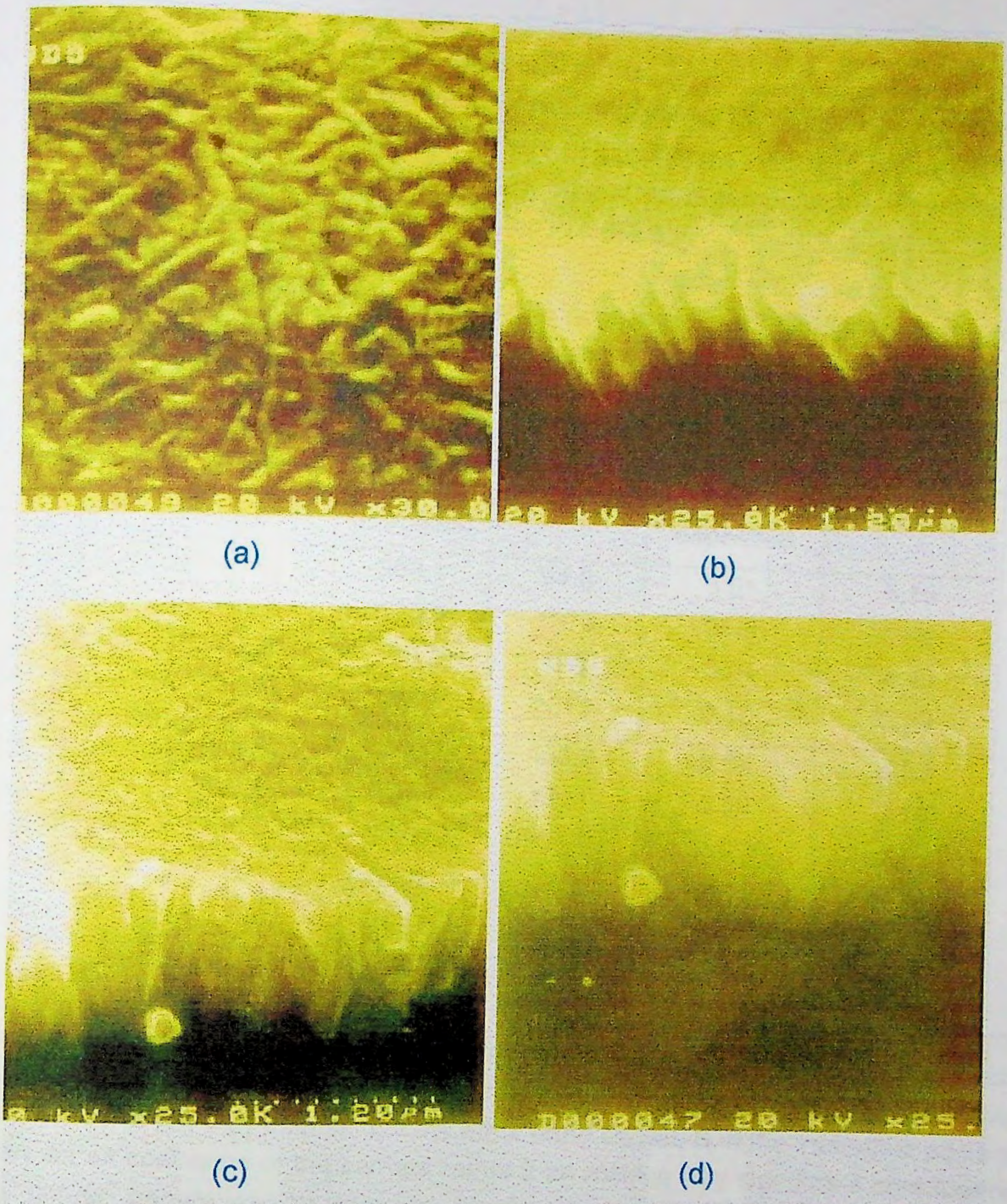

(a) (b)

(c) (d)

Fig. 4.2.4 SEM micrograph of CdS films prepared at (a) Ts=200°C, (b) Ts=250°C, with 50% $CdCl_2$ and 50% Thiourea composition; (c) 40% $CdCl_2$ with 60% Thiourea (d) 60% $CdCl_2$ with 40% Thiourea, (c) and (d) are at co nstant Ts=250°C.

4.2.3 Electrical properties

4.2.3.1 Hall effect and carrier concentration

Using Van der Pauw method the Hall mobility (μ_H) and carrier concentration (n) have been determined for our sample at a constant magnetic field of 8.85 K.G. We have limited our observation only at room temperature. The obtained values for the CdS thin films are tabulated in table 3.

Table 3: Values of Hall mobility and carrier concentration of CdS films at the room temperature with different deposition parameter.

$CdCl_2$: $SC(NH_2)_2$	Substrate temperature (°C)	Hall mobility (cm^3/V-sec.)		Carrier concentration x10^{14} (cm^{-3})	
		As deposited	Annealed	As deposited	Annealed
40:60	250	203.1	94.8	3.91	5.10
45:55		42.70	1273	26.5	0.49
50:50		195.2	138	5.24	4.45
55:45		4663	2312	0.10	0.29
50:50	150	531	458.8	3.64	4.53
	200	1226	1321	0.28	0.13
	250	476	231.9	4.07	4.16
	300	856	687.8	0.28	0.26
	350	1011	601.7	0.84	1.67

All the CdS films were found to show n-type conductivity. The n-type conductivity in CdS films is mainly due to the excess Cd in the film. Other defects and foreign impurities can also form donor levels in the band gap of the films, but their effect is not very intense. On the other hand excess S in the interstitial position can act as scatterers of the carriers rather than making any significant contribution to carrier generation mechanism. Among the (various other) native defects incorporation of Cl atom from spraying solution. A part of this halide (Cl) acts like donors but another part causes deviations from stoichiometry in the form of cation vacancies (one cation vacancy being formed for each two halide ions incorporated) which in terns are compensated by the donors. Thus Cl can reduce conductivity by reducing carriers in the films.

From table 3 it is observed that the obtained values of μ_H and n are of expected order of magnitude but are rather scattered with respect to, both preparation condition, substrate temperature and solution composition. The scattered nature of our mobility and carrier concentration results may be due to the fact that the deposition conditions of the films were not constant. Carrier concentration was found to be low, this low value of carrier concentration in an apparently stoichiometric film may seem to be due to a bigger compensation ratio of the samples and the films may be considered as partly compensated semiconductors.

4.2.3.2 DC conductivity

Electrical resistivity have been measured from room temperature to 300°C. Films deposited at substrate temperature 250°C with 50% $CdCl_2$ have their electrical resistivities about 100_{Ω}-cm at room temperature. Figure 4.2.5 shows the variation of the resistivity (ρ) with substrate temperature and solution composition. Substrate temperature has a remarkable effect on the resistivity. From curve (a) of figure 4.2.5 it is observed that the resistivity decreases with substrate temperature reaches to a minimum value and then increases with further increase substrate temperature. From curve (b) of figure 4.2.5 a slight increase of resistivity with the increase of $CdCl_2$ composition up to 50% is noticeable but above this composition resistivity starts to decrease. This may be an indication that excess Cd is the main source of donors and lower percentage of thiourea can provide S^{-2} ion vacancies. On the other hand interstitial S atom can produce acceptors levels just above the valence band as has been mentioned by Achour et al.[11] and provide acceptors for carrier compensation in the samples. Except these native defects other foreign impurities from the working solution may also be incorporated in the film during its growth. These non- deliberate foreign atoms are not chemical doping and thus deviation from CdS stoichiometry is probably less.

In the as deposited films resistivities remain higher than that of the annealed films. Annealing in vacuum decreases the resistivities about 75% and is true for all samples either deposited at various substrate temperatures or with various $CdCl_2$ compositions. The nature of variation of resistivity with temperature for different substrate temperature and solution composition of $CdCl_2$ are shown in figure 4.2.6 and 4.2.7 respectively. Temperature coefficient of resistivity is negative for all our samples.

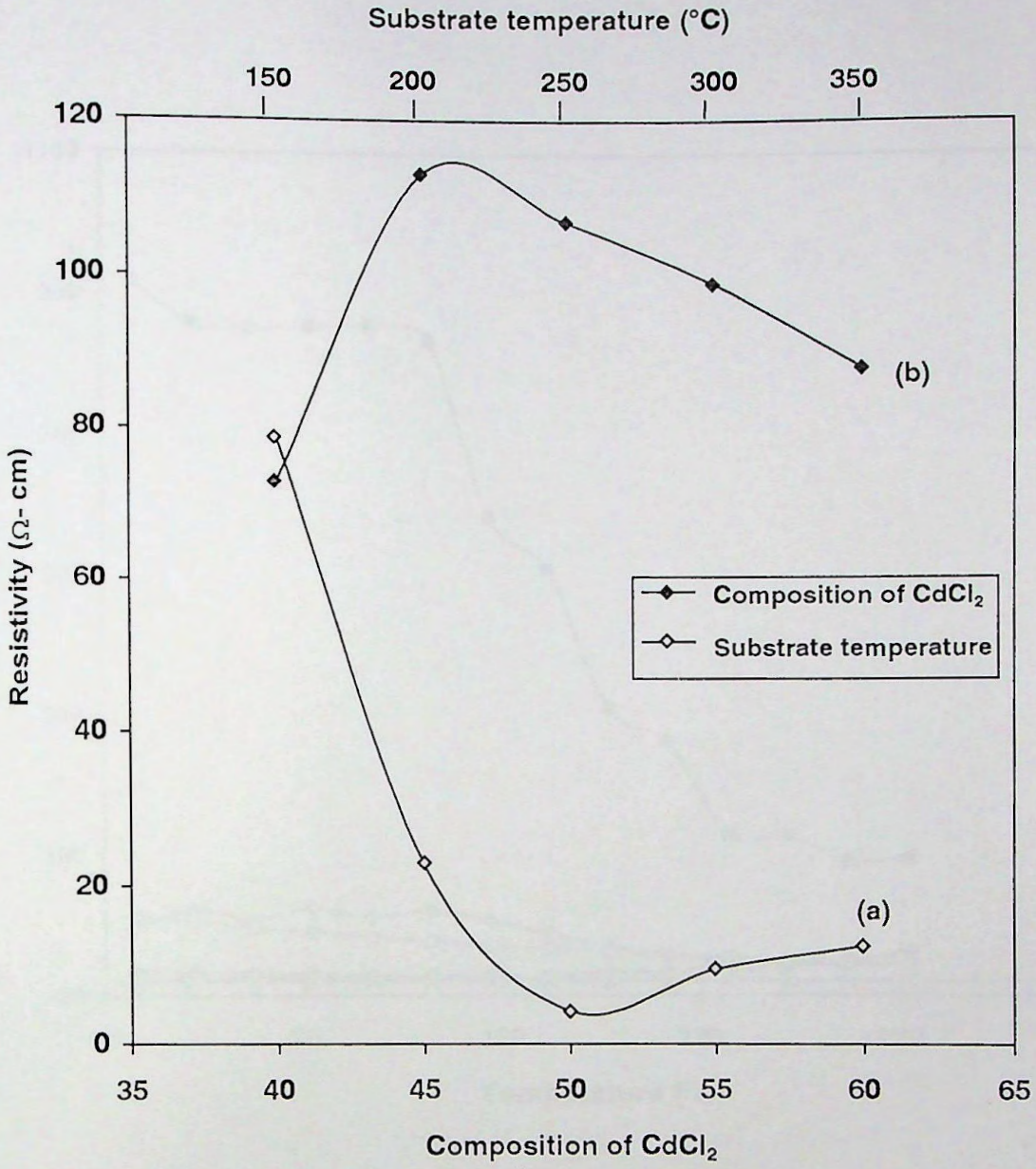

Fig. 4.2.5 Resistivity with (a) substrate temperature of CdS films (b) composition of $CdCl_2$.

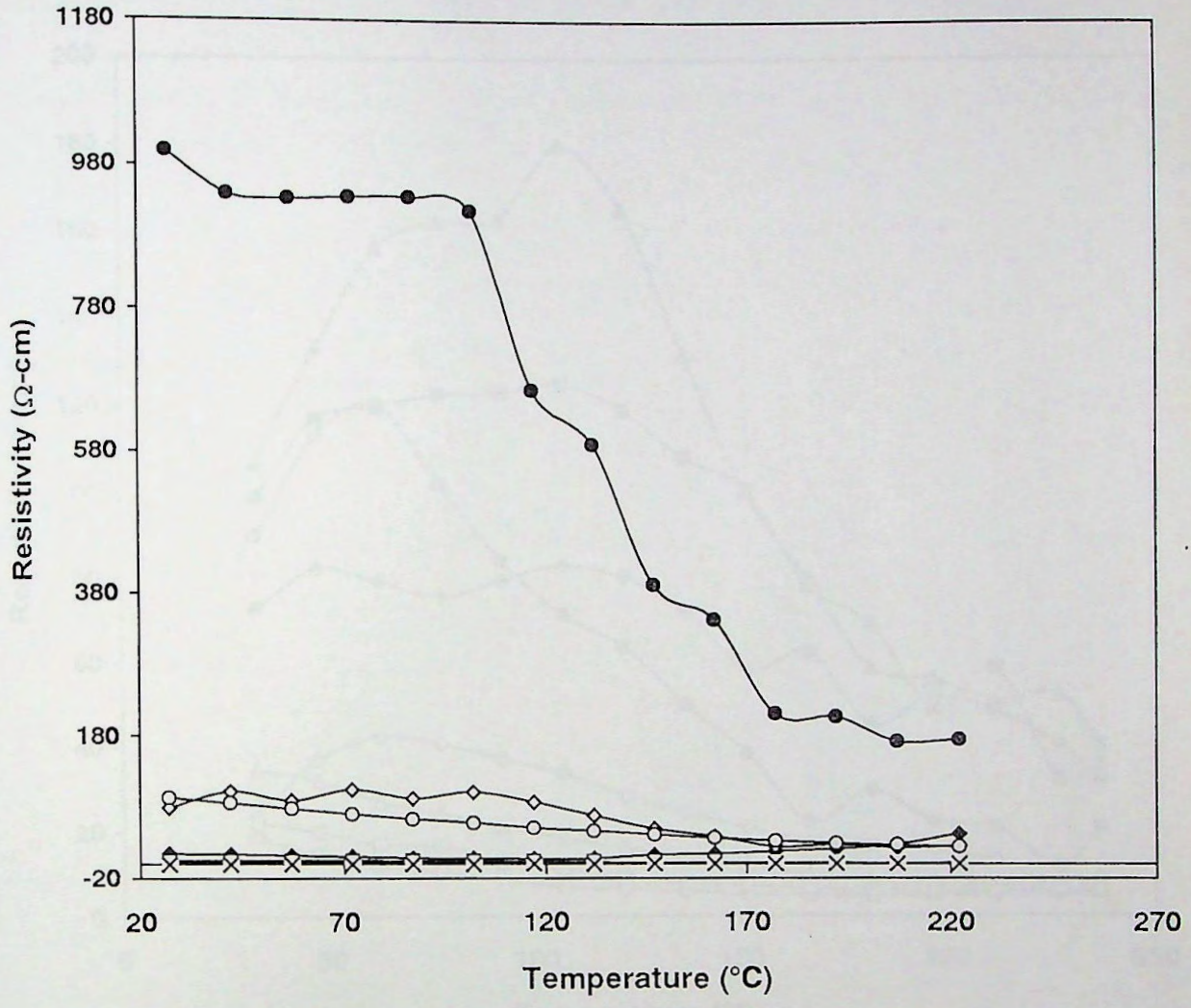

Fig. 4.2.6. Variation of resistivity with temperature for different substrate temperature for CdS films.

i) Ts=150°C-◆-as deposited,-◇-annealed
ii) Ts=200°C-●-as deposited,-○-annealed
iii) Ts=250°C-▲-as deposited,-△-annealed
iv)Ts=300°C-■-as deposited,-□-annealed
v) Ts=350°C-✳-as deposited,-x-annealed.

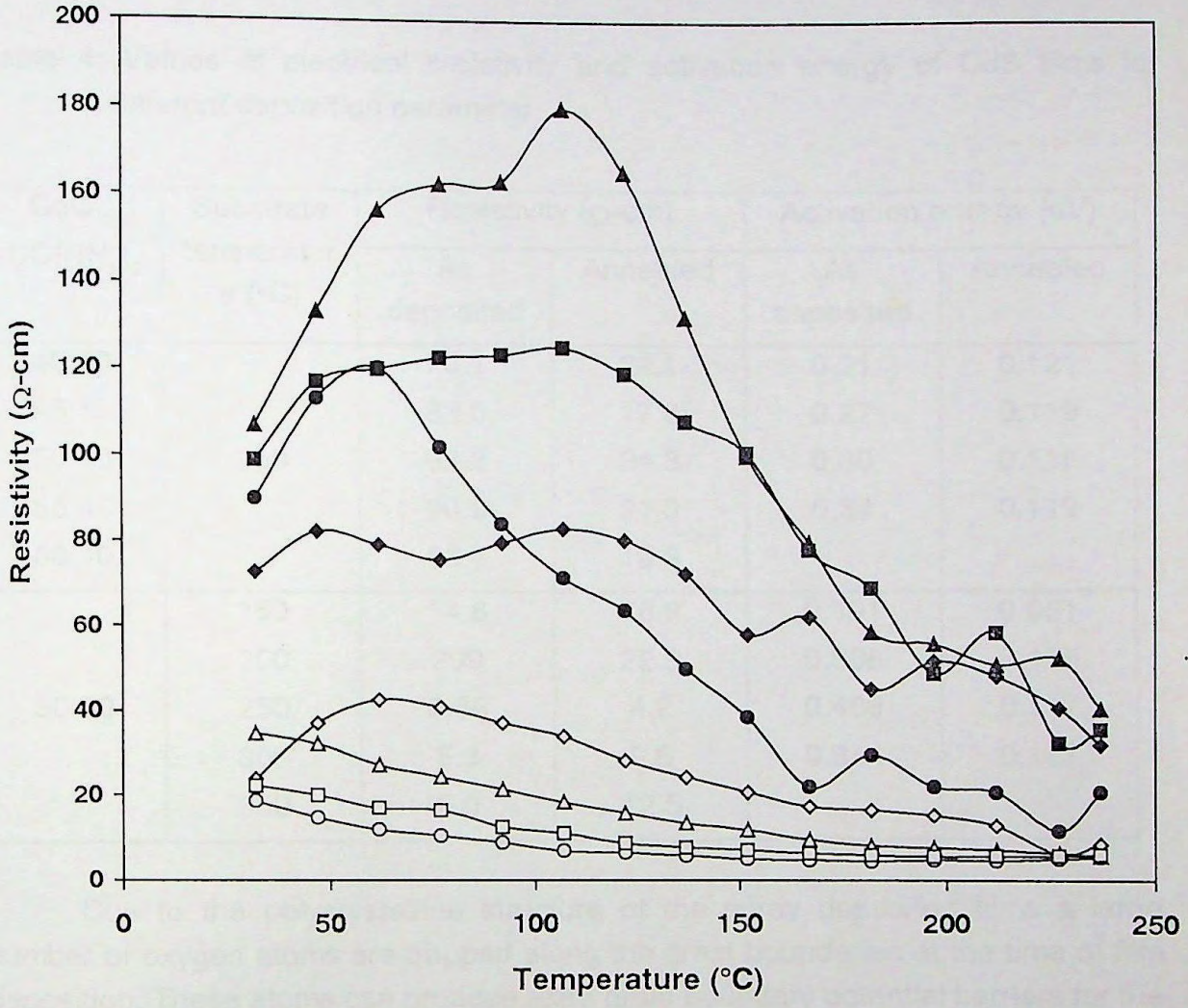

Fig. 4.2.7. Variation of resistivity with temperature for different solution composition.

i) 40% $CdCl_2$ as deposited, annealed ii) 45% $CdCl_2$ as deposited, annealed
iii) 50% $CdCl_2$ as deposited, annealed iv)55% $CdCl_2$ as deposited, annealed.

The activation energy of the annealed films has been obtained from $\ln\sigma$ versus inverse of temperature T plot. Figure 4.2.8 and 4.2.9 show the plot of $\ln\sigma$ versus 1/T curves for films of different thickness and Ts respectively. Resistivity and activation energy of our films with different deposition parameter is shown in table 4. From table 4 it can be seen that for annealed film activation energy remain almost same for all the samples but vary slightly in the case of as deposited films.

Table 4: Values of electrical resistivity and activation energy of CdS films for different deposition parameter.

$CdCl_2$:$SC(NH_2)_2$	Substrate temperature (°C)	Resistivity (Ω-cm)		Activation energy (eV)	
		As deposited	Annealed	As deposited	Annealed
40:60	250	70.1	22.1	0.21	0.121
45:55		82.0	17.6	0.27	0.119
50:50		93.2	34.3	0.30	0.118
55:45		90.8	21.0	0.34	0.119
60:40		86.7	19.8		
50:50	150	14.6	78.8	0.191	0.061
	200	999	22.9	0.636	0.115
	250	0.38	4.2	0.468	0.117
	300	5.3	9.6	0.844	0.127
	350	5.0	12.5		

Due to the polycrystalline structure of the spray deposited films a large number of oxygen atoms are trapped along the grain boundaries at the time of film deposition. These atoms can produce extra grain boundary potential barriers for the carriers in the conduction path leading to high resistivity. On subsequent annealing in vacuum these barriers are minimized in many respect and the activation energy is lowered accordingly[12].

4.2.3.3 Thermoelectric power

Thermoelectric power measurements were made for five different films of thickness 2689Å, 3929Å, 5204Å, 6738Å and 8266Å for solution composition of 50% $CdCl_2$. Films were prepared at substrate temperature 250°C. Thermal emf was measured as a function of temperature from 30°C to 170°C.

Figure 4.2.10 shows the variation of thermal emf developed between the two end points of the films with increasing the temperature difference. From figure we found that the thermal emf increases linearly with temperature difference in every cases. For the thermoelectric power measurements copper wires of high quality were used. As the absolute value of TEP of copper is only 1.7 μV/K compared to very large TEP of our experimental films, it was neglected in comparison to the TEP of our samples.

Thermoelectric power has been calculated from the thermal emf of the curves of fig. 4.2.10. Thermoelectric power is one of the most important experiment for the determination of the type of the carriers that dominates the material and TEP is also the most sensitive method of studying the variation in the Fermi level. When one end of the metal semiconductor junction is heated the mobile charge carriers tends to diffuse from hot junction to cold junction. So the sign of the potential developed at the cold junction will have same sign as the carriers. Thus from the polarity of the thermal emf, the type of the sample can be tentatively determined. For our films the observed negative value of thermal emf indicates that the carrier is n-type.

Fig. 4.2.11 shows the TEP plot of a set of five films with different thickness as a function of reciprocal temperature. From figure it is found that near the room temperature TEP value increases slightly with the increases in temperature for relatively thinner films (2689Å, 3929Å, 5204Å) but the value decreases for thicker films (6738Å, 8266Å). At higher temperature the value remains constant with temperature for all films. The observed results is in accordance with the observation of Phahle[13] for thicker films, who found that TEP varied as reciprocal of temperature at low temperatures while at high temperatures TEP is independent of temperature. Goswami and Ojha[14] have also found that TEP is nearly independent of temperature above 300K for other thicker specimen.

It is well known[15-17] that, according to classical size effect theory, the thermoelectric power of thin film is a function of film thickness. Fig. 4.2.12 shows the plot of TEP as a function of thickness for three different temperatures. It is seen from the figure that TEP of the films is a function of thickness for all three temperatures.

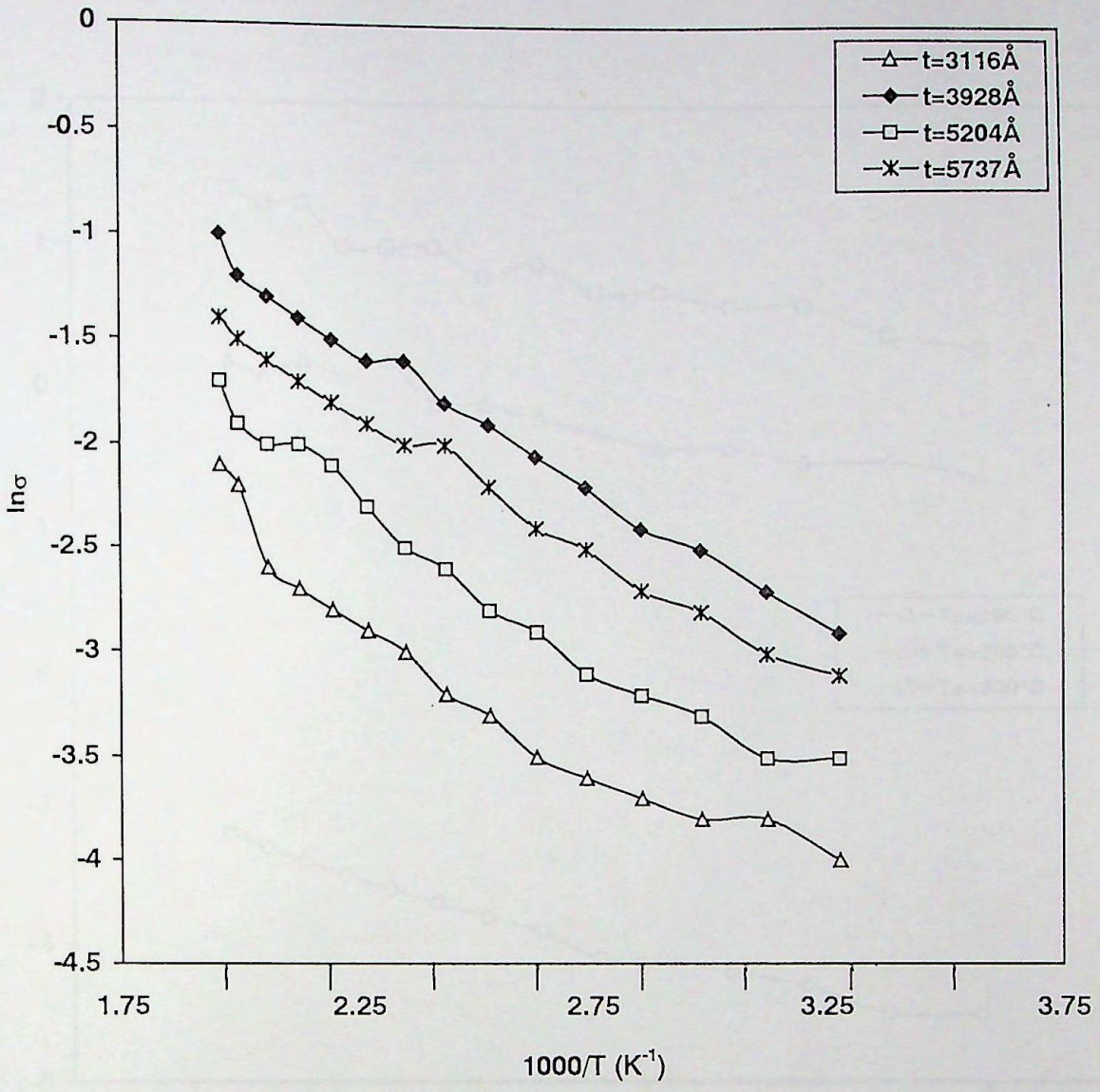

Fig. 4.2.8. Variation of $\ln_{\sigma}$ with 1/T for different thickness of CdS films.

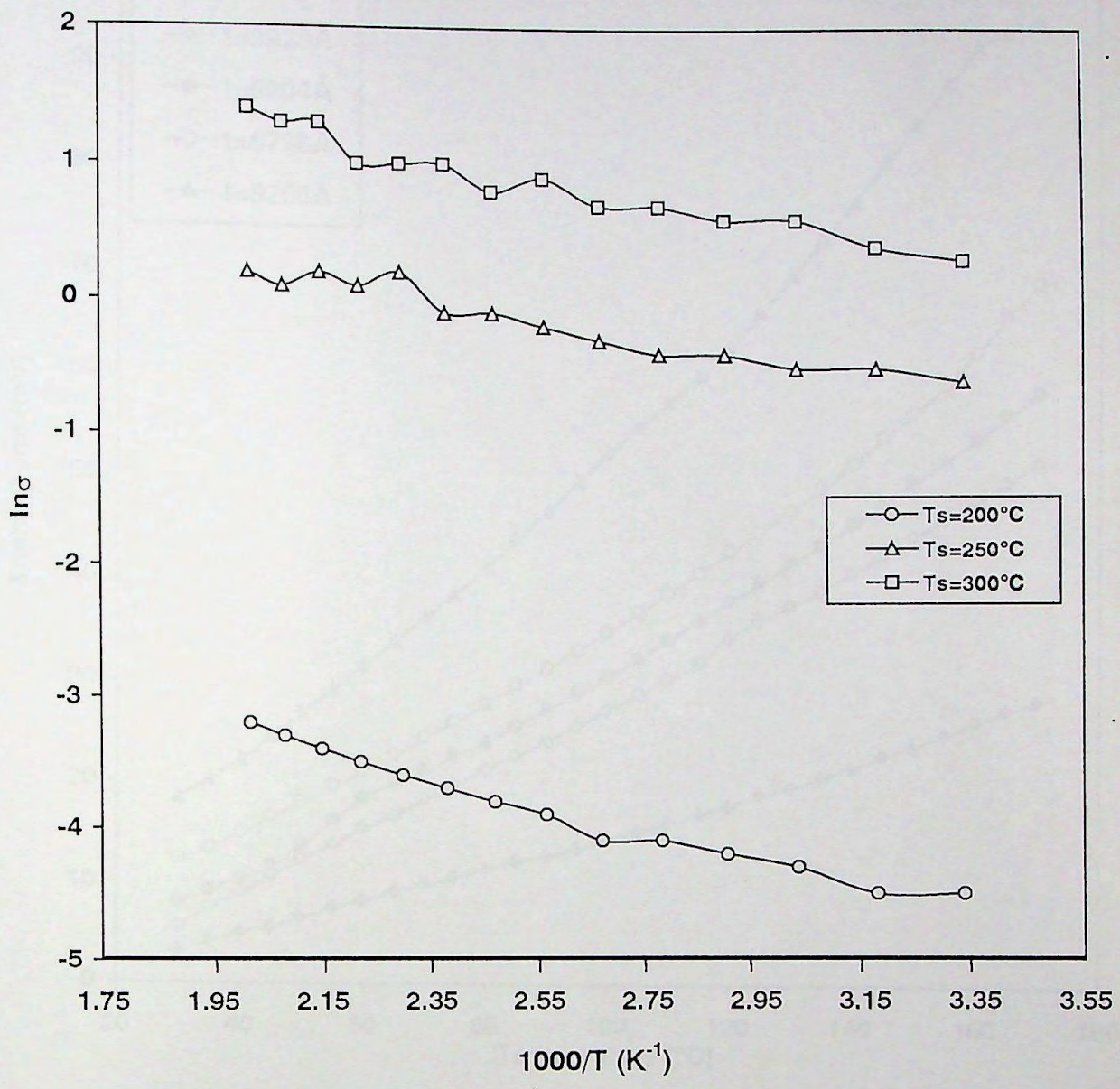

Fig. 4.2.9 Variation of $\ln\sigma$ with 1/T for different substrate temperature for annealed CdS films.

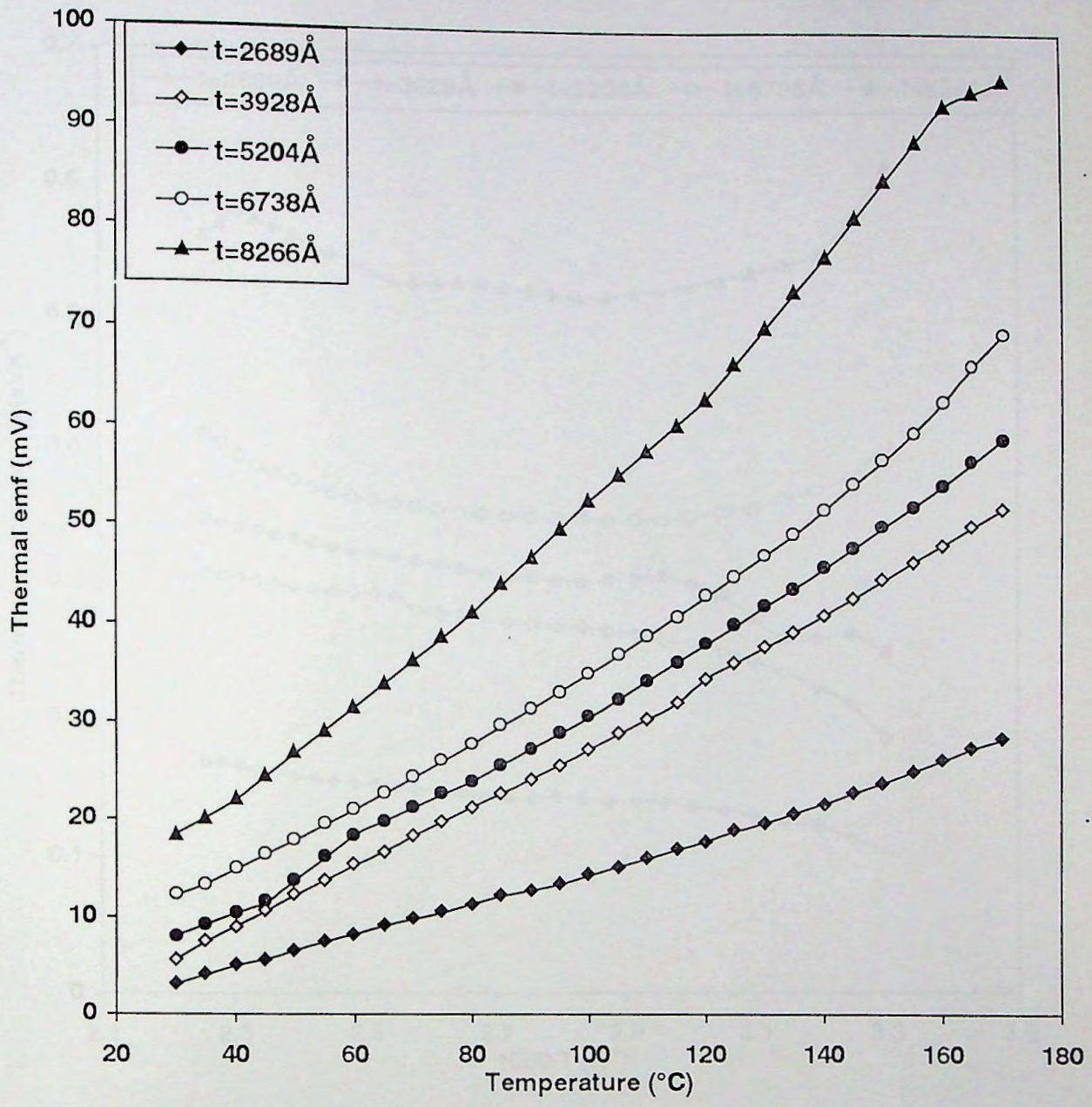

Fig. 4.2.10 Variation of thermal emf with temperature for different thickness for CdS films.

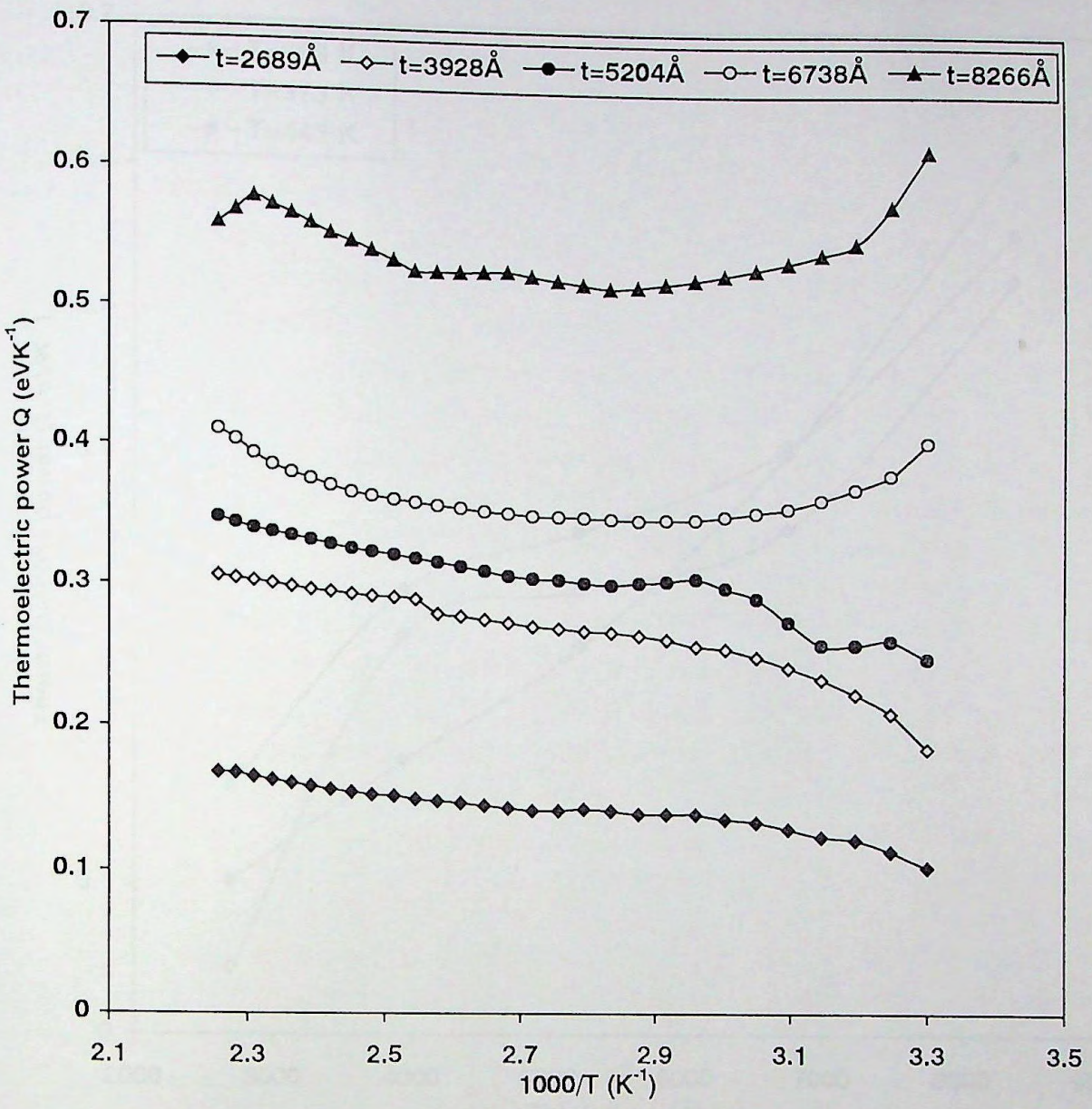

Fig. 4.2.11 Variation of thermoelectric power with 1/T for different thickness of CdS films.

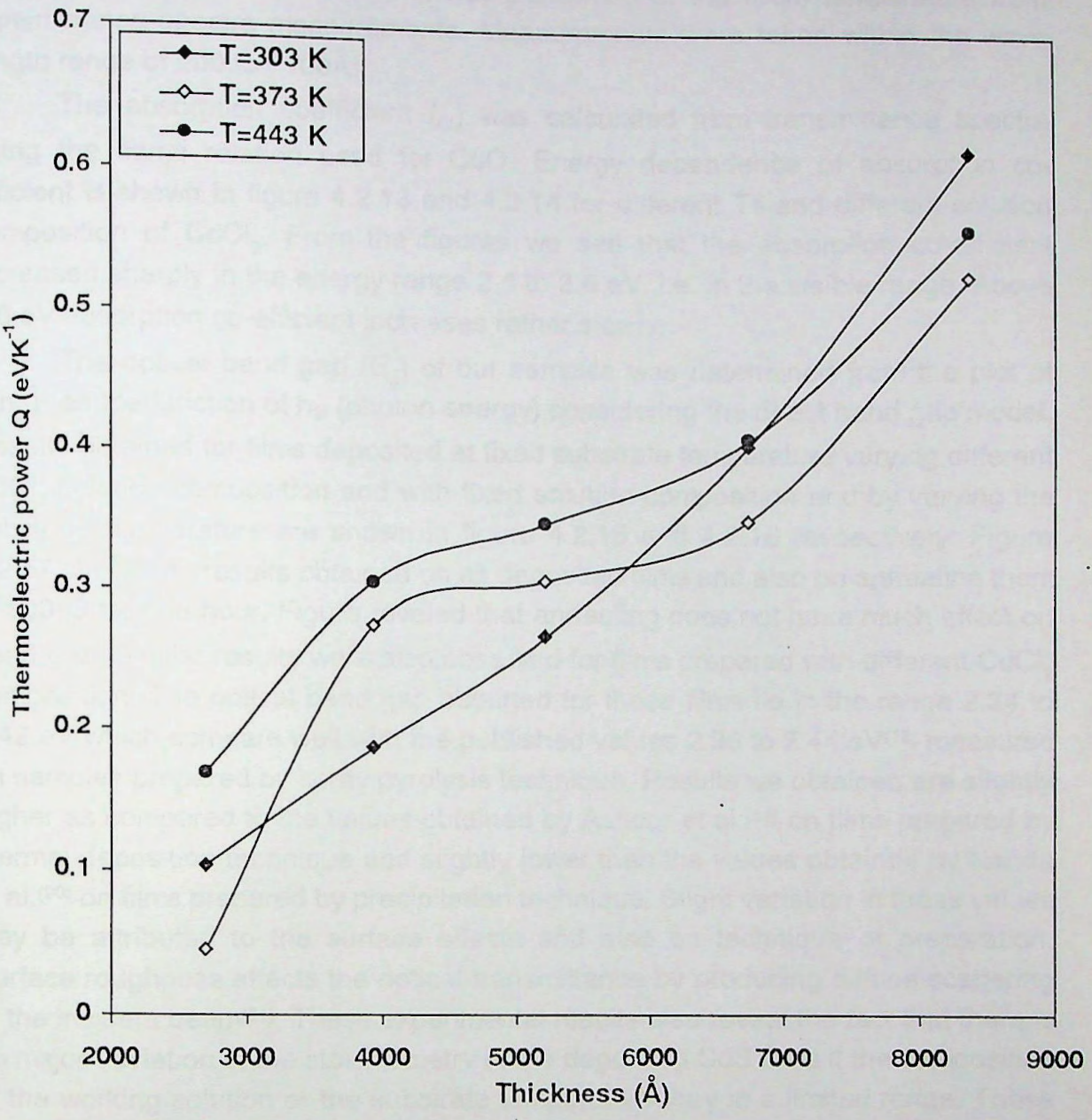

Fig. 4.2.12 Variation of thermoelectric power with thickness for different temperature for CdS films.

4.2.4 Optical properties

The optical characterization was performed at the room temperature from transmittance spectra measurements. Measurements were taken within the wave length range of 200 to 1100Å.

The absorption coefficient (α) was calculated from transmittance spectra using the same relation used for CuO. Energy dependence of absorption co-efficient is shown in figure 4.2.13 and 4.2.14 for different Ts and different solution composition of $CdCl_2$. From the figures we see that the absorption co-efficient increased sharply in the energy range 2.4 to 2.6 eV. i.e. in the visible range. Above 2.6 eV absorption co-efficient increases rather slowly.

The optical band gap (E_g) of our samples was determined from the plot of $(\alpha h_\nu)^2$ as the function of h_ν (photon energy) considering the direct band gap model. Results obtained for films deposited at fixed substrate temperature varying different $CdCl_2$ solution composition and with fixed solution composition and by varying the substrate temperature are shown in figure 4.2.15 and 4.2.16 respectively. Figure 4.2.17 shown the results obtained on as deposited films and also on annealing them at 300°C for one hour. Figure reveled that annealing does not have much effect on band gap. Similar results were also observed for films prepared with different $CdCl_2$ composition. The optical band gap obtained for these films lie in the range 2.34 to 2.42 eV which compare well with the published values 2.36 to 2.44 eV[18] measured on samples prepared by spray pyrolysis technique. Results we obtained are slightly higher as compared to the values obtained by Ashour et al.[19] on films prepared by thermal deposition technique and slightly lower than the values obtained by Nanda et al.[20] on films prepared by precipitation technique. Slight variation in these values may be attributed to the surface effects and also on technique of preparation. Surface roughness affects the optical transmittance by producing diffuse scattering of the incident beam[21]. These experimental results also reveal the fact that there is no major deviation of the stoichiometry of the deposited CdS films if the composition of the working solution or the substrate temperature vary in a limited range. These observations agree well with the observation of Krunks et al.[22]. In the as deposited films band gap remain slightly higher than that of the annealed films. This could be due to the slight improvement of crystallinity of the film on annealing. Optical band gap obtained on CdS films we prepared under different deposition conditions are shown in table 5.

Table 5: Values of the optical band gap of CdS films with different deposition parameters

$CdCl_2$:$SC(NH_2)_2$	Substrate temperature (°C)	Band gap (eV)	
		As deposited	Annealed
30:70	250	2.34	
40:60		2.40	2.42
45:55		2.42	
50:50		2.40	2.42
55:45		2.40	
60:40		2.40	2.42
50:50	150	2.36	2.40
	200	2.40	2.42
	250	2.40	2.42
	300	2.42	
	350	2.34	

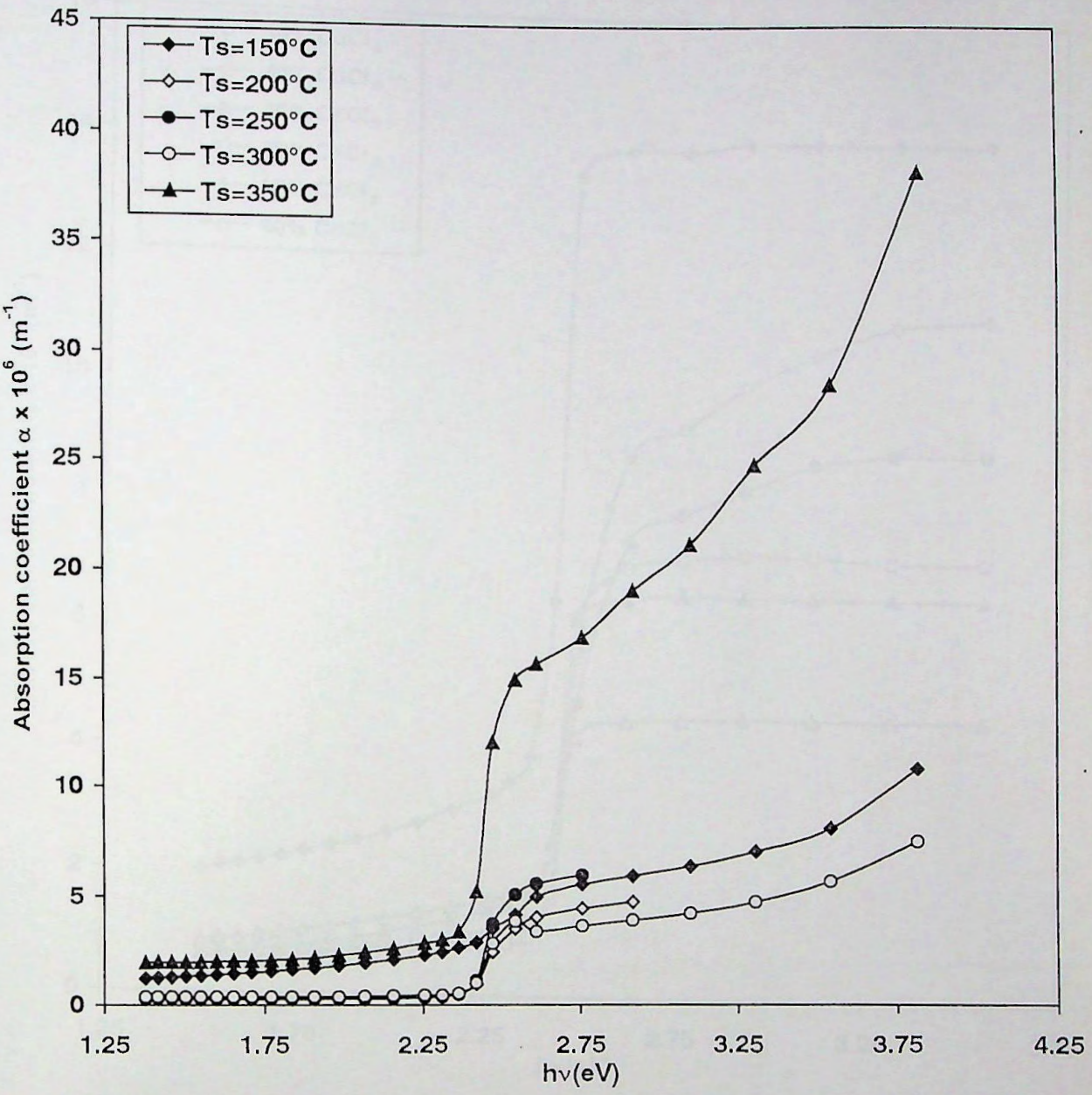

Fig. 4.2.13 Variation of absorption coefficient with photon energy for different substrate temperature.

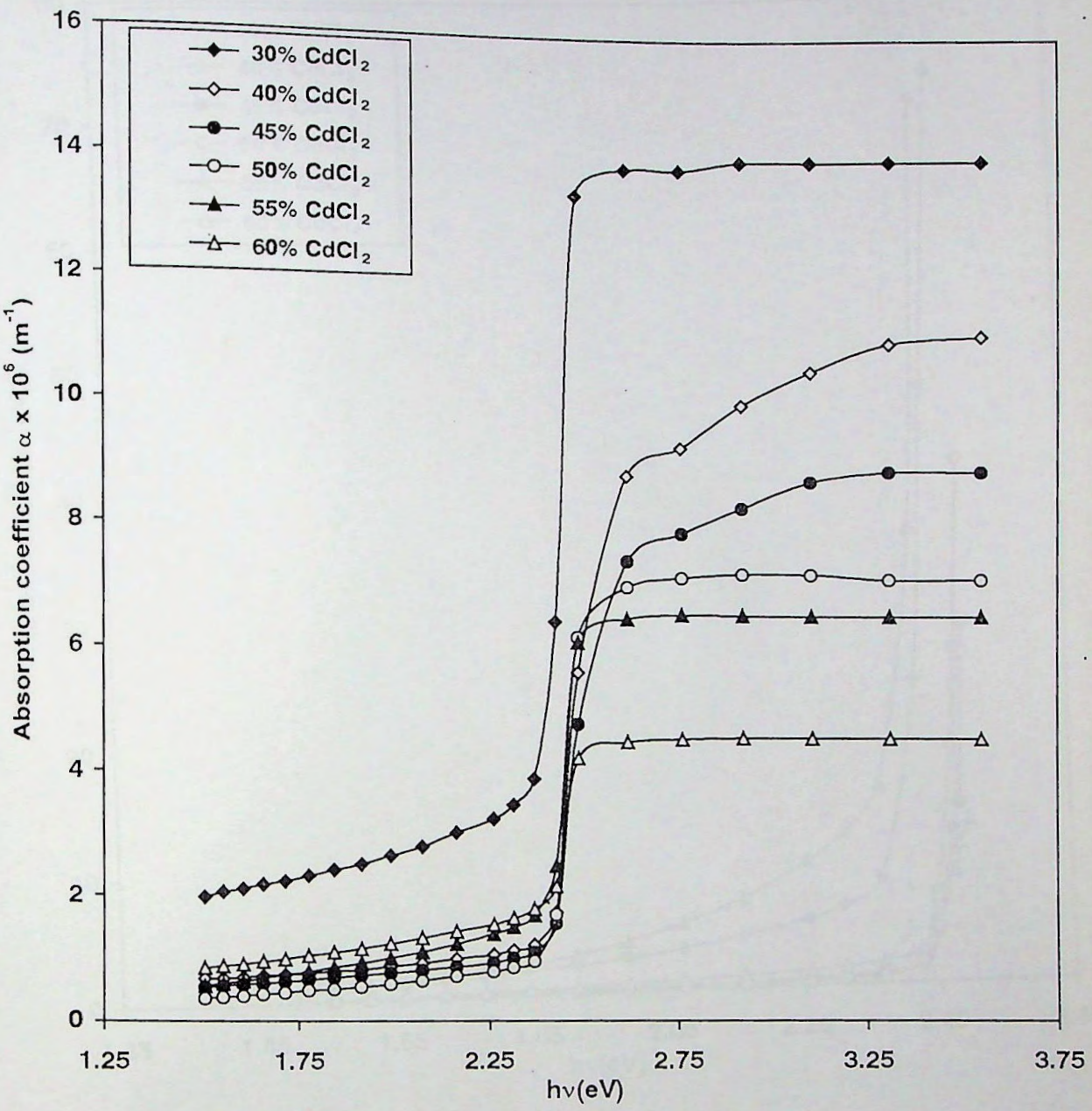

Fig. 4.2.14 Variation of absorption coefficient with photon energy for different solution composition for CdS films.

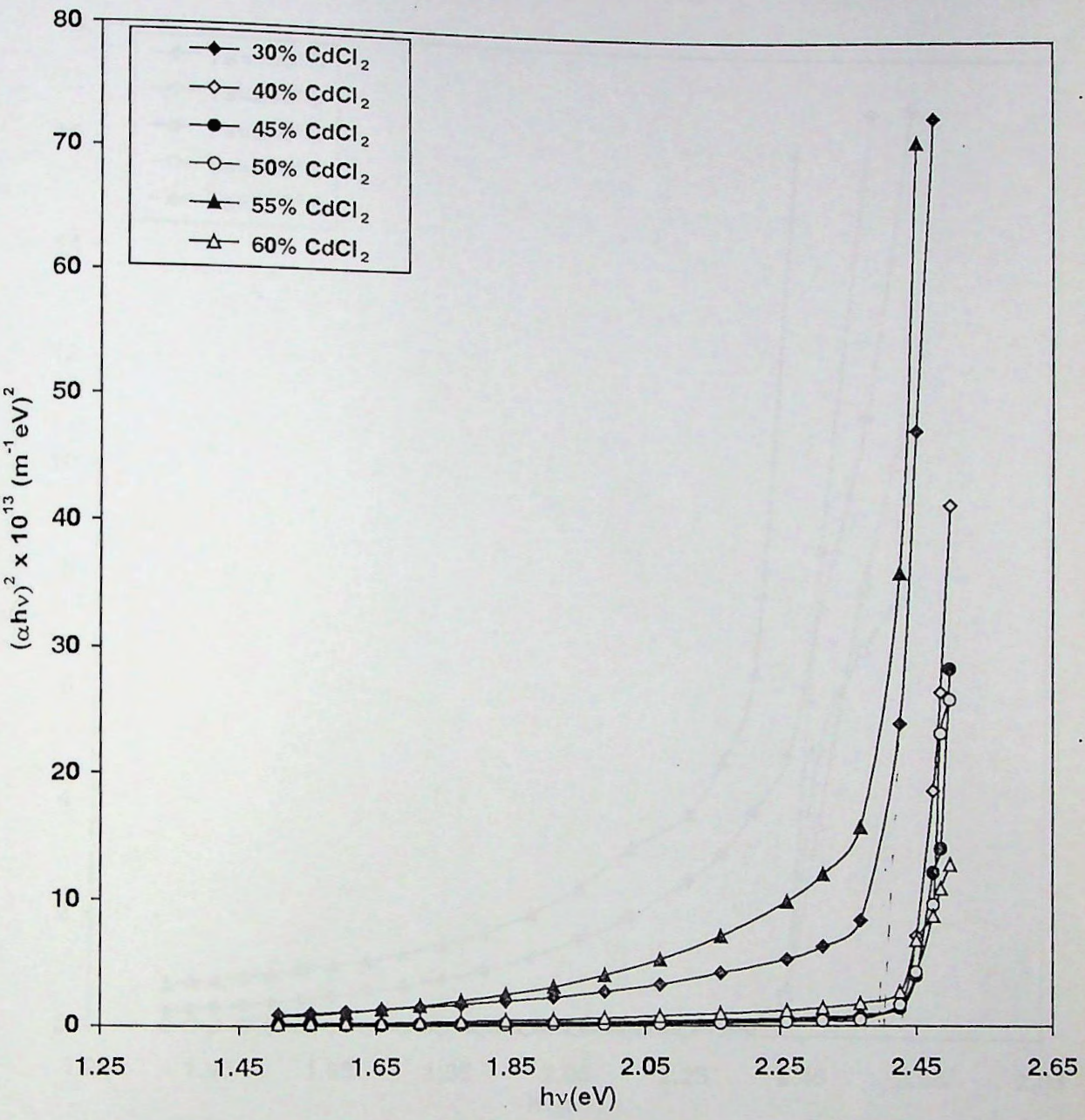

Fig. 4.2.15 Variation of $(\alpha h\nu)^2$ with photon energy for different solution composition for CdS films.

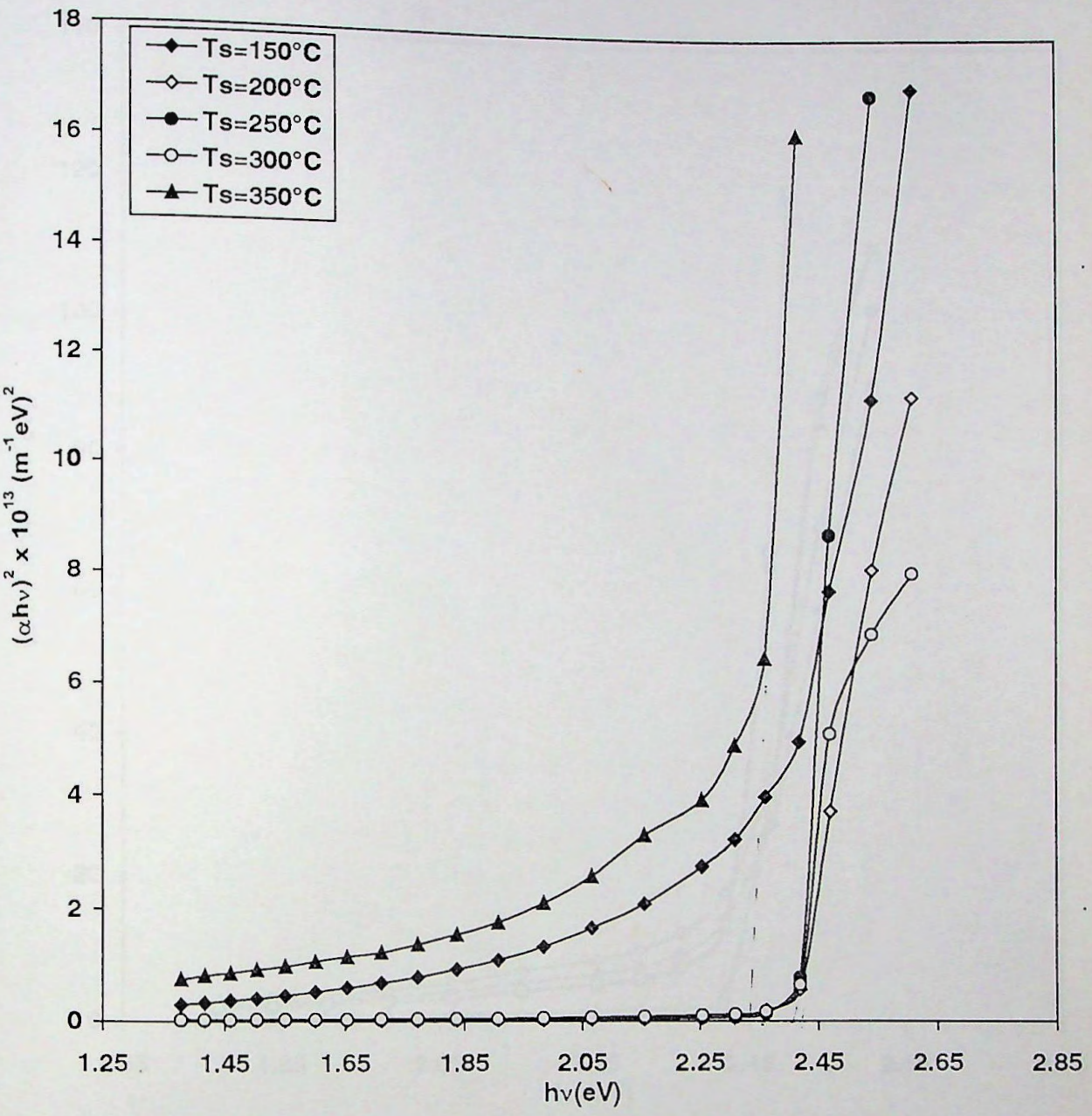

Fig. 4.2.16 Variation of $(\alpha h\nu)^2$ with photon energy for different substrate temperature for CdS films.

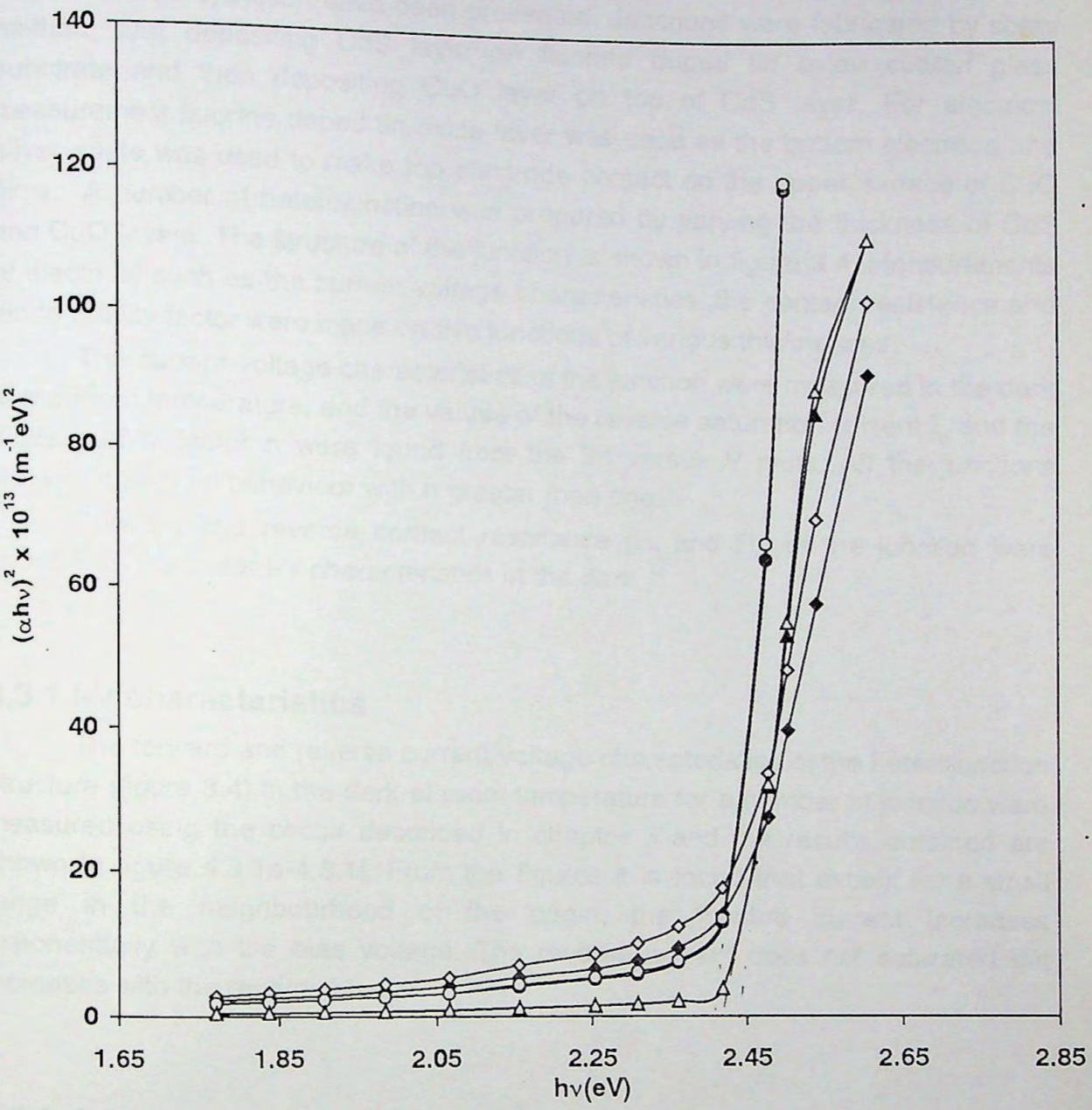

Fig. 4.2.17 Variation of $(\alpha h_\nu)^2$ with photon energy for different substrate temperature both as deposited and annealed.

i) Ts=150°C as deposited, annealed, ii) Ts=200°C as deposited, annealed
iii) Ts=250°C as deposited, annealed.

4.3 Studies on the CuO/CdS heterojunction

In this part of the chapter the results of the investigations carried on CuO/CdS heterojunction have been presented. Junctions were fabricated by spray method, first depositing CdS layer on fluorine doped tin oxide coated glass substrate and then depositing CuO layer on top of CdS layer. For electrical measurement fluorine doped tin oxide layer was used as the bottom electrode and silver paste was used to make top electrode contact on the upper surface of CuO films. A number of heterojunction was prepared by varying the thickness of CdS and CuO layers. The structure of the junction is shown in figure 3.4. Measurements of electrical such as the current-voltage characteristics, the contact resistance and diode quality factor were made on five junctions of various thicknesses.

The current-voltage characteristics of the junction were measured in the dark at the room temperature, and the values of the reverse saturation current I_o and the diode quality factor n were found from the lnI versus V plots. All the junctions showed non-ideal behaviour with n greater than one.

Forward and reverse contact resistance (R_f and R_r) of the junction were found from the linear I-V characteristics in the dark.

4.3.1 I-V characteristics

The forward and reverse current-voltage characteristics of the heterojunction structure (figure 3.4) in the dark at room temperature for a number of junction were measured using the circuit described in chapter 3 and the results obtained are shown in figure 4.3.1a-4.3.1f. From the figures it is found that except for a small range in the neighbourhood of the origin, the forward current increases exponentially with the bias voltage. The reverse current does not saturated but increases with the reverse bias.

4.3.2 Junction resistance

Junction forward and reverse contact resistances were calculated from the slope of the curves of the figures 4.3.1 from their straight line portion. The results are incorporated in table 6.

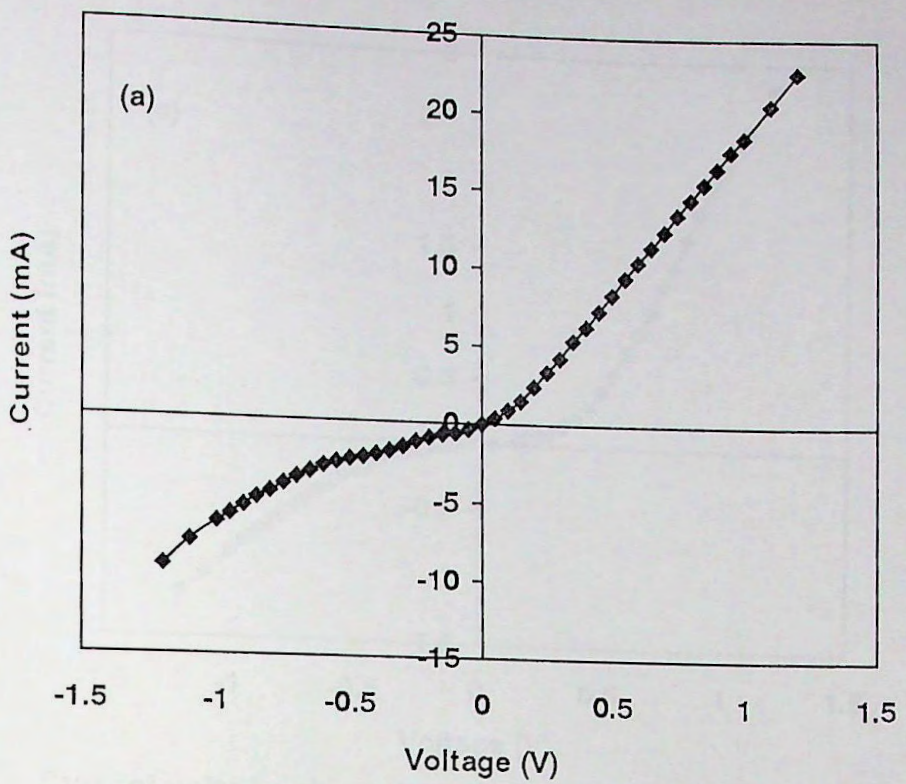

Fig. 4.3.1a Current voltage characteristics of CuO/CdS junctions with CuO=673 Å and CdS=6734 Å.

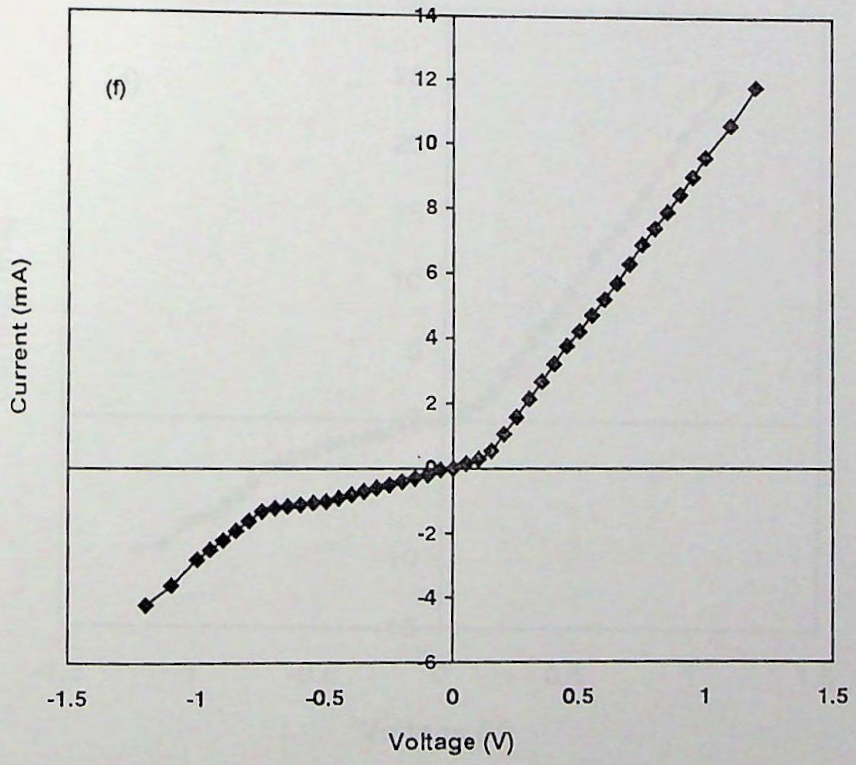

Fig. 4.3.1b Current voltage characteristics of CuO/CdS junctions with CuO=552 Å and CdS=5068 Å.

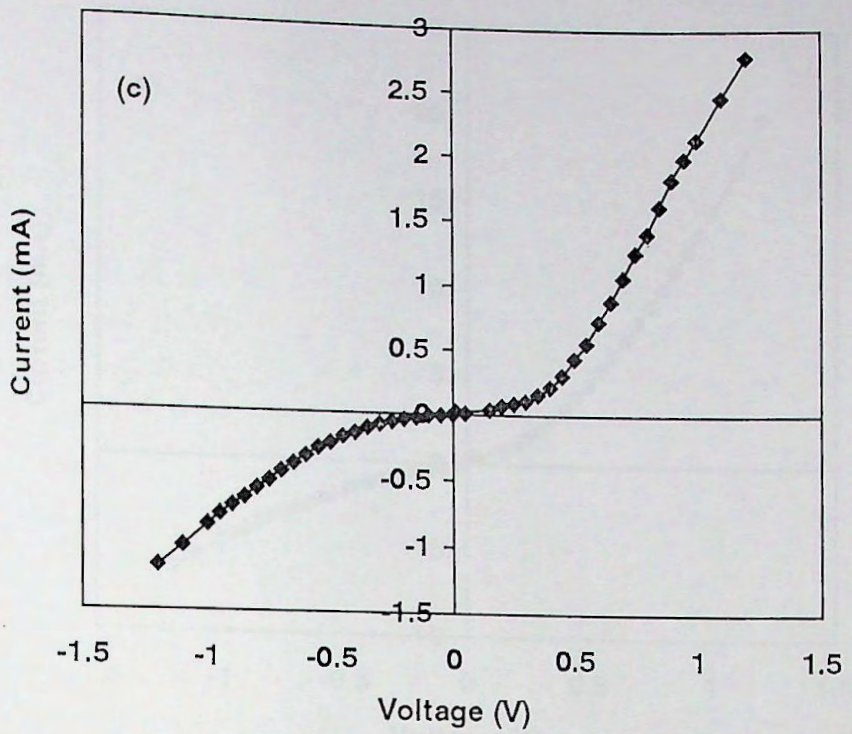

Fig. 4.3.1c Current voltage characteristics of CuO/CdS junctions with CuO=491 Å and CdS=1706 Å.

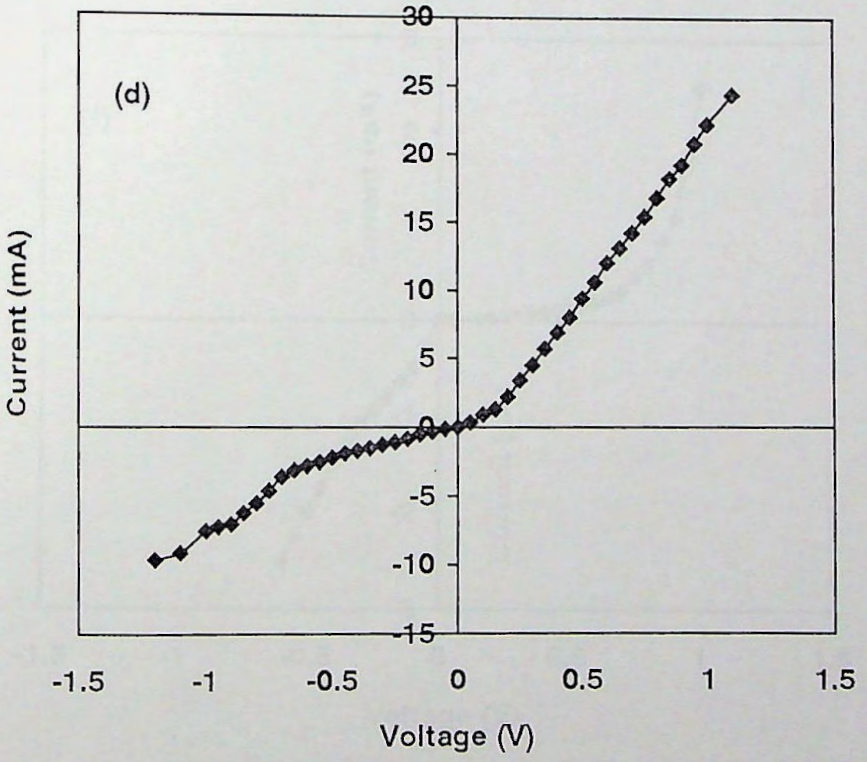

Fig. 4.3.1d Current voltage characteristics of CuO/CdS junctions with CuO=1277 Å and CdS=2058 Å.

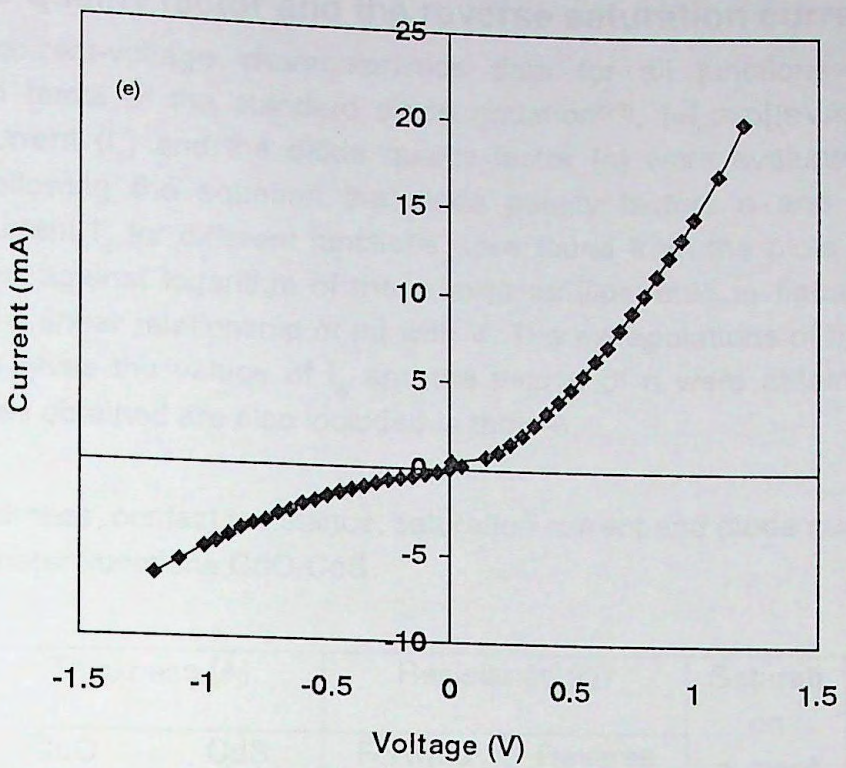

Fig. 4.3.1e Current voltage characteristics of CuO/CdS junctions with CuO=561 Å and CdS=2878 Å.

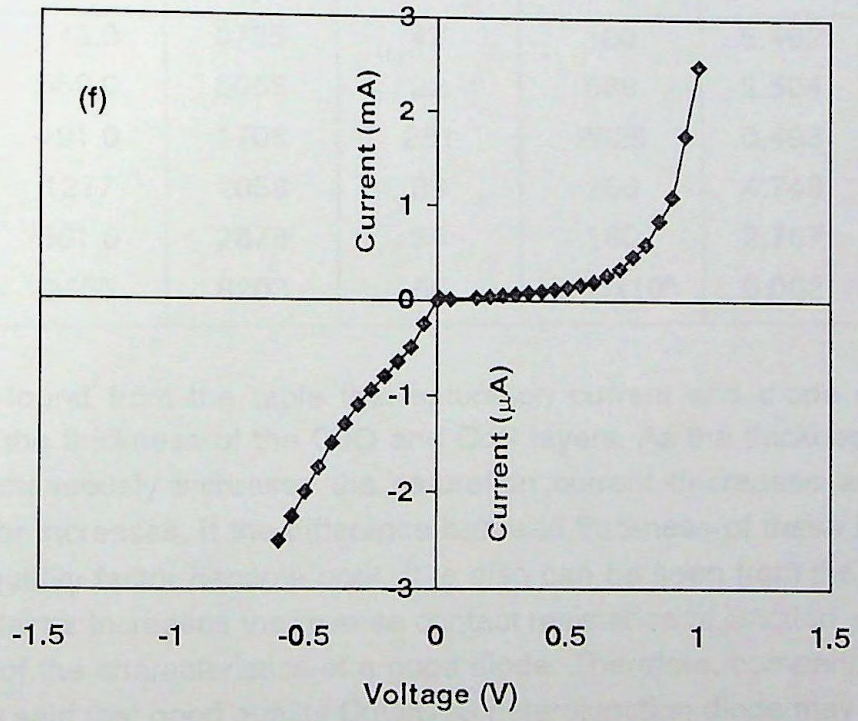

Fig. 4.3.1f Current voltage characteristics of CuO/CdS junctions with CuO=2455 Å and CdS=8203 Å.

4.3.3 Diode quality factor and the reverse saturation current

The current-voltage charachteristics data for all junctions have been annalysed in terms of the standard diode equation[23], $I=I_o\exp[(eV/nKT)-1]$. The saturation current (I_o) and the diode quality factor (n) were evaluated from this equation. Following the equation the diode quality factors n and the reverse saturation current I_o for different junctions were found from the plots of the open circuit voltage against logarithm of the current as illustrated in figure 4.3.2. The curves show a linear relationship of lnI with V. The extrapolations of these straight lines to V=0 gives the values of I_o and the values of n were obtained from the slopes. Values obtained are also included in table-6.

Table 6: Thickness, contact resistance, saturation current and diode quality factor of the heterojunctions CuO/CdS.

Heterojunctions	Thickness (Å)		Resistance (Ω)		Saturation current $x10^{-3}$ I_o (Amp.)	Diode quality factor n
	CuO	CdS	Forward	Reverse		
S1	673.0	6735	47	100	5.462	1.25
S2	552.0	5068	92	688	2.504	1.33
S3	491.0	1706	281	2625	0.493	1.47
S4	1277	2058	39	266	4.748	1.54
S5	561.0	2878	35	160	2.767	1.62
S6	2455	8203	66	$2.65x10^6$	0.002	7.00

It is found from the table that saturation current and diode quality factor depend on the thickness of the CuO and CdS layers. As the thickness of both the layers simultaneously increases the saturation current decreases and the diode quality factor increases. If the difference between thickness of these layers is high the diode quality factor become poor. It is also can be seen from the table that as the quality factor increases the reverse contact resistance of junction increases and this is one of the characteristics of a good diode. Therefore, comparing data in the table it may said that good quality CuO/CdS heterojunction diode may be fabricated by depositing thick CuO and CdS layers of comparable thickness.

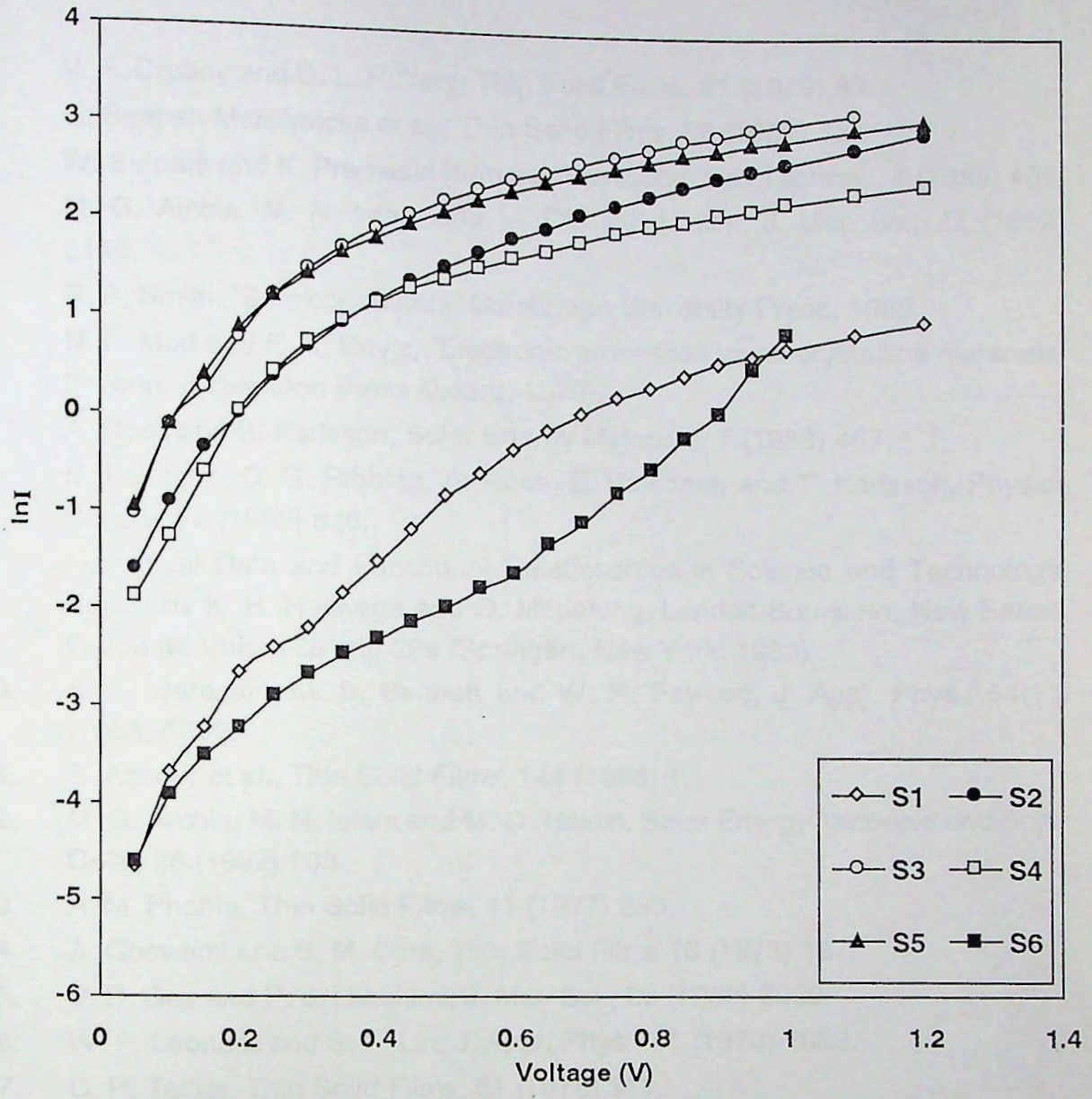

Fig. 4.3.2 Variation of lnI with voltage .

Reference

1. V. F. Drobny and D. L. Pulfery, Thin Solid Films, 61 (1979) 89.
2. G. Beensh-Marchwicka et al., Thin Solid Films, 88 (1982) 33.
3. W. Siripala and K. Premasiri Kumara, Semicond. Sci. Technol., 4 (1989) 465.
4. M. G. Ambia, M. N. Islam and M. Obaidul Hakim, J. Mat. Sc., 27 (1992) 5159.
5. R. A. Smith, "Semiconductors" Cambridge University Press, 1968.
6. N. F. Mott and E. A. Davis, "Electronic processes in noncrystalline metarials" 2nd edn. (Clarendon Press Oxford, 1979).
7. A. Ross and B. Karlsson, Solar Energy Materials, 7 (1983) 467.
8. B. Karlsson, C. G. Ribbing, A. Roos, E. Valkonen and T. Karlsson, Physica Scripta, 25 (1982) 826.
9. Numerical Data and Functional Relationships in Science and Technology, Edited by K. H. Hellwege and O. Madelung, Landolt-Bornstein, New Series, Group III, Vols. 17a and 22a (Springer , New York, 1982)
10. A. S. Baranski, M. S. Bennett and W. R. Fawcett, J. Appl. Phys., 54(11) (1983) 6390.
11. S. Achour et al., Thin Solid Films, 144 (1986) 1.
12. M. G. Ambia, M. N. Islam and M. O. Hakim, Solar Energy Materials and Solar Cells, 28 (1992) 103.
13. A. M. Phahle, Thin Solid Films, 41 (1977) 235.
14. A. Goswami and S. M. Ojha, Thin Solid Films 16 (1973) 187.
15. V. D. Das and P. J. Lakshimi, J. Mat. Sci., 23 (1988) 3869.
16. W. F. Leonard and S. F. Lin, J. Appl. Phys., 41 (1970) 1862.
17. C. R. Tellier, Thin Solid Films, 51 (1978) 311.
18. B. K. Gupta and O. P. Agnihotri, Solid State Commu., 23 (1977) 295.
19. A. Ashour, N. El-Kadry, S. A. Mahmoud, Thin Solid Films, 269 (1995) 117.
20. K. K. Nanda, S. N. Sarangi, S. Mohanty, S. N. Sahu, Thin Solid Films, 322 (1998) 21.
21. K. L. Chopra and S. R. Das, Thin Film Solar Cells, Penum Press, New York, 1983.
22. M. Krunks, E. Mellikov and E. Sork, Thin Solid Films, 140 (1986) 105.
23. B. L. Sharma and R. K. Purohit, Semiconductor heterojunction, Pergamm Oxford, 1974.

CHAPTER FIVE

CONCLUSIONS AND FUTURE WORK

CONCLUSIONS AND FUTURE WORK

5.1 Conclusions

CuO and CdS thin films were deposited by spray pyrolysis process under different physical conditions, and various properties of the samples have been studied. CuO/CdS heterojunctions were also fabricated and their current-voltage characteristics have been investigated.

CuO thin films have been prepared from aqueous solution of $CuCl_2$ under different physical conditions such as (i) maintaining solution concentration and spray time fixed but varying substrate temperature (ii) keeping solution concentration and substrate temperature fixed and varying spray time and (iii) keeping spray time and substrate temperature fixed and varying solution concentration.

It was found that film growth rate decreases and film thickness increases with time of spray. Film thickness decreases as the substrate temperature increases but it increases with solution concentration when sprayed for a constant time.

X-ray diffraction studies of the films deposited under different conditions show that films obtained are of fine crystalline structure with characteristic peaks of CuO phase. The structure of the material deposited is monoclinic with lattice parameter a=4.704Å, b=3.414Å and c=5.004Å.

DC (dark) conductivity measurements show that films deposited at higher substrate temperature have relatively low resistivity and the value increases slightly with the increase in film thickness and annealing lowers the value slightly. The conductivity show a single activation energy, E_σ=0.13 eV in the temperature range 293 to 403 K. Value of activation energy in addition to other behaviours indicate that conduction takes place through hopping in the band gap. Hall effect studies show a positive Hall constant at room temperature and samples are p-type with carrier concentrations in the range 10^{15} to 10^{16} cm^{-3} up to a film of 6000Å thickness.

Thermoelectric power of a number of films having different thickness have been measured by integral method and it was found that TEP varies with temperature but it becomes almost independent of temperature at high temperature, which is the characteristics of pinning of Fermi levels. It was also found that Fermi levels start from 0.118 eV above the valence band edge for film of higher thickness (6000Å) and move towards the band edge, and finally enters the extended band at lower film thickness.

Optical measurements were made in the UV-visible region and the material was found to be direct band gap semiconductor. The band gap varies slightly with deposition temperature and thickness of the films and the values lie in the range 1.3 to 1.5 eV.

CdS thin films were also prepared by the same process as mentioned above from aquous solution of $CdCl_2$ and $SC(NH_2)_2$ with 0.1M solution concentration and under different deposition conditions.

Crystallographic properties of CdS films were investigated by X-ray diffraction analysis. It was found that crystallinity of the films depends on deposition conditions and in all cases the material has hexagonal structure with a=4.136Å and c=6.713Å. Scanning electron microscope studies of these films show a columnar growth of the crystal grains 0.3-0.5 μm size, which are uniformly distributed over the substrate surface. All the films were polycrystalline with small grain size.

Hall effect measurements show CdS material deposited is n-type semiconductor with carrier concentration of the order 10^{14} cm^{-3}. This low value of carrier concentration may be due to the compensation effect, and the films considered are partly compensated semiconductors. Electrical resistivity has been measured from room temperature to 300°C and it was found that substrate temperature has a remarkable effect on the resistivity. Freshly deposited films' resistivity is higher than that of annealed films and the activation energy of annealed films remain almost same for all sample but varies slightly in the case of freshly deposited film.

Thermoelectric power measurements on the films show that TEP value increases almost linearly with thickness of the film, and the value change slightly near room temperature but remain almost temperature independent at higher temperature for all films.

Optical measurements show that CdS also is a direct band gap semiconductor. Optical band gap changes slightly with substrate temperature and annealing of films does not have much effect on this value. The values obtained for CdS lie in the range of 2.34 to 2.4 eV.

CuO/ CdS heterojunctions have been fabricated by first depositing CdS on fluorine doped tin oxide coated glass and then depositing CuO layer over CdS layer. Number of junctions were made by varying the thickness of CdS and CuO layers. From current-voltage characteristics it was found that diode quality factor depends on the thickness of the layers. Good quality diode may be fabricated by depositing relatively thick CuO and CdS layers of comparable thickness.

5.2 Future work

In our present work we have studied the structural, electrical and optical properties of CuO and CdS thin films. For further work the following may be considered:

1) study of electrical properties at low temperature to understand physical transport behaviour better,
2) photo sensitive behaviour has not been continued in the present work and may be a future project.
3) to control the resistivity characteristics further doping of the film may be considered in addition to increase of thickness of the films for making a good heterojunction or solar cell,
4) CuO/CdS heterojunction has been prepared primarily but to fabricate solar cells all their properties such as temperature and thickness dependence of diode quality factor, fill factor, solar cell efficiencies etc. are to be investigated.

PUBLICATION

1. Preparation and characterization of CdS thin films prepared by spray pyrolysis, M. Muhibbullah, M.G.M. Chowdhury and M.O. Hakim, Proceedings of international workshop on recent developments in condensed matter physics and nuclear science, R.U., Rajshahi, Bangladesh, 28 Oct - 1 Nov. 1996, Vol. I, p. 213-216.
2. Electrical and optical properties of spray deposited polycrystalline CdS thin films. M. Muhibbullah, M.O. Hakim and M.G.M. Chowdhury, Journal of Bangladesh Academy of Sciences, Dhaka, Bangladesh, Vol. 24, No. 1, (2000), 1-7.
3. Properties of spray deposited polycrystalline CdS thin films, M. Muhibbullah, M.G.M. Chowdhury and M.O. Hakim, The Nucleus (A Quarterly Scientific Journal, Islamabad, Pakistan), Vol. 27(1-2), (2000), 95-100.
4. Preparation and Characterization of copper (II) oxide thin film by chemical spray. M.O. Hakim, M. Muhibbullah and M.G.M. Chawdhury, J. Mat. Sci., (to be published).
5. Seebeck effect in polycrystalline CuO thin films prepared by spray pyrolysis, M. Muhibbullah, M.O. Hakim and M.G.M. Chowdhury, Thin Solid Films (to be published).
6. Study of the thermoelectric effect of CdS films, M. Muhibbullah, M.G.M. Chowdhury and M.O. Hakim (under preparation).